Technische Universität München

Fakultät für Medizin

p22phox promotes placental dysfunction and fetal death in a model of obesity and type 2 diabetes

Linda Li

Vollständiger Abdruck der von der Fakultät für Medizin der Technischen Universität München zur Erlangung einer

Doktorin der Medizinischen Wissenschaft (Dr. med. sci.)

genehmigten Dissertation.

Vorsitz: apl. Prof. Dr. Klaus-Peter Janssen

Prüfer*innen der Dissertation:

1. Prof. Dr. Agnes Görlach
2. Prof. Dr. Uta Behrends (schriftliche Beurteilung)
   apl. Prof. Dr. Vanadin R. Seifert-Klauss (mündliche Prüfung)

Die Dissertation wurde am 13.04.2023 bei der Technischen Universität München eingereicht und durch die Fakultät für Medizin am 16.08.2023 angenommen.

p22phox promotes placental dysfunction and fetal death in a model of obesity and type 2 diabetes

by

Linda Li

A Dissertation

Submitted to the
Department of Medicine
Technical University of Munich

In fulfillment of the requirement for the degree of
doctor of medicine

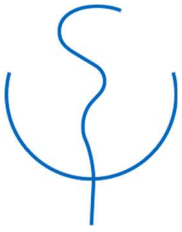

2023

Dedication

I dedicate this thesis to my family.

Thank you for your continuous love and support throughout these years.

Table of Contents

1. Publications

Parts and contents of this dissertation have been submitted for publication in the Journal of Biological Chemistry [1].

2. List of abbreviations

ADA	American Diabetes Association
α-SMA	Alpha smooth muscle actin
AUC	Area under the curve
BM	Body mass
BMI	Body mass index
BSA	Bovine serum albumin
CT	Computed tomography
CYBA	Cytochrome b-245 alpha chain
CYBB	Cytochrome b-245 beta chain
DAB	3,3'-Diaminobenzidine
DAPI	4′,6-Diamidino-2-phenylindole
dH_2O	Distilled water
DMSO	Dimethyl sulfoxide
DNA	Deoxyribonucleic acid
dNTPs	Deoxyribonucleoside triphosphates
DPBS	Dulbecco's phosphate buffered saline
EDTA	Ethylenediaminetetraacetic acid
eNOS	Endothelial nitric oxide synthase
ER	Endoplasmic reticulum
FAD	Flavin adenine dinucleotide
FELASA	Federation for laboratory animal science associations
FFPE	Formalin-fixed paraffin-embedded
Fig.	Figure
GCT	Glucose challenge test
GD	Gestational day
GDM	Gestational diabetes mellitus
GLUT	Glucose transporter
H&E	Haematoxylin and Eosin
HFD	High-fat diet
HIER	Heat-induced epitope retrieval
HRP	Horseradish peroxidase
IADPSG	The International Association of the Diabetes and Pregnancy Study Groups
IHC	Immunohistochemistry
IpGTT	Intraperitoneal glucose tolerance test
IpITT	Intraperitoneal insulin tolerance test
IUGR	Intrauterine growth restriction
IVC	Individually ventilated cages
KO	Knockout
MCP-1	Monocyte chemoattractant protein 1
MRI	Magnetic resonance imaging
mRNA	Messenger ribonucleic acid
NADPH	Nicotinamide Adenine Dinucleotide Phosphate
NAFL	Non-alcoholic fatty liver
NAFLD	Non-alcoholic fatty liver disease
NAL	Nasal-anal length
NASH	Non-alcoholic steatohepatitis
NFD	Normal-fat diet
NGSP	National Glycohemoglobin Standardization Program
NOX	NADPH oxidase
NOXA1	NOX activator 1
NOXO1	NOX organizer 1
O.C.T.	Optimal cutting temperature
OGTT	Oral glucose tolerance test
PAS	Periodic acid-Schiff
PBS	Phosphate buffered saline
PCR	Polymerase chain reaction
RNA	Ribonucleic acid
ROS	Reactive oxygen species
RT	Room temperature
SDS	Sodium dodecyl sulfate
SFA	Saturated fatty acids
SGA	Small for gestational age
ssDNA	Single-stranded DNA
Tab.	Table
TAE	Tris-acetate-EDTA
TRIS	Tris(hydroxymethyl)aminomethane
T2DM	Type 2 diabetes mellitus
VEGF	Vascular endothelial growth factor
WGA	Wheat germ agglutinin
WHO	World Health Organization
WT	Wildtype
4-HNE	4-Hydroxynonenal
8-OHdG	8-Hydroxy-2'-deoxyguanosine

3. Abstract

Obesity and diabetes are major health problems worldwide and the prevalence of these diseases has constantly been increasing over the last decades. Excess intake of high-caloric food as in the case of "Western diets" is regarded as one of the main risk factors in the development of these metabolic diseases.

Maternal obesity and diabetes are associated with adverse pregnancy outcomes for both mother and offspring. These high-risk pregnancies often involve gestational hypertension, preeclampsia, gestational diabetes, congenital anomalies, preterm birth and perinatal deaths. Reactive oxygen species (ROS) and ROS-mediated oxidative stress are believed to play a crucial role in the development of obesity, diabetes and the concomitant pregnancy complications.

Although NADPH oxidases represent a major source of ROS, their role in the pathogenesis of obesity, diabetes and adverse pregnancy outcomes is not completely understood.

The aim of this work was a) to evaluate the role of the NADPH oxidase subunit p22phox in the development of obesity and diabetes, and b) to investigate its impact on obesity/diabetes-associated pregnancy complications.

To achieve these goals a high-fat diet (HFD) mouse model in female p22phox-deficient nmf333 mutant and wildtype (WT) mice was established. Mice were fed with HFD for 20 weeks and during pregnancy. Controls chowed regular food (normal-fat diet, NFD). At the age of 25 weeks mice were mated. Dissection was performed at gestational day (GD) 17.5. It was shown that WT mice with functional p22phox developed an obese phenotype in response to 20 weeks of HFD compared to the nmf333 HFD group. In addition, WT HFD mice presented signs of glucose intolerance, increased fasting blood glucose levels, and insulin resistance compared to WT NFD fed mice and nmf333 HFD littermates. Glucose intolerance in WT HFD mice was maintained during pregnancy. Moreover, livers of pregnant WT HFD mice exhibited signs of non-alcoholic fatty liver disease (NAFLD) in transition to non-alcoholic steatohepatitis (NASH) and oxidative stress whereas nmf333 HFD mice remained unharmed. Fetal death rate was significantly higher in WT HFD mice compared to nmf333 HFD mice. Fetal mass and fetal/placental mass ratio were significantly lower in WT HFD pregnancies than in nmf333 HFD pregnancies. Upon analysis of the placenta, we could demonstrate that placentas of WT HFD mice but not of nmf333 HFD mice showed a significant increase in ROS-mediated placental lipotoxicity as well as vascular remodeling. Finally, this study demonstrated that

oxidative stress and lipid accumulation was also increased in fetal livers of WT HFD but not of nmf333 HFD dams.

In conclusion, this work showed that p22phox promotes HFD-induced obesity and obesity-related diseases such as type 2 diabetes mellitus and NAFLD/NASH, and impairs fetal survival via intrauterine growth restriction and fetal deaths, due to increased oxidative stress, lipotoxicity and placental vascular remodeling.

4. Introduction

4.1. Obesity

Obesity is one of the leading health problems worldwide [2]. It is described as a medical disorder that is not only a disease by itself but also leads to severe comorbidities [3]. The World Health Organization (WHO) defines obesity as a body mass index (BMI) ≥ 30.0 kg/m^2 and subdivides it into 3 different grades of obesity: 1 (BMI 30.0 to < 35.0 kg/m^2), 2 (BMI 35.0 to < 40.0 kg/m^2) and 3 (BMI > 40.0 kg/m^2). Overweight on the other hand is defined as BMI ≥ 25.0 to < 30.0 kg/m^2 [4].

4.1.1. Epidemiology

According to WHO the worldwide prevalence of obesity has constantly been increasing, nearly tripling since 1975 [4]. In 2016 almost 2 billion adults were overweight and among them over 650 million were obese. These numbers equate to 39% of the global adult population being overweight and 13% being obese [1, 4]. But not only adults have been facing this global threat, even childhood overweight and obesity has become a major problem. In 2019 approximately 38 million children aged < 5 years have been considered overweight or obese. Between 5-19 years old children and adolescents, the prevalence even reached 340 million which is more than four times higher than in 1975 (2016) [4].

Estimates suggest that by 2025 2.7 billion adults will be overweight, over 1 billion adults will be affected by obesity and among them 177 million will be severely obese, if the current trend is maintained [2].

4.1.2. Obesity as primary risk factor for metabolic syndrome

Body fat distribution has been associated with different comorbidities. While adolescent truncal subcutaneous fat accumulation positively correlates with the development of atherosclerosis in adulthood, central fat accumulation on the other hand is associated with insulin resistance [5]. However, abdominal obesity can be seen as the key trigger for the so-called metabolic syndrome, a cluster of several severe clinical conditions consisting of abdominal obesity alongside excessive waist circumference, systemic hypertension, insulin resistance or type 2 diabetes mellitus and atherogenic dyslipidemia such as impaired triglycerides or HDL

cholesterol [3, 6, 7]. Metabolic syndrome has become a rising challenge of modern world. Initially being a disease of the Western world, it has now become a global problem due to the rapid spread of "westernization". The risk underlying this syndrome comprise the retention and promotion of high-morbidity diseases such as type 2 diabetes mellitus, coronary artery diseases and stroke, making it a challenge for both health care and economy [8].

4.2. Diabetes mellitus

Diabetes mellitus comprises a group of heterogeneous diseases characterized by chronic hyperglycemia. It has long been subdivided into type 1 diabetes, type 2 diabetes and gestational diabetes, but several more uncommon forms of diabetes have been confirmed and added to this syndrome in the last decade [9, 10].

4.2.1. Epidemiology

Diabetes mellitus is considered as a major global health threat. 1 in 11 adults worldwide suffer from diabetes mellitus, amongst them 90% have type 2 diabetes mellitus, making it the main pillar in the rapidly emerging global epidemic of this disease [10, 11].

4.2.2. Clinical classification

The WHO classifies diabetes mellitus into six main categories which are type 1 and type 2 diabetes, hybrid forms of diabetes, other specific types of diabetes, unclassified diabetes and hyperglycemia during pregnancy (Table 1) [12].

4.2.3. Clinical appearance and diagnosis

Given the rising incidences of type 2 diabetes mellitus (T2DM) and gestational diabetes mellitus (GDM) the healthcare system is faced with the importance of early and accurate diagnosis.

4.2.3.1. Type 2 diabetes mellitus

Type 2 diabetes mellitus (T2DM) is the most common type of diabetes, usually arising after 40 years of age [1, 13]. Individuals suffering from T2DM exhibit increased insulin resistance in skeletal muscle and liver as well as impaired β-cell function [1, 14]. The former is compensated

by increased β-cell secretion of insulin, but glucose intolerance and consequently chronic hyperglycemia arise once the pancreatic β-cells fail to cope with the increased requirement of insulin, eventually leading to diabetes [14, 15]. Studies have demonstrated that patients display declining insulin sensitivity already decades before onset of T2DM, alongside gradually increasing fasting and postprandial hyperglycemia [16]. At the present, age and obesity are regarded as major risk factors for T2DM. Especially obesity leads to changes in the insulin-signaling pathway causing increased insulin resistance of tissues [9]. Upon recommendation of the American Diabetes Association (ADA), diabetes can be diagnosed by means of plasma glucose or HbA1c values [17], the latter being a glycated hemoglobin and an accepted diagnostic test for T2DM as well as a clinical parameter for glycemic control in diabetic patients [18] (Table 2).

Since 1980 the number of people with T2DM has been steadily growing; while in 1980s the number comprised 108 million, in 2014 it already reached 422 million. Worldwide, the prevalence of T2DM in adults adds up to 8.5% (2014) [19].

Type of diabetes	Brief description
Type 1 diabetes	β-cell destruction (mostly immune-mediated) and absolute insulin deficiency; onset most common in childhood and early adulthood
Type 2 diabetes	Most common type, various degrees of β-cell dysfunction and insulin resistance; commonly associated with overweight and obesity
Hybrid forms of diabetes	
Slowly evolving, immune-mediated diabetes of adults	Previously referred to as latent autoimmune diabetes of adults (LADA)
Ketosis-prone type 2 diabetes	Presents with ketosis and insulin deficiency but later does not require insulin; not immune-mediated
Other specific types	
Monogenic diabetes - Monogenic defects of β-cell function - Monogenic defects in insulin action	Caused by specific gene mutations
Diseases of the exocrine pancreas	Various conditions that affect the pancreas can result in hyperglycemia (trauma, tumor, inflammation, etc.)
Endocrine disorders	Occurs in diseases with excess secretion of insulin-antagonistic hormones
Drug-or chemical-induced	Can impair insulin secretion or destroy β-cells
Infection-related diabetes	Some viruses are associated with direct β-cell destruction
Uncommon specific forms of immune-mediated diabetes	Associated with rare immune-mediated diseases
Other genetic syndromes associated with diabetes	Genetic disorders and chromosomal abnormalities
Unclassified diabetes	Diabetes which does not clearly fit into other categories
Hyperglycemia first detected during pregnancy	
Diabetes mellitus in pregnancy	Type 1 or type 2 diabetes first diagnosed during pregnancy
Gestational diabetes mellitus	Hyperglycemia below diagnostic thresholds for diabetes in pregnancy

Table 1: Clinical classification of diabetes mellitus. Adapted after [12].

Accompanied by a concomitant increase in premature mortality, approximately 1.6 million deaths were estimated to be caused directly by diabetes mellitus in 2016 and 2.2 million to be brought on by high blood glucose in 2012. Hence, diabetes is regarded as one of the worldwide leading causes of death [19].

FPG ≥ 126 mg/dL (7.0 mmol/L). Fasting is defined as no caloric intake for at least 8 h.
Or
2-h PG ≥ 200 mg/dL (11.1 mmol/L) during **OGTT**. The test should be performed as described by the WHO, using a glucose load containing the equivalent of 75 g anhydrous glucose dissolved in water.
Or
HbA1c ≥ 6.5% (48 mmol/mol). The test should be performed in a laboratory using a method that is NGSP certified and standardized to the DCCT assay.
Or
In a patient with classic symptoms of hyperglycemia or hyperglycemic crisis, a random **PG ≥ 200mg/dl** (11.1 mmol/L).

Table 2: Criteria for the diagnosis of diabetes. Adapted after [17]. Abbreviations: DCCT - Diabetes Control and Complications Trial; FPG - fasting plasma glucose; OGTT - oral glucose tolerance test; PG - plasma glucose.

4.2.3.2. Gestational diabetes mellitus and type 2 diabetes mellitus in pregnancy

As one of the most common medical complications of pregnancy gestational diabetes mellitus (GDM) is defined as hyperglycemia that evolves during pregnancy but disappears after birth. Currently, several conditions are regarded as major GDM risk factors including maternal overweight and obesity, advanced age at gravidity, previous history of GDM, family history of T2DM and ethnicity [20]. WHO comprises two groups under the term “hyperglycemia first detected during pregnancy” (Table 1).

One is diabetes mellitus (type 1 or type 2 diabetes) in pregnancy which is defined by the same diagnosis criteria as in the non-pregnant; the other is named gestational diabetes where hyperglycemia is lower than the defined glucose threshold values [12]. At present, two equivalent strategies for screening and diagnosis of GDM are approved (Table 3). The “one-step” method involves a 75-g OGTT at 24-28 weeks of gestation recommended by the IADPSG. The older “two-step” method, consisting of a screening test followed by a diagnostic test, comes with a 50-g (non-fasting) glucose challenge test (GCT) and is complemented with a 100-g OGTT if the GCT exceeds the defined glucose threshold [17, 20].

One-step method
75-g OGTT. At 24-28 weeks of gestation in women not previously diagnosed with diabetes; performed in the morning after an overnight fast of at least 8 h. The diagnosis of GDM is made when any of the following plasma glucose values are met or exceeded: • Fasting: 92 mg/dl (5.1 mmol/L) • 1 h: 180 mg/dl (10.0 mmol/L) • 2 h: 153 mg/dl (8.5 mmol/L)
Two-step method
Step 1: 50-g GCT (non-fasting). At 24-28 weeks of gestation in women not previously diagnosed with diabetes. If plasma glucose level measured after 1 h is ≥ 130, 135, or 140 mg/dL (7.2, 7.5, or 7.8 mmol/L), proceed to 100-g OGTT.
Step 2: 100-g OGTT (fasting). The diagnosis of GDM is made when at least two of the following four plasma glucose levels are met or exceeded: • Fasting: 95 mg/dl (5.3 mmol/L) • 1 h: 180 mg/dl (10.0 mmol/L) • 2 h: 155 mg/dl (8.6 mmol/L) • 3 h: 140 mg/dl (7.8 mmol/L)

Table 3: Screening methods for diagnosis of GDM. Adapter after [17]. Abbreviations: OGTT, oral glucose tolerance test; GCT, glucose challenge test.

4.3. Comorbidities and adverse outcomes associated with obesity and type 2 diabetes mellitus

Obesity and T2DM are, however, often accompanied by additional metabolic comorbidities and possible adverse outcomes, which independently contribute to the global health burden, and on the other hand can even affect the offspring.

4.3.1. Development of fatty liver disease

Concomitant to the continuous rise of metabolic diseases such as obesity, metabolic syndrome and T2DM, associated liver abnormalities such as non-alcoholic fatty liver disease (NAFLD), and the more severe non-alcoholic steatohepatitis (NASH) have also been shown to exert a growing influence on the world health. The worldwide prevalence of NAFLD was estimated to be 24% in 2016 [21] with the highest numbers present in the Middle East (~32%) and South America (30,45%), followed by Asia (27%) as well as the US (24,13%) and Europe (23,71%) [22]. NAFLD/NASH cases are estimated to further increase over the next decades with 100.9 million NAFLD and 27 million NASH cases by 2030 merely in the US. In parallel, the incidence of decompensated liver cirrhosis is forecasted to increase by 168% and that of hepatocellular carcinoma (HCC) by 137%, leading to growing numbers of excess liver deaths [23].

The term NAFLD comprises the spectrum of fatty liver, steatohepatitis and liver cirrhosis individuals without significant alcohol consumption. It can become manifest in non-alcoholic fatty liver (NAFL) with only hepatic steatosis or more severe NASH with inflammation and hepatocytic damage [24]. The latter is furthermore accompanied by fibrosis that can progress to cirrhosis and concomitant adverse hepatic outcomes such as liver failure, need for transplantation and liver cancer (Table 4) [24, 25]. NAFLD is often (incidentally) diagnosed via non-invasive imaging techniques, for example ultrasound, CT and MRI. Clinical features such as the presence of metabolic comorbidities or elevated liver enzymes can contribute to the diagnosis [25]. NASH on the other hand requires a liver biopsy for definite diagnosis which in addition enables to determine the grade of fibrosis [25].

NAFL	Presence of hepatic steatosis with no evidence of hepatocellular injury in the form of ballooning of the hepatocytes or no evidence of fibrosis. Minimal risk of progression to cirrhosis and liver failure.
NAFLD	Entire spectrum of fatty liver disease without significant alcohol consumption, ranging from fatty liver to steatohepatitis and cirrhosis
NASH	Presence of hepatic steatosis and inflammation with ballooning with or without fibrosis. Progression to cirrhosis, liver failure and liver cancer possible.
NASH Cirrhosis	Presence of cirrhosis with current or previous histological evidence of steatosis or steatohepatitis

Table 4: NAFLD and related definitions. Adapted after [24].

Major risk factors in the development of NAFLD and NASH are the presence of metabolic syndrome and T2DM [26]. Thereby, the association between NAFLD and the metabolic syndrome is presumed to be bidirectional, implying that NAFLD could predispose to the development of metabolic syndrome features, which on the other hand could exacerbate NAFLD or increase the risk of development in individuals without a pre-existing diagnosis [26]. Furthermore, individuals suffering from T2DM are regarded as high-risk groups. Many studies have identified a higher prevalence of NAFLD in patients with T2DM [27-30]. In addition, patients with T2DM and NAFLD also show a higher incidence of NASH and advanced liver fibrosis [31, 32].

4.3.2. Effect of obesity and type 2 diabetes mellitus on mother and offspring

In pregnancy the placenta is the key organ essential for the maternal-fetal supply of oxygen and nutrients to the developing fetus. The placenta uses maternal resources for its own supply but at the same time allows fetal growth, mediating maternal metabolic disturbances on the fetus [20]. These metabolic changes mainly include hyperglycemia, elevated fatty acids and amino acid concentration in the maternal circulation [20].

Contents of the following paragraphs have been submitted for publication [1].

Maternal obesity is associated with adverse outcomes both for mother and offspring. Pregnant women with increased bodyweight are more likely to develop maternal pathologies such as gestational hypertension, preeclampsia or gestational diabetes, but also hold greater risks for the offspring such as fetal growth restriction, preterm birth, fetal adiposity, congenital anomalies and perinatal death [1, 33, 34]. Furthermore, placentas of overweight and obese women have been described to be heavier at birth and to exhibit an increased amount of lipids, macrophages and proinflammatory mediators [35]. Studies of obesity in animal models have shown a decrease in birth and fetal weight and alterations in glucose homeostasis and endocrine metabolism in offspring [36, 37].

Hyperglycemia during pregnancy has also been described to affect both mother and offspring. Maternal outcomes comprise short- and long-term risks such as preeclampsia, cesarean section, future diabetes and cardiovascular complications later in life [1, 38-41]. Embryonic and fetal complications include anomalies of the cardiovascular and neural tube system, but also preterm delivery, congenital anomaly and stillbirth [42-44]. Similar findings were observed in the Hyperglycemia and Adverse Pregnancy Outcome (HAPO) Study, a worldwide study comprising more than 25.000 pregnant women. Primary and secondary outcomes included increased birth weight, primary cesarean delivery, clinical neonatal hypoglycemia, premature delivery, shoulder dystocia or birth injury, as well as need for intensive neonatal care and preeclampsia [45]. Furthermore, animal models of diabetic embryopathy have shown the association of maternal hyperglycemia to increased fetal teratogenesis and congenital malformations, especially of the cardiovascular system [46-48].

The causative underlying mechanisms of these adverse pregnancy outcomes are thought to be linked to oxidative stress [1, 49]. Excessive reactive oxygen species have been described in obesity and diabetes [1, 50, 51] and accumulating evidence points to an association between reactive oxygen species and pregnancy complications [1, 52, 53].

4.4. Reactive oxygen species and NADPH oxidases

Reactive oxygen species (ROS) play an important role in mediating both physiological and pathophysiological signal transduction. They are produced in various subcellular compartments such as the cytoplasm, cell membrane, the ER, mitochondria and peroxisomes [54-56]. Because of their high reactivity, ROS can easily interact with many cellular molecules including nucleic

acids, proteins and lipids, hereby causing damage to the cells [57]. Yet, ROS have also been described to be fundamental for cellular homeostasis by promoting cell survival, cell growth, differentiation and immune signaling [56]. Hence, a balance between oxidants and antioxidants is crucial for maintaining normal cellular function, given that any disruption will lead to oxidative stress and subsequent human diseases [57].

4.4.1. Different types of reactive oxygen species

Contents of the first paragraph have been submitted for publication [1].

ROS are a group of highly reactive, oxygen-composed molecules generated by the partial reduction of oxygen [1, 56]. They can be classified into two types: 1) species with unpaired electrons (free oxygen radicals), such as: superoxide anion ($O_2^{\bullet -}$) and hydroxyl radical ($OH^{\bullet}$), and 2) non-radicals: e.g. hydrogen peroxide (H_2O_2) [1, 58].

$O_2^{\bullet -}$ can be reduced either spontaneously or through a reaction with superoxide dismutase (SOD), through the Haber-Weiss reaction [59, 60], or in reaction with nitric oxide radical ($NO^{\bullet}$) [61]. H_2O_2 can react with reduced transition metals – called the Fenton reaction [62] – to form $OH^{\bullet}$ and OH^- or $OOH^{\bullet}$ and H^+, when combined with Fe^{2+} or Fe^{3+}, respectively [61].

4.4.2. NADPH oxidases

Contents of this chapter have been submitted for publication [1].

NADPH oxidases are a family of membrane-bound enzymes which produce superoxide anion ($O_2^{\bullet -}$) with NADPH serving as electron donor [1, 63]. The phagocyte NADPH oxidase was the first identified NADPH oxidase, which plays a decisive role in the innate immune defense against bacteria [64].

The heterodimeric membrane-bound core catalytic complex of phagocyte NADPH oxidase, referred to as cytochrome b558, consists of two proteins: $p22^{phox}$ and NOX2 (formerly known as $gp91^{phox}$). The enzyme activity is tightly regulated by several cytosolic proteins, termed $p47^{phox}$, $p40^{phox}$, $p67^{phox}$ and the GDP-bound GTPase Rac [65]. Phosphorylation of $p47^{phox}$ leads to enzyme activation and translocation of the cytosolic proteins to the membrane. Electron transfer is then induced upon assembly of the heterohexameric enzyme complex, more precisely upon interaction between $p67^{phox}$ and active, GTP-bound Rac with the cytochrome (Fig.1) [66].

Over the time homologous proteins to NOX2 have been identified [63]. NOX1, previously termed as mox1, was first cloned in 1999 [67]. It was found to be mostly expressed in colon, prostate and vascular endothelial cells, but not in leukocytes [67]. Subsequently, more homologs i.a. NOX3, NOX4, NOX5 [68] as well as DUOX1 and DUOX2, initially described as thyroid oxidases [69], were discovered. Together, they form the family of NADPH oxidases.

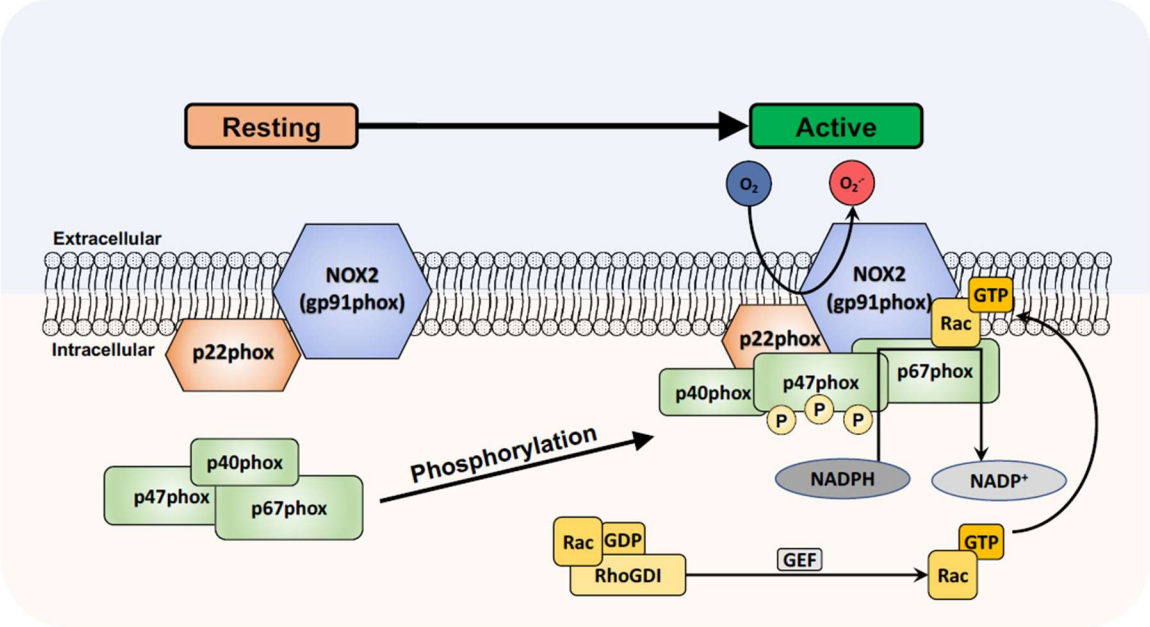

Figure 1. Structure of phagocytic NADPH oxidase.
In resting cells, $gp91^{phox}$ and $p22^{phox}$ form the membrane-bound cytochrome b558. Upon activation the cytosolic subunits $p40^{phox}$, $p47^{phox}$, $p67^{phox}$ and Rac translocate to the membrane to form the activated NADPH complex. Adapted from [70].

All seven homologs are characterized by a multi-protein complex, however, differences in their membrane localization and protein components have been observed (Fig. 2) [1, 71]. The conserved structural domains include: (1) a COOH-terminus containing a NADPH-binding site and a FAD-binding site, (2) six conserved transmembrane domains, and (3) four heme-binding histidines, thereof two in the third and two in the fifth transmembrane domain. Some family members contain additional features, such as EF-hands or an additional NH_2-terminal transmembrane domain [1, 63, 71].

4.4.2.1. The NOX homologs

The prototype of NADPH oxidases contains NOX2 as the catalytic subunit and was termed phagocyte NADPH oxidase due to its expression in phagocytes. Providing a respiratory burst response, NOX2-containing NADPH oxidases serve as essential players in the innate immune defense against phagocytosed bacteria [64]. Mutations in the CYBB gene coding for NOX2

result in chronic granulomatous disease [72]. But expression of NOX2 has also been reported in other non-phagocytic cells, such as neurons, cardiomyocytes, vascular smooth muscle and endothelial cells, skeletal muscle cells and hepatocytes [63].

NOX1 was the first homolog of NOX2 that was described [67], and was initially named mox1. Its mRNA was found to be expressed in colon, prostate, uterus, vascular smooth muscle cells, but not in phagocytes [67]. Similar to the active NOX2-containing complex, functional NOX1-containing NADPH oxidases require cytosolic subunits, NOXO1 and NOXA1, homologs of $p47^{phox}$ and $p67^{phox}$ along with membrane-bound $p22^{phox}$ and GTPase Rac for full activation (Fig. 2) [71, 73]. NOX1 activity has been associated with various physiological and pathophysiological mechanisms, e.g. immune defense in inflammatory bowel disease, regulation of smooth muscle growth, blood pressure and neural differentiation but also with increased cell proliferation resulting in cancer, especially colon adenocarcinoma [71].

NOX3 has been initially identified in fetal organs [68]. In the adult, it is highly expressed in specific portions of the inner ear, namely the vestibular and cochlear sensory epithelia [74]. Vestibular defects of the mutant “head-tilt” mice (R96, R542 and vst mutant mice) were described as a consequence of mutations in the NOX3 gene [75]. Additional cytosolic subunits or Rac are not needed for basal activity, however their presence leads to enhanced NOX3 activity [63, 71, 74].

The NOX4 homolog was originally described to be mainly expressed in the kidney [76, 77]. With approximately 37% similarity to NOX2 it is more distant than NOX1 and NOX3 [65]. NOX4 mRNA expression has been found in various other tissues such as osteoclasts, endothelial, smooth muscle and hematopoietic stem cells, fibroblasts, neurons, keratinocytes, and melanoma cells [63]. Its function has been associated with cell differentiation, cell survival and migration, insulin signaling, apoptosis and oxidative stress in cardiac dysfunction [71]. NOX4 is a $p22^{phox}$-dependent enzyme, but does not require cytosolic subunits or Rac for its function [63]. In contrast to the other enzymes, it has been discussed to also generate H_2O_2 [78].

NOX5 was discovered in 2001 by two different groups [68, 79]. It is the most distant isoform with only 27% similarity to NOX2 [65]. To date five splice variants have been described [80]. In contrast to other homologs, NOX5 does not require $p22^{phox}$ or other cytosolic subunits for activation [81]. Instead, it possesses an intracellular NH_2-terminus with a Ca^{2+}-binding EF-hand domain (Fig. 2) [79, 81]. NOX5 mRNA has originally been described to be mainly expressed

in testis, spleen and lymph nodes, but NOX5 variants have also been discovered in endothelial cells [68, 79, 82].

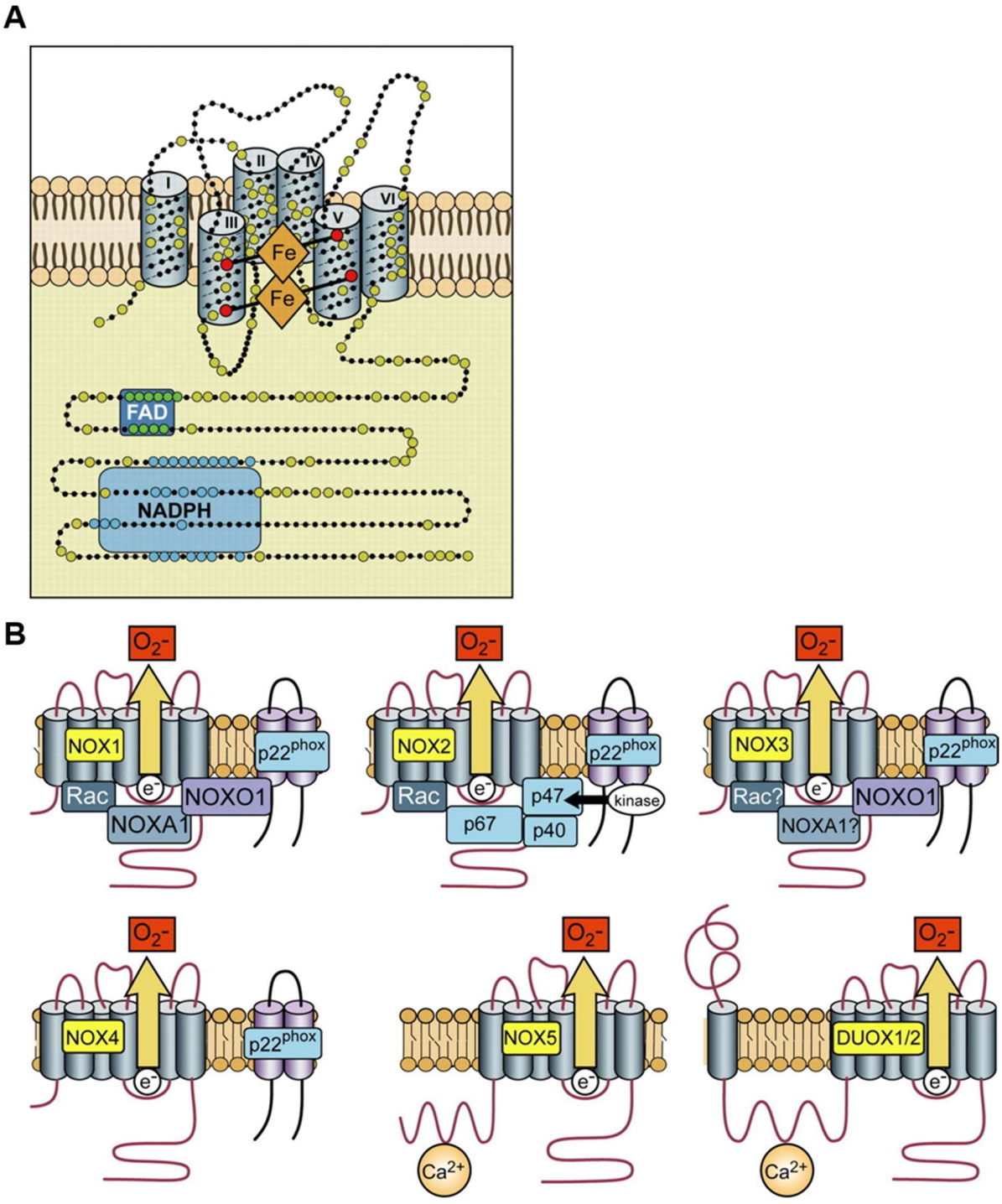

Figure 2. The NOX homologs and their structure.
(A) All NOX homologs consist of six transmembrane domains and a NADPH/FAD site at the COOH terminus. **(B)** Additional proteins needed for activation of certain members include $p22^{phox}$, $p67^{phox}$, $p47^{phox}$, $p40^{phox}$ as well as Rac. Adapted from [63].

DUOX1 and DUOX2 (also known as thyroid oxidases) differ from the NOX isoforms by possessing a seventh transmembrane domain and an extracellular peroxidase domain in addition to the Ca^{2+}-binding EF-hand domain which is also present in NOX5 [69]. Similar to NOX5, DUOX1/2 function is not fully dependent on $p22^{phox}$ [83, 84]. DUOX1 and DUOX2 have been found to be highly expressed in the thyroid, airway epithelia and the prostate [69, 84-86].

4.4.2.2. The subunit p22phox

Parts of the first paragraph have been submitted for publication [1].

p22phox is a membrane-bound subunit, crucial for the activation of NOX1-4 [1, 87-90]. It forms the flavocytochrome b558 together with NOX2 [91]. In humans the gene for p22phox, CYBA, is located on chromosome 16 [1, 63]. Mutations in the CYBA gene can lead to chronic granulomatous disease [1, 92]. Previous studies have reported ubiquitous expression of p22phox mRNA [93-95]. Major functions of p22phox comprise binding to NOX proteins for their stabilization, and interaction with cytosolic subunits [63].

However, NOX5 forms an exception since its activation is mainly regulated by Ca^{2+} concentration [81]. As for DUOX1/2, a potential requirement of p22phox for enzyme activation is still under debate since DUOX has been demonstrated to coimmunoprecipitate with p22phox, but no evidence for enhanced DUOX activity when co-expressed with p22phox has been provided so far [84, 96, 97].

Taken together, p22phox plays a major part in activation of most NOX isoforms.

4.4.3. Other sources of reactive oxygen species

While NADPH oxidases serve as a major source of enzymatically generated ROS, the latter can also be produced non-enzymatically. On an intracellular level the mitochondrial respiratory chain is primarily responsible for the production of ROS [98-100]. The electron transport chain consists of four complexes, namely complex I-IV, with complexes I and III being major sites of superoxide formation mainly due to leaking electrons [101-103]. However, mitochondrial enzymes such as the nitric oxide synthase, α-ketoglutarate dehydrogenase, 2-oxoacid dehydrogenase and pyruvate dehydrogenase also considerably contribute to the production of superoxide radicals and hydrogen peroxide [104-106].

In addition, ROS can also be generated in various cellular compartments aside from mitochondria. These include the ER, lysosomes and peroxisomes [103]. The latter participates in lipid metabolism and is able to produce H_2O_2 [107]. Interestingly, peroxisome-generated H_2O_2 has been shown to play a major part in non-esterified fatty acid-mediated lipotoxicity of pancreatic β-cells [108].

4.4.4. Role of reactive oxygen species in the development of obesity and type 2 diabetes mellitus

Contents of the following two paragraphs have been submitted for publication [1].

Oxidative stress and ROS are involved in the pathogenesis of various diseases such as obesity, diabetes and cardiovascular disorders [1, 109-111]. Excess energy supply which is common in obesity can lead to mitochondrial dysfunction and increased ROS signaling [1, 50, 112]. Previous evidence has shown that high-fat diet/obesity increases ROS production which is associated with disturbed mitochondrial integrity [113, 114]. In addition to defects in mitochondrial metabolism, NADPH oxidases also play a significant role in extensive superoxide production in obesity and the metabolic syndrome [109, 115, 116]. Furthermore, peroxisomes are presumed to considerably contribute to increased ROS signaling in obesity [117].

ROS generation is also increased in obesity-related diseases such as T2DM. T2DM is characterized by insulin resistance and pancreatic β-cell dysfunction, and ROS have been shown to participate in the progression of both [118, 119]. The underlying mechanisms comprise the production of advanced glycation end products (AGE) and ROS by the glycation reaction and activation of the electron transport chain, both in consequence of hyperglycemia [120]. Furthermore, membrane-bound NADPH oxidases are stimulated by AGEs and high insulin levels, thereby contributing to the accumulation of ROS [120]. Enhanced activity of the mitochondrial respiratory chain and NADPH oxidases are believed to be the major sources of ROS in pancreatic β-cells [1, 121], promoting glucose toxicity in these cells [122, 123]. Moreover, expression of ROS markers has been found to be increased under diabetic conditions [124]. Lipotoxicity is also accused of promoting β-cell dysfunction. High concentrations of free fatty acids (FFA) have been shown to induce ROS production in pancreatic islets, contributing to the disruption of insulin secretion and β-cell deterioration [125-127].

5. Aim of the study

Obesity and diabetes are major health problems worldwide and the number of patients suffering from these diseases is continuously increasing. Intake of high-caloric food describes one of the main risk factors in the development of these metabolic diseases. Maternal obesity and diabetes are associated with adverse pregnancy effects for both mother and offspring. ROS and ROS-mediated oxidative stress are believed to play a crucial role in the pathogenesis of obesity and T2DM and to contribute to adverse pregnancy outcomes associated with these diseases. NADPH oxidases are considered a major source of ROS generation. p22phox is an essential subunit of several members of the NOX family. However, the particular link between obesity/T2DM and p22phox-dependent NADPH oxidases is not completely understood.

The aim of this work is therefore to assess the role of p22phox in the development of obesity and diabetes *in vivo* and to evaluate potential adverse effects on pregnancy. Specifically, the following questions are addressed:

Is p22phox involved in the development of HFD-induced obesity and T2DM?

Does p22phox contribute to the development of GDM during pregnancy?

Does p22phox play a role in potential adverse effects during pregnancy and how do they manifest themselves?

6. Materials and Methods

6.1. Materials

6.1.1. Equipment: Laboratory

Item	Supplier
Adjustable volume pipettes	Gilson
Analytical balance BP 301S	Sartorius
Analytical balance BP 4100S	Sartorius
Analytical balance EMB-220-1	Kern & Sohn GmbH
Analytical balance PCB 350-3	Kern & Sohn GmbH
Anesthetizing box	Harvard Apparatus
Aperio AT2 digital slide scanner	Leica Biosystems
Axiocam 506 color	Zeiss
Axioscope 2 801672	Zeiss
Bel-Art mouse restrainer w/ dorsal access	Fisher Scientific
Bonn artery scissor with ball tip 9cm 14086-09	Fine Science Tools
Capsulefuge PMC-060	TOMY Digital Biology
Centrifuge Biofuge pico	Heraeus
Centrifuge Biofuge fresco	Heraeus
Centrifuge Biofuge stratos	Heraeus
Centrifuge Megafuge 1.0R	Heraeus
Cooling Plate COP 20	Medite
Cooling Plate COP 30	Medite
Cryostat Leica CM 1850	Leica Biosystems
Dewar carrying flask	KGW Isotherm
Digital Caliper	Unknown
Electrophoresis chambers	Bio-Rad
Fine scissor	Fine Science Tools
Forceps	Fine Science Tools
Gel Doc 2000	Bio-Rad
Gene-Disc heat sealer HS-01	Corbett Research
Glass jar DURAN®	Schott AG
Herafreeze ultra-low temperature freezer	Thermo Scientific
Herasafe biological safety cabinet	Thermo Scientific
Incubator Kelvitron	Heraeus
Leica HI 1220 flattening table	Leica Biosystems
Leica MZ7.5 stereomicroscope	Leica Microsystems
Liebherr Comfort refrigerator	Liebherr
Lightsource Spectra X	Lumencor
Magnetic stirrer MR 3000	Heidolph Instruments
MED-100 fridge	Kirsch
Microm AP 280-2 tissue embedding system	Microm
Microm STP-120 spin tissue processor	Microm
Microplate reader “Safire”	Tecan

Microtome HM 355S	Thermo Fisher Scientific
Microwave Severin 900 & Grill	Severin
Nano Drop 2000c	Thermo Fisher Scientific
Objective plan 1.0x 10446275	Leica Microsystems
Olympus IX83 inverted microscope	Olympus
OneTouch Verio IQ blood glucose meter	OneTouch
OneTouch Verio test strips	OneTouch
OptiMOS sCMOS camera	QImaging
O/R light Hanaulux 2003	Heraeus
PH meter, GLP pH540	WTW
Pipette “Multipette plus”	Eppendorf
Pipette “Pipetman”	Gilson
Pipette “Pipetus”	Hirschmann Laborgeräte
Pipette „Pipetboy acu“	Integra Biosciences
Plate shaker Polymax 1040	Heidolph Instruments
Power supply, Power Pac 200	Bio-Rad
Power supply, Power Pac 300	Bio-Rad
Roller mixer RM 5 No. 348	Assistant
Roller mixer LLG-uniROLLER 6 digital	LLG Labware
Scanner WF-2630	Epson
Shaker IKA MTS 2 electronic	IKA
Shaker IKA MTS 4 electronic	IKA
Sonopuls ultrasonic homogenizer	Bandelin
Spring scissor	Fine Science Tools
Staining jar according to Hellendahl	DWK Life Sciences
Staining jar with glass tray	Marienfeld Superior
Thermocycler GeneAmp PCR System 9700	Applied Biosystems Life Technologies
Thermomixer comfort 1,5ml	Eppendorf
Tissue Float Bath 1052	GFL GmbH
Tube Rotator Type 3000 A251258	Fröbel Labortechnik GmBH
Versilic hand protector 161090	Saint Gobain
Video copy processor P91W	Mitsubishi
Vortex-Genie 2	Scientific Industries
X-ray cassettes IEC 60406	Kisker Biotech

6.1.2. Equipment: Animal facility

Item	**Supplier**
Bottle with cap	Tecniplast
Breeding feed for mouse V1124-300	Ssniff Spezialdiäten GmbH
Cage lid	Tecniplast
Double sided changing station C S5	Tecniplast
EF D12492 (II) mod. 60kJ% fat diet	Ssniff Spezialdiäten GmbH
Inner fitting lid	Tecniplast
IVC	Tecniplast
IVC Racks	Tecniplast
Maintenance feed for rat/mouse V1534-300	Ssniff Spezialdiäten GmbH
SkyFlow	Tecniplast

6.1.3. Laboratory consumables

Item	Supplier
Aluminium foil	Carl Roth
Amersham Protran 0,45µm nitrocellulose blotting membrane	GE Healthcare Life Sciences
Aquatex	Merck
BD Microlance 3 needles 26G	BD Medical
Cellstar cell culture multiwell plates	Greiner Bio-One
Cryobox	Kisker
CryoPure tube	Sarstedt
Entellan new	Merck
Eppendorf tubes	Eppendorf
Falcons	BD Biosciences
Falcon pipettes	BD Biosciences
Gloves (latex)	Sempermed
Gloves (nitril)	Kimberly-Clark
Kimtech Science Precision Wipes	Kimberly-Clark
Metal base molds	Leica Biosystems
Microscope cover glasses 24x60mm	VWR
Microscope slides Menzel-Gläser	Thermo Scientific
Microscope slides SuperFrost Plus	VWR
Microtome blades C35	Feather
Mini Super HT pap pen	Biotium
Mounting Medium	Dako
Multi-Adapter	Sarstedt
Nail polish	Various brands
Paraffin	Merck
Peel-A-Way® Embedding Mold (truncated)	Polysciences
Petri dish	Fisher Scientific
Pipette filter tips	Biozym Scientific
Pipette tips	Gilson
Plastic transfer pipettes	Thermo Fisher Scientific
Reaction tubes, 4-stripe	Biozym Scientific
Reaction tubes, 8-stripe	Thermo Fisher Scientific
Rotilabo tissue embedding cassettes K116.1	Carl Roth
Slidebox 100 place HS15994C	Heathrow Scientific
S-Monovette, EDTA	Sarstedt
Surgical Disposable Scalpel	B. Braun
Syringe, sterile	B. Braun
Syringe filter, sterile, 0.22 µm	Merck Millipore
Tissue-Tek Cryomold molds	Sakura Finetek
Tissue-Tek O.C.T. Compound	Sakura Finetek
Whatman filter paper 30mm 19,0cm x 100m	GE Healthcare Life Sciences
WypAll Towels	Kimberly-Clark

6.1.4. Chemicals

Chemical/ Reagent	Supplier
Acetic acid glacial	Carl Roth
Acetone	Sigma Aldrich
Agarose Standard	Carl Roth
Albumine Fraction V (pH 7.0)	AppliChem
Amido black 10 B	Carl Roth
Bond Breaker	Thermo Fisher Scientific
Bromophenol blue	Sigma Aldrich
$CaCl_2$	Sigma Life Science
Cell Lysis Buffer (10x) #9803	Cell Signaling Technology
Clear-Rite 3	Thermo Scientific
p-Coumaric Acid	Sigma Aldrich
Dako Wash Buffer 10x	Dako
DMSO	Sigma Aldrich
Direct Red 80	Sigma Aldrich
Dithiothreitol	GE Healthcare
DPBS, w/o: Ca and Mg, sterile filtered	PAN Biotech
D-(+)-Glucose	Sigma Life Science
D-(+)-Sucrose for molecular biology	AppliChem
EDTA	Carl Roth
Eosin G 0,5%, aqueous	Morphisto
Ethanol, absolute	Sigma-Aldrich
Ethanol Rotipuran ≥99,8 %	Carl Roth
Ethanol 99.5% denaturated with 1% MEK	VWR Chemicals
Ethidium bromide	Carl Roth
Formalin 37%	Carl Roth
Glycerol 85%	GE Healthcare
Glycerol 99,5%	GERBU
Glycine	GE Healthcare
HCl	Carl Roth
Haematoxylin after MAYER unleavened	Morphisto
HIER citrate buffer pH 6.0 (10x)	Zytomed Systems
HIER EDTA buffer pH 8.0 (10x)	Zytomed Systems
HIER T-EDTA buffer pH 9.0 (10x)	Zytomed Systems
Hoechst 33342, H1399	Thermo Fisher Scientific
H_2O_2 30%	Carl Roth
KH_2PO_4	Merck
Liquid DAB + Substrate chromogen system	Dako
Lithium carbonate	Carl Roth
Luminol	Sigma Aldrich
Magnesium carbonate hydroxide	Sigma Life Science
$MgCl_2$	Sigma Life Science
Methanol	VWR
2-Methylbutane	Carl Roth
NaCl 0,9%	B. Braun
NaCl	Carl Roth

$NaHCO_3$	Merck
NaH_2PO_4	Merck
Na_2HPO_4	Carl Roth
Naphthol blue black	Sigma Aldrich
Na3VO4	Merck
NEBuffer 3	New England Biolabs
Oil Red O	Sigma-Aldrich
Oil Red O color solution	Merck
Orange G	Sigma Aldrich
PBS Tablets, pH 7.4	Life Technologies / ChemSolute
Picric acid solution 1,3% in H_2O (saturated)	Sigma Life Science
Ponceau S solution for electrophoresis (0.2 %)	SERVA
Propanol-2	Carl Roth/VWR Chemicals
Quick-Load 100bp DNA Ladder	New England Biolabs
Rhodamine-WGA	Vector Laboratories
Rotiphorese Gel 30 (37,5:1)	Carl Roth
Roti-Quant 5x	Carl Roth
SDS	GE Healthcare
Skim milk powder for blotting	SERVA
Smoky HCl 37%	Merck
Sodium acetate	Carl Roth
TRIS	Carl Roth
Triton X-100	Sigma Aldrich
Xylene (mixture of isomers) ≥98.5%, AnalaR NORMAPUR®	VWR Chemicals

6.1.5. Drugs

Drug	**Supplier**
Insuman® Rapid 40 I.E./ml	Sanofi-Aventis

6.1.6. Kits and Ready-to-use reagents

Kits	**Supplier**
PAS Staining Kit HP01	Carl Roth

6.1.7. Buffers

Tissue lysis buffer for genotyping:

1M TRIS-HCl pH 8.0	50 mM
EDTA 0.5M	0.1 M
5M NaCl	0.1 M
20% SDS	1%

dissolved in dH_2O and autoclaved

10x Orange G loading buffer:

Glycerol	30% (v/v)
Orange G	0.2% (w/v)

dissolved in dH_2O

10x TAE electrophoresis buffer:

TRIS	0.5 M
Sodium acetate	0.2 M
EDTA	0.02 M

adjusted pH to 7.4 and stored at RT

0.1M Phosphate buffer:

NaH2PO4	25 mM
Na2HPO4	75 mM

dissolved in dH_2O [pH 7.3]

6.1.8. Solutions

6.1.8.1. Tissue preservation solutions

20% Sucrose stock solution:

Sucrose	20 g
PBS 0.1M	80 ml

aseptically prepared and stored at 4°C

O.C.T/Sucrose compound:

O.C.T compound	25 ml
20% Sucrose	25 ml

shaken for several hours until homogeneous solution and stored at 4°C

6.1.8.2. Histology solutions

Picro-sirius Red solution:

Direct Red 80	0.5 g
Picric acid, aqueous solution	500 ml

stored at RT

Acidified Water:

Acetic acid glacial	5 ml
dH_2O	1 L

stored at RT

6.1.9. Enzymes

Item	Supplier
Bsl I – RE	New England Biolabs
Proteinase K (recombinant), PCR Grade	Thermo Scientific
Taq DNA Polymerase (5 U/µl)	Bioron

25x Protease Inhibitor Mix:

cOmplete, EDTA-free Protease Inhibitor Cocktail	1 Tab.
dH_2O	2 ml

vortexed and stored at 4°C

6.1.10. Primary antibodies

Antigen	Host species	Number	Supplier	Dilution
α-SMA	mouse	M0851	Dako	1:100
CD31	rat	DIA-310	Dianova	1:20
F4/80	rabbit	70076S	Cell Signaling Technology	1:125
8-OHdG	mouse	15A3	Abcam	1:125

6.1.11. Secondary antibodies

Secondary antibodies fluorophore conjugated:

Host species	Target	Conjugate	Wavelength	Dilution	Number	Supplier
goat	mouse	Alexa Fluor 488	488 nm (green)	1:200	A-11029	Invitrogen
goat	mouse	Alexa Fluor 594	594 nm (red)	1:200	A-11032	Invitrogen

Secondary antibodies horse radish peroxidase conjugated:

Host species	Target	Conjugate	Dilution	Number	Supplier
goat	mouse	HRP	1:10000	401253	Merck Millipore
goat	rabbit	HRP	1:200/1:10000	401393	Merck Millipore
goat	rat	Micropolymer HRP	-	MP-7444	Vector Laboratories
rabbit	goat	HRP	1:10000	401515	Merck Millipore

6.1.12. Software

Software	Supplier
Adobe Photoshop CS3 Extended	Adobe Systems
Aperio ImageScope	Leica Biosystems
CellSens Dimension	Olympus
Excel	Microsoft
GraphPad PRISM Version 5	GraphPad Software
HP Precisionscan Pro	Hewlett-Packard
ImageJ	National Institutes of Health
ZEN 2.3 lite	Zeiss

6.2. Methods

Contents of this chapter have been submitted for publication [1].

6.2.1. Animal experiments

All animal procedures were performed in accordance with the European directive 86/609/EEC and approved by the local legislative committee for animal welfare (Government of Upper Bavaria, Munich, Germany) under the reference number AZ.55.2.1.54-2532-94-13 [1].

6.2.1.1. Nmf333 mouse line

A.B6 Tyr^{+}-Cyba^{nmf333}/J were originally obtained from Jackson Laboratories [1]. The p22phox-deficient mouse strain (nmf333 mice) carries a single point mutation in exon 5 of the CYBA gene located on chromosome 8 (coding for p22phox) which causes the substitution of the amino acid tyrosine (Y) to histidine (H) at position 121 (Fig. 3A) [1, 128]. This leads to Y121H, a missense mutation that can be identified by restriction digestion with Bsl1 restriction enzyme [128].

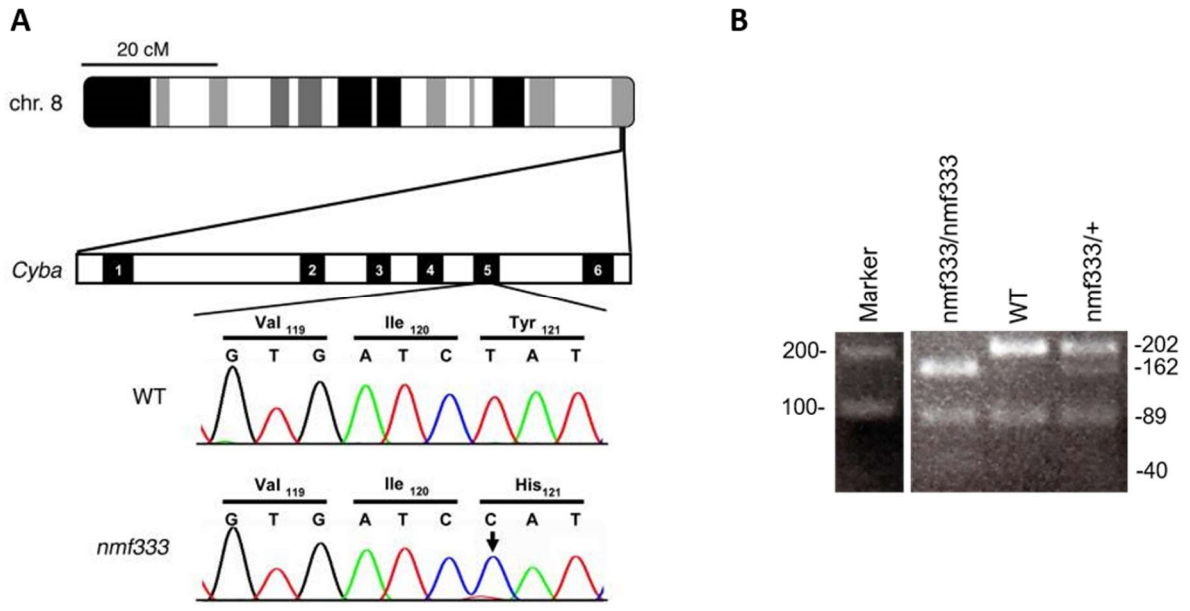

Figure 3. Missense mutation Y121H in the CYBA gene of the nmf333 mouse strain.
(A) The T to C point mutation (marked with arrow) causes the amino acid tyrosine (Y) to be replaced by histidine (H) at position 121 on exon 5 of the CYBA gene. Adapted after [128]. **(B)** Genotyping of nmf333 mouse strain: after digestion with restriction enzyme Bsl1 homozygous nmf333 (nmf333/nmf333) mice exhibit digestion products of 162 bp and 89 bp, WT mice show products of 202 bp and 89 bp, heterozygous nmf333 (nmf333/+) mice have 3 bands of 202 bp, 162 bp and 89 bp.

Genotyping results show WT alleles with digestion products of 202 bp and 89 bp. Homozygous nmf333 alleles exhibit products of 162 bp, 89 bp and 40 bp, the latter being not visible. Heterozygous nmf333 mice have three bands of 202 bp, 162 bp and 89 bp (Fig. 3B).

6.2.1.2. High-fat diet mouse models

Mice were held in individually ventilated cages under pathogen-free conditions under 12/12h cycle light/darkness with ad libitum access to water and food. Nmf333 mice were mated and pups were separated by gender and genotype at 3 weeks of age [1].

To investigate the dietary impact on the development of obesity and type 2 diabetes mellitus (T2DM) female, 5-week-old, nmf333 and wildtype (WT) mice consisting of nmf333 littermate controls and C57BL/6J mice (Charles River), were put either on normal-fat diet (NFD, 13% fat, 68% carbohydrates, 19% protein) or high-fat diet (HFD, ssniff EF D12492 (II), 60% fat, 21% carbohydrates, 19% protein) for 20 weeks [1].

At 25 weeks of age (20 weeks of diet) mice were mated with males of the appropriate genotype which were kept on NFD, and achieved pregnancy within 3-5 weeks. Pregnant mice were sacrificed at gestational day (GD) 17.5 and fetuses were extracted [1].

6.2.1.3. Measurements

6.2.1.3.1. Body mass

Starting from the age of 5 weeks the body mass (BM) for all mice was determined bi-weekly during the course of the experiment [1].

6.2.1.3.2. Nasal-anal lengths

At the age of 25 weeks the nasal-anal length (NAL) was measured using a digital caliper in order to determine the body length [1].

6.2.1.3.3. Body mass index

Body mass index (BMI) was calculated using the formula [1]:

$$BMI = \frac{BM\ (g)}{NAL\ (cm)^2}$$

6.2.1.3.4. Lee's index of obesity

Lee's index of obesity (LIO) was calculated according to the formula described by Simson et al. [1, 129]:

$$LIO = 10^4 \times \frac{\sqrt[3]{BM\ (g)}}{NAL\ (mm)}$$

6.2.1.3.5. Blood glucose levels

Starting from the age of 5 weeks, blood glucose levels were measured every two weeks [1]. For that, mice were fasted for 6 h. Then the tip of the tail was cut, the resulting blood drop was collected with a glucose test strip and the glucose level was determined by a glucose meter.

6.2.1.3.6. Intraperitoneal glucose tolerance test

At the age of 5, 15 and 25 weeks as well as at gestational day 10, mice were fasted for 6 h, and intraperitoneal glucose tolerance tests (ipGTT) were performed [1]. In brief, a glucose solution of 0.9 g of glucose was dissolved in 5 ml of distilled water (0.18 mg/µl) and filtrated. After fasting 1.5 mg/g (body mass) glucose was intraperitoneally injected. Glucose levels were measured at time points 0, 20, 40, 60, 80, 100 and 120 min after the injection by a glucose meter.

6.2.1.3.7. Intraperitoneal insulin tolerance test

Intraperitoneal insulin tolerance tests (ipITT) were performed as previously described [1, 130]. 23-weeks-old mice were fasted for 4 h. After fasting, 0.5 U/kg BM insulin (Insuman Rapid) were intraperitoneally injected. Glucose levels were measured by a glucose meter at time points 0, 10, 20, 30, 40, 50, 60, 70, 80 and 90 min after injection.

6.2.1.4. Euthanasia

At the experimental end points mice were euthanized using carbon dioxide (CO_2) exposure followed by cervical dislocation.

6.2.1.4.1. Organ removal

After blood withdrawal the vascular system was flushed with 1x PBS solution in order to clear vessels from remaining blood clots [1].

The following paragraph has not been submitted for publication.

The right lobe of the liver was partly incised. Then, the left ventricle was punctured and 1x PBS solution was injected until the liver tissue visibly brightened. Eventually organs, i.e. liver, pancreas, kidneys, spleen, white and brown fat were collected. They were primarily detached from excess fat or connective tissue and then put on the analytical balance for determining the organ mass. Afterwards, organs were washed in PBS, carefully wiped off excessive fluid and divided into sections. For histology, specimens were either placed in tissue embedding cassettes and kept 48 hours in 4% formalin solution, or put in cryomolds filled with the O.C.T/Sucrose solution, gradually frozen in a Styrofoam containing liquid nitrogen and stored at -20°C.

6.2.1.4.2. Dissection of placenta and fetus

The following sections have not been submitted for publication.

Prior to dissection of the abdominal organs the uterus containing the fetuses was taken out and put in PBS to wash off blood and secretions. The total number of living and dead fetuses was counted. Dead fetuses were identified by notably smaller size or black discoloration compared to living fetuses (Fig. 4) [131]. After transferring the uterus to a clean Petri dish filled with PBS, the uterus was opened using a bonn artery scissor with the ball tip facing the fetus in order to avoid destruction of the fragile skin.

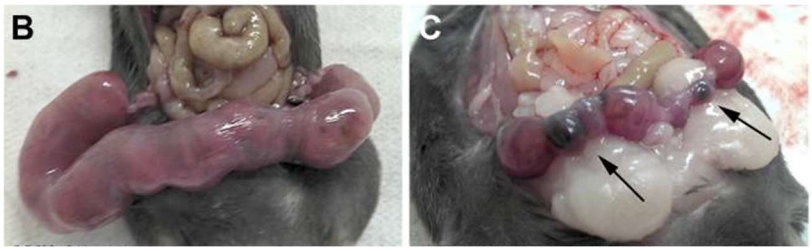

Figure 4. Living and dead fetuses.
Dead fetuses (marked with black arrows) can be distinguished from living ones by notedly smaller size and black discoloration. Adapted after [131].

Since fetuses and placentas were still surrounded by the yolk sac, the latter was removed by gently pulling with forceps. Placentas were separated from fetuses by cutting through the umbilical cord and the placental mass was measured. Placentas were eventually prepared for

either histology, cryopreservation or molecular analysis as described in the section above. Fetuses were put in a clean Petri dish. The umbilical cord was teared through above the umbilicus. Fetuses were washed in PBS, gently wiped off excessive fluid and balanced. Parts of the fetuses were processed for histology and cryopreservation. For molecular analysis fetal hearts and livers were dissected. Therefore, fetuses were put in an empty Petri dish. The fetal body was opened via median incision using the Leica MZ7.5 stereomicroscope. Access to the inner thorax was enabled through median sternotomy and the heart was dissected. The abdomen was opened by median laparotomy. After extracting the liver, the gallbladder was removed. Hearts and livers were put in tubes, immediately frozen in liquid nitrogen and stored at -80°C.

6.2.2. Histology

6.2.2.1. Tissue processing

Dissected tissues designated for histology were processed either for formalin-fixed paraffin-embedding or cryofixation depending on the intended staining methods. Since formalin fixation and dehydration required for paraffin embedding eliminate certain structures, such as adipocytes and lipid droplets [132], special processing techniques for visualizing e.g. lipids are needed.

6.2.2.1.1. Formalin fixation

Formalin-fixed paraffin-embedding is a standard procedure used in histology. Tissues need to be fixated and dehydrated since paraffin wax is not soluble in water or alcohol. Therefore, the paraffin solvent xylene is used. After dehydration, tissues are embedded in paraffin and cut into micron thin sections. Before staining, rehydration of the tissue is necessary, since most of the dyes used are aqueous.

Specimens were put in embedding cassettes and immersed in 4% formalin solution for 48 hours at 4°C. Afterwards the solution was replaced with 70% ethanol and kept at 4°C until dehydration [1]. Embedding cassettes were put in the metal basket provided by the dehydration machine. Dehydration was performed using a descending series of alcohol consisting of one change of 70% isopropyl alcohol, two changes of 80% isopropyl alcohol, two changes of 96% isopropyl alcohol, three changes of 100% isopropyl alcohol, two changes of the isoparaffinic-based xylene substitute Clear-Rite 3 and two changes of fluid paraffin.

After dehydration, cassettes were retrieved and warmed alongside differently sized metal molds on the paraffin embedding station. Specimens were extracted from the embedding cassettes and placed in the center of the metal molds. The molds were filled with liquid paraffin, avoiding formation of air bubbles. Subsequently, molds were put on a cooling plate (-5°C), allowing hardening of the paraffin and thereby fixing of the tissue. The labeled cassettes were then placed on top, the molds were filled up with liquid paraffin without thawing and carefully put back onto the cooling plate. After a while, paraffin blocks containing the specimens were carefully detached from the metal molds and stored at 4°C.

For sectioning, formalin-fixed paraffin-embedded (FFPE) specimens were cut using the microtome HM 355S (Thermo Fisher Scientific) [1]. The paraffin blocks were fixed with the clip. Trimming was performed until tissues were visible. Then, micron thin sections were cut by smoothly turning the crank handle, thereby preventing fissure or curling. Depending on the embedded tissue, thickness of the sections varied from 2 to 5 µm. Cut sections remained on the metal support and were transferred into dH_2O blended with a lacing of 90% ethanol, using an object slide. Subsequently, sections were converted into a warm water bath (40°C) enabling expansion and smoothing of the paraffin on the water surface. Next, paraffin sections were carefully transferred onto the object slide and put on the tub rim to air-dry. After a few minutes specimen holders were placed on a heating table (42°C) allowing condensation. The object slides were dried for 24 hours and stored at 4°C.

Before staining, FFPE sections were cleared of paraffin. For this rehydration process sections were incubated at 55°C overnight to melt the paraffin. Then, sections were immersed in xylene and descending alcohol concentrations as specified in the respective paragraphs. For section preservation, tissue specimens were dehydrated using ascending alcohol concentrations and xylene, enabling mounting with a resinous mounting medium. The latter was applied on the coverslip which was carefully placed on the object slides, avoiding formation of air bubbles. The glass slides were left to dry overnight, cleaned of excessive mounting medium and stored at room temperature (RT).

6.2.2.1.2. Cryofixation

Since formalin fixation and dehydration cause deterioration of adipocytes and lipid droplets, another fixation method for lipid analysis was used.

Labelled cryomolds were filled with O.C.T/20% sucrose compound [1] and tissue specimens of placenta and fetus were put in the center. Molds were placed on a styrofoam panel and gradually frozen with liquid nitrogen [1]. Specimens were stored at -20°C.

For sectioning, the cryostat Leica CM 1850 (Leica Biosystems) was used with working temperatures of -20°C [1]. Frozen tissue blocks were unhinged from the ductile cryomolds and mounted on metal stamps using Tissue-Tek O.C.T compound. Stamps were placed in the cryostat to allow hardening of the O.C.T compound. After solidification stamps were fixed in the holding device. The cutting routine was overall similar to FFPE sectioning. However, sections were much thicker, ranging from 10 to 12 µm, and were only cut to the upper margin so that the sections were loose but not detached from the block. They were directly transferred onto object slides. After air-drying for about 10 minutes, object slides were stored at -20°C.

6.2.2.2. Staining

Bright-field images were captured using Zeiss Axioscope 2 light microscope, or scanned with Leica Aperio AT2 digital slide scanner [1]. For digital processing and quantification ImageJ, a Java-based image processing and analysis program was used. Fluorescence stainings were analyzed using Olympus IX83 inverted microscope and Olympus cellSens software.

6.2.2.2.1. Immunohistochemical staining

FFPE sections were rehydrated through two changes of xylene, 100% ethanol and 96% ethanol, respectively, and one change of 70% ethanol, each spanning 5 min. Sections for fluorescence detection were subsequently washed in running tap water for 2 min, whereas those for chromogenic detection were washed in two changes of PBS (5 min each).

Heat-induced epitope retrieval (HIER) was performed for antigen retrieval. For that, sections were immersed in either citrate antigen retrieval buffer (pH 6.0) or EDTA antigen retrieval buffer (pH 8.0 or pH 9.0) depending on the primary antibody (see table below), and cooked in a microwave for several minutes at 750 W to the boiling point. The procedure was repeated up to a total boiling time of 20 min.

Primary antibody	HIER antigen retrieval buffer
α-SMA	EDTA pH 8.0
CD31	Citrate pH 6.0
F4/80	Citrate pH 6.0
8-OHdG	T-EDTA pH 9.0

In this study two different methods – fluorescence and chromogenic detection – for detecting bound antibodies were used:

1. Visualization by fluorescence detection by using fluorophore-conjugated secondary antibodies:

Fluorophores have excitation and emission spectra of certain wavelengths enabling simultaneous incubation of multiple fluorophore-conjugated secondary antibodies on one section since they can be extinguished by their individual excitation wavelength. Counterstaining of nuclei was performed using Hoechst 33342, a fluorescent stain for nucleic acids. It emits cyan-colored light at an excitation/emission wavelength of 361/497 nm.

Immunofluorescence stainings were performed as follows [1]:

After establishing liquid barriers, sections were washed by sequential immersion in: 1x PBS, followed by 0.2% Triton X-100 in 1x PBS and again in 1x PBS for 5 min. Then, sections were blocked with 3% BSA dissolved in 1x PBS for 2 h at RT. Afterwards, sections were drained from excessive BSA and were incubated with the primary antibody in a humid chamber overnight at 4°C. The primary antibody was diluted in PBS as stated below:

Primary antibody	Dilution
α-SMA	1:100
8-OHdG	1:125

The next morning, sections were consecutively washed in 1x PBS, followed by 0.2% Triton X-100 in 1x PBS and again in 1x PBS for 5 min in order to clean specimens of excessive primary antibody solution. Sections were then incubated with the corresponding secondary antibody at a dilution of 1:200 for 2 h in a humid chamber at RT, followed by three washing steps with 1x PBS for respectively 2 min. Counterstaining of nuclei was performed by incubating sections with Hoechst 33342 diluted 1:10.000 for 1 min at RT. After three washing steps with 1x PBS for 2 min each, object slides were mounted with DAKO mounting medium and coverslips, sealed with nail-polish and stored at 4°C in the dark.

2. Visualization by chromogenic detection by using DAB (3,3'-diaminobenzidine), a horseradish peroxidase substrate [133]:

For this detection method the Liquid DAB + Substrate Chromogen System by Dako was used [1].

After HIER, sections were left in the retrieval buffer for 10-15 min to cool down and washed in 1x PBS for 3-4 min. Peroxidase blocking was performed in 3% H_2O_2 diluted in 1x PBS for 10 min followed by two washing steps with 1x Dako wash buffer for 5 min. After establishing the liquid barriers, sections were incubated for 2 h at 4°C with the primary antibody diluted in 1x PBS as follows:

Primary antibody	Dilution
CD31	1:20
F4/80	1:125

Then, sections were again washed with 1x Dako wash buffer in two washing steps of 5 min, followed by incubation with the secondary antibody in a dilution of 1:200 for 2 h at RT. After two washing steps in 1x Dako wash buffer, sections were incubated with DAB for approximately 3-5 min until a brown color change could be observed. Object slides were then quickly submerged in dH_2O to stop the reaction and subsequently washed under running tap water for 3 min. Counterstaining was performed with Mayer's Haematoxylin for 30 s followed by bluing under running tap water for 5 min. Sections were mounted with Aquatex and coverslips, and left to air-dry.

6.2.2.2.2. 8-Hydroxy-2'-deoxyguanosine staining

FFPE liver sections (4 µm) as well as placenta and fetus sections (2 µm) were stained with an antibody against 8-hydroxy-2'-deoxyguanosine (8-OHdG) and quantified by capturing 4 image sections of 40x magnifications using Olympus IX83 inverted fluorescence microscope [1]. Multichannel images (DAPI, GFP Slider, CY5) were exported as .tif files and analyzed with ImageJ [1]. The image analysis was performed using an automated protocol executed by a macro according to Guirado et al. [1, 134]. For that, images were split into four equal parts (see Appendix B 10.1). Then, the area of nuclei was selected on the DAPI (blue) image and the selection was used on the GFP Slider (green) image to measure the intensity (mean gray value) of the selected area (see Appendix A Fig. 1 and Appendix B 10.2).

6.2.2.2.3. Alpha-smooth muscle actin staining

FFPE placenta sections (2 µm) were cut lengthwise in order to assess the placental labyrinth as a whole and stained with an antibody against alpha-smooth muscle actin (α-SMA). For quantification, 4 image sections of 10x magnification were captured using the fluorescence microscope [1]. Multichannel images (DAPI, GFP Slider) were exported as .tif files and analyzed with ImageJ using the macro described by Guirado et al. [1, 134]. Images were split into four equal parts and quantification was performed on GFP Slider images (see Appendix B 10.3). Integrated density, which is the product of area and mean gray value, was measured for the images, respectively.

6.2.2.2.4. F4/80 staining

FFPE liver sections (5 µm) were stained with an antibody against F4/80. To quantify the amount of antibody-bound antigen, 10 bright-field images of 20x magnifications were captured [1]. Image analysis was performed with ImageJ's color threshold [1]. Hue, saturation and brightness were adjusted to the brown reaction sites and respective area values within the set threshold were measured (see Appendix A Fig. 2).

6.2.2.2.5. Wheat germ agglutinin staining

The following paragraph has not been submitted for publication.

For delineation of cell membranes, FFPE placenta cross sections (2 µm) were stained with Rhodamine labelled wheat germ agglutinin (WGA). Rhodamine is a conjugated fluorophore with an excitation/emission maximum of 550/575nm, making it appear red when observed through a fluorescence microscope. The nuclei were visualized with DAPI (1:10000) staining [135]. WGA quantification was performed by taking 4 fluorescence image sections of 40x magnifications. Multichannel images (DAPI, CY5) were exported as .tif files and analyzed with ImageJ according to Guirado et al. [134]. Therefore, images were first split into four equal parts and the automated analysis was performed on CY5 images (see Appendix B 10.4). Mean gray values was measured for all images.

6.2.2.2.6. Hematoxylin-Eosin staining

Hematoxylin-Eosin (H&E) staining of FFPE liver (3.5 µm) and FFPE placenta (2µm) cross sections were analyzed with regard to general morphology [1]. Liver sections were analyzed for necrotic spots and lipid droplets. The H&E stain combines two dyes, namely haematoxylin and eosin. Haematoxylin is a cationic basic dye of deep purple-blue color. Application of haematoxylin to FFPE sections results in blue stains of basophilic structures, such as nuclei, endoplasmic reticulum and ribosomes, since they have an affinity for basic dyes. Eosin on the other hand is an acidic dye of red-pink color and stains proteins, resulting in pink cytoplasm and extracellular matrix [136]. For H&E staining FFPE sections were rehydrated through two changes of xylene, 100% ethanol and 96% ethanol, respectively, and one change of 70% ethanol, each spanning 5 min. The descending series of alcohol was followed by two washing steps with dH_2O for 2 min. Subsequently, FFPE sections were immersed in Mayer's Haematoxylin for 15 min. Sections were then blued in lukewarm running tap water for 5 min, followed by immersion in 0.5% acidified aqueous eosin solution for 3 min. After three washing steps in dH_2O for 1.5 min each, sections were dehydrated in 70 % ethanol, two changes of 96% ethanol and 100% ethanol for 1 min, respectively. Sections were immersed in two changes of xylene for 3 min, mounted with Entellan® and coverslips, and left to air-dry overnight. The number of necrotic spots was counted for 10 bright-field image sections in 10x magnifications. For quantification of lipid droplets, 10 frames with 20x magnifications were captured. Measurement of the area values was performed with ImageJ. The obtained RGB image was split into three color channels. Analysis was conducted on the green channel image exhibiting the highest contrast. For each biological replicate the threshold was set according to the extent of lipid droplets (see Appendix Fig. 3).

6.2.2.2.7. Picrosirius Red staining

Sirius Red is a strong anionic dye which is able to stain collagen by reacting with its sulphonic acid groups. It is one of the few dyes able to solely stain collagen fibers in tissue [137]. For assessing fibrosis, the amount of stained collagen was analyzed in FFPE liver cross sections (3.5µm). FFPE tissues were stained according to the protocol by Candace Adamo, Griendling Lab [1, 138]. Picrosirius Red solution and acidified water were prepared one day prior to staining (see 6.1.8.2) [1]. Rehydration was conducted through three changes of xylene of 5 min, followed by two changes in 100% ethanol, one in 96% ethanol, 90% ethanol and 80% ethanol, respectively, each spanning 2 minutes. Sections were then washed in dH_2O for 2 min and

immersed in Picrosirius Red solution for 1 h. After staining, sections were washed twice in acidified water for 2 min, respectively. After removing excessive water, specimens were immersed in three changes of 100% ethanol (1 min each) and two changes of xylene (3 min each). Sections were mounted with Entellan® and coverslips and left to air-dry overnight. 10 bright-field image frames with 20x magnifications were acquired and the amount of collagen was measured via ImageJ's color threshold function [1]. Hue, saturation and brightness were adjusted to the red fibers and respective area values within the set threshold were measured (see Appendix A Fig. 4).

6.2.2.2.8. Periodic acid–Schiff reaction

Periodic acid–Schiff (PAS) reaction was used to detect glycol-conjugates in tissues. FFPE liver (5 µm) and placenta (3.5 µm) cross sections were stained using the PAS Staining Kit (Carl Roth) [1]. The staining solutions were filtrated before use. Counterstaining of cell nuclei was ensured using acidic Hemalum® solution according to Mayer provided by the kit. De-waxing and rehydration of the sections was performed as described in 6.2.2.2.6. Sections were immersed in 1% periodic acid solution for 10 min and washed using tap water (10 min) and two changes of dH_2O (each 2 min). Next, sections were immersed in Schiff's reagent at RT for 20 min. After rinsing in warm tap water (>35°C) for 5 min and dH_2O for 1 min, counterstaining was performed using Hemalum® solution according to Mayer. Sections were blued in running tap water for 15 min. Dehydration and preservation were done as described in 6.2.2.2.6. For automated PAS reaction analysis, 10 bright-field images in 20x magnifications of liver and placenta sections were taken, the latter comprising decidua basalis and decidua-labyrinth intersection [1]. PAS-positive areas of the liver were measured using the color threshold function in ImageJ (see also Appendix B 10.5) [1]. Color threshold values for automated placenta analysis were set in comparison to the labyrinth region which does not hold glycol-conjugates and thus exhibits no PAS reaction. Respective area values were determined for the set color threshold.

6.2.2.2.9. Oil Red O staining

For lipid analysis, Oil Red O staining was performed on frozen sections [1]. Stock and working solutions were prepared according to Mehlem et al. [1, 139]. Placenta and fetus cryosections (12 µm) were equilibrated to RT for 10 min. Tissue sections were incubated with Oil Red O solution for 5 min. Counterstaining was performed by immersing sections with Mayer's

Haematoxylin for 15 s. Sections were dipped 3x in lithium solution and rinsed under running tap water for 30 min. Sections were mounted with Aquatex and coverslips, left to air-dry for 10 min and sealed with nail polish. Bright-field images were taken within 24 h to prevent precipitation of the dye thereafter. 10 image sections were captured in 40x magnifications per biological replicate [1]. Using ImageJ hue, saturation and brightness in the color threshold were set to best match the stained lipid droplets when compared with the original image (see Appendix A Fig. 5 and Appendix B 10.5) [1]. Results were obtained by measuring the area values of the selected regions within the threshold.

6.2.3. Molecular biological techniques

The following subchapters have not been submitted for publication.

6.2.3.1. Genomic DNA extraction

Genomic DNA was extracted from mouse ears according to the manufacturer instruction. Ears were dissolved in 500 µl of lysis buffer containing 15 µl of 20 mg/ml proteinase K. Samples were incubated overnight at 56°C in an Eppendorf thermomixer. The next day 250 µl of 5 M NaCl was added to the lysates and solutions were thoroughly mixed. Samples were spun down at 13.000 rpm for 15 min at RT and 600 µl of the top phases were immediately transferred into new tubes. After adding 400 µl isopropanol to each tube, solutions were mixed by inversion and again spun down at 13.000 rpm for 15 min at RT. The supernatants were carefully removed by aspiration. The DNA sediments were subsequently washed with 1 ml of 70% ethanol kept at RT, mixed by inversion and spun down at 13.000 rpm for 10 min at RT. Supernatants were removed as completely as possible and DNA pellets were left at RT to air-dry for up to 1 h. Finally, the latter were dissolved in 50 µl 0.1x TE buffer by incubating at 37°C for 10 min while gently shaking and stored at -20°C for later analysis.

6.2.3.2. Polymerase chain reaction

Polymerase chain reaction (PCR) was performed using a Thermocycler GeneAmp PCR System 9700 following our laboratory's standard protocol. 25 µl reaction volume consisted of:

	[µl]
H_2O	18.25
10x buffer with $MgCl_2$	2.5
dNTPs (10 mM)	0.25

Primer-F (10 µM)	0.25
Primer-R (10 µM)	0.25
DMSO	1.0
Taq (5 U/µl)	0.5
DNA	2

The PCR reaction program was set as follows:

Denaturation	94 °C	05:00 min

40 cycles:

Denaturation	94 °C	00:30 min
Annealing	59 °C	01:00 min
Extension	72 °C	01:00 min

Final phase:

Extension	72 °C	07:00 min

Termination:

Cooling	4 °C	∞

The PCR product was stored at 4 °C.

Digestion of the PCR product with BslI restriction enzyme

The digestion mix (20 µl sample volume) was prepared as listed below and incubated at 55°C overnight.

	[µl]
NEB buffer 3	2
Bsl1	0.5
H_2O	2.5
PCR product	15

6.2.3.3. Gel electrophoresis

In order to visualize the digested PCR products, gel electrophoresis was performed according to our laboratory's standard protocol. Ethidium bromide was used as a dye. The resulting DNA bands were visualized using UV light.

The digestion mix was run on a 3% agarose gel. For that 3.0 g of agarose was mixed with 100 ml of 1x TAE buffer in an Erlenmeyer flask and boiled in the microwave until the solution

became clear. Evaporation was compensated by adding dH_2O. Then 5 µl of ethidium bromide was added and the solution was mixed by carefully slewing the flask. The agarose solution was poured into a plastic tray and assembled with the loading comb. After polymerization for 30 min at RT, the comb was removed and the solid gel was transferred into the electrophoresis chamber and submerged with 1x TAE buffer. 2 µl of orange loading buffer were added to the PCR products. Subsequently, the wells were loaded and 5 µl of Quick-Load 100bp DNA Ladder were used as a marker. After connection of the electrodes, gels were run for about 60 min at 90 V and monitored by observing the loading buffer. DNA bands were visualized using the UV camera Gel Doc 2000 and Quantity One software.

6.3. Statistics

The following paragraph has been submitted for publication [1].

Statistical analyses were performed using Prism5 (GraphPad Software, version 5.01) and Microsoft Excel 2019. Data are expressed as means with standard deviation (s.d.), or standard error of the mean (s.e.m.). Outliers were excluded from the data sets by quantification of z-scores. One-way or two-way analysis of variance (ANOVA) were used for comparisons between multiple groups, followed by Tukey's multiple-comparisons test or Bonferroni test. Differences were considered significant when $p < 0.05$.

7. Results

Data, contents and parts of the following subchapters have been submitted for publication [1] unless otherwise stated.

7.1. Effects of high-fat diet on metabolism

7.1.1. p22phox promotes high-fat diet-induced obesity

In this study, the role of the NADPH oxidase subunit p22phox in fetal survival was evaluated in a model of maternal obesity and type 2 diabetes mellitus (T2DM) [1]. Therefore, 5-weeks-old female wild type (WT) and nmf333 mutant mice lacking functional $p22^{phox}$ due to a point mutation in the CYBA gene [128] were fed with a high-fat diet (HFD, 60% kcal fat) for 20 weeks. Controls chowed normal-fat diet (NFD, 13% kcal fat).

Following 20 weeks of HFD feeding, WT HFD mice showed an increase in body mass index (BMI) as well as in Lee's index of obesity (Fig. 5A/B) [1].

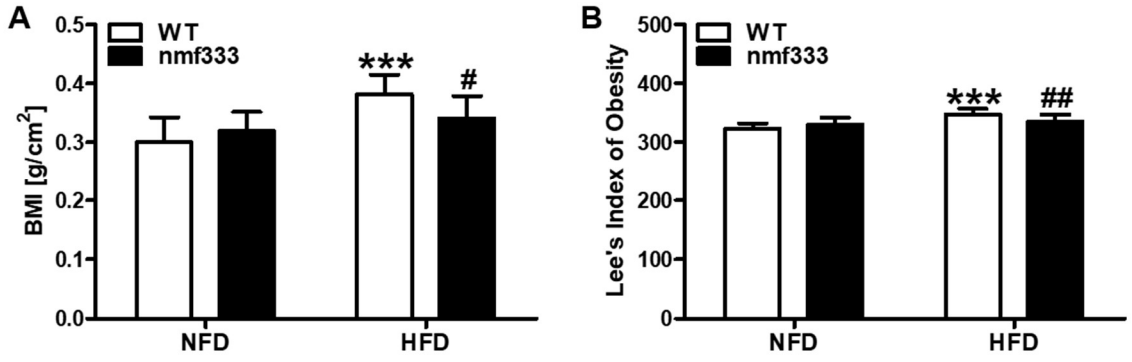

Figure 5. p22phox promotes HFD-induced obesity and visceral adiposity [1].
(A-B) 5-weeks-old wild type mice (WT) and mice deficient of p22phox due to a point mutation in the CYBA gene (nmf333) were HFD fed for 20 weeks. Controls received NFD. Body masses and nasal-anal lengths were measured at age 25 weeks, and: **(A)** body mass index (BMI) and **(B)** Lee's index of obesity were calculated. Data are means ± s.d., n = 16-21, ***p < 0.001 WTNFD vs. WTHFD, #p < 0.05, ##p < 0.01 WTHFD vs. nmf333HFD by one-way ANOVA and Tukey's multiple-comparisons test.

7.1.2. p22phox promotes high-fat diet-induced glucose intolerance and insulin resistance

Since obesity is linked to the development of T2DM in experimental rodent models and human subjects [140-143], glucose tolerance, intrinsic blood glucose levels and insulin resistance were assessed in all mice groups during the 20-week HFD feeding (Fig. 6) [1].

Glucose tolerance was assessed by intraperitoneal glucose tolerance test (ipGTT) at weeks 10 (Fig. 6A) and 20 (Fig. 6B) of diet [1]. At week 10 of HFD, the WT HFD group had significantly higher blood glucose values compared to NFD control littermates starting from 20 min after i.p. glucose injection, while the nmf333 HFD group had values comparable to NFD control mice (Fig. 6A). Interestingly, although glucose values were higher in WT HFD mice, the recovery curve of blood glucose levels was shaped similarly to the curves of the other groups, practically reaching the same end-point at 120 min (Fig. 6A). However, ipGTT performed at week 20, showed higher blood glucose values in WT HFD mice at 20 min and slower recovery curves with blood glucose levels not reaching the basal values even at 120 min pointing to fully developed glucose intolerance, a feature missing in NFD controls and nmf333 HFD mice (Fig. 6B).

To substantiate the observed impaired glucose metabolism in HFD, intrinsic blood glucose levels were determined bi-weekly after 6 h of fasting (Fig. 6C) [1]. Although intrinsic blood glucose levels after 6 h starvation showed a tendency to increase within the first 4 weeks of HFD feeding, a significant increase was observed in WT HFD mice compared to NFD controls starting at week 12 of HFD (Fig. 6C). From week 14 of HFD a significant decrease in fasting blood glucose levels of nmf333 HFD mice compared to WT HFD littermates was observed, pointing to a role of p22phox in the regulation of blood glucose levels in the HFD/obesity model (Fig. 6C).

Next, insulin resistance was evaluated by intraperitoneal insulin tolerance test (ipITT) at 18 weeks of HFD (Fig. 6D) [1]. WT HFD mice showed an increase in blood glucose levels already 70 min after insulin injection compared to WT NFD mice, while blood glucose levels remained low in the nmf333 HFD group, suggesting a role of p22phox in insulin resistance following HFD (Fig. 6D).

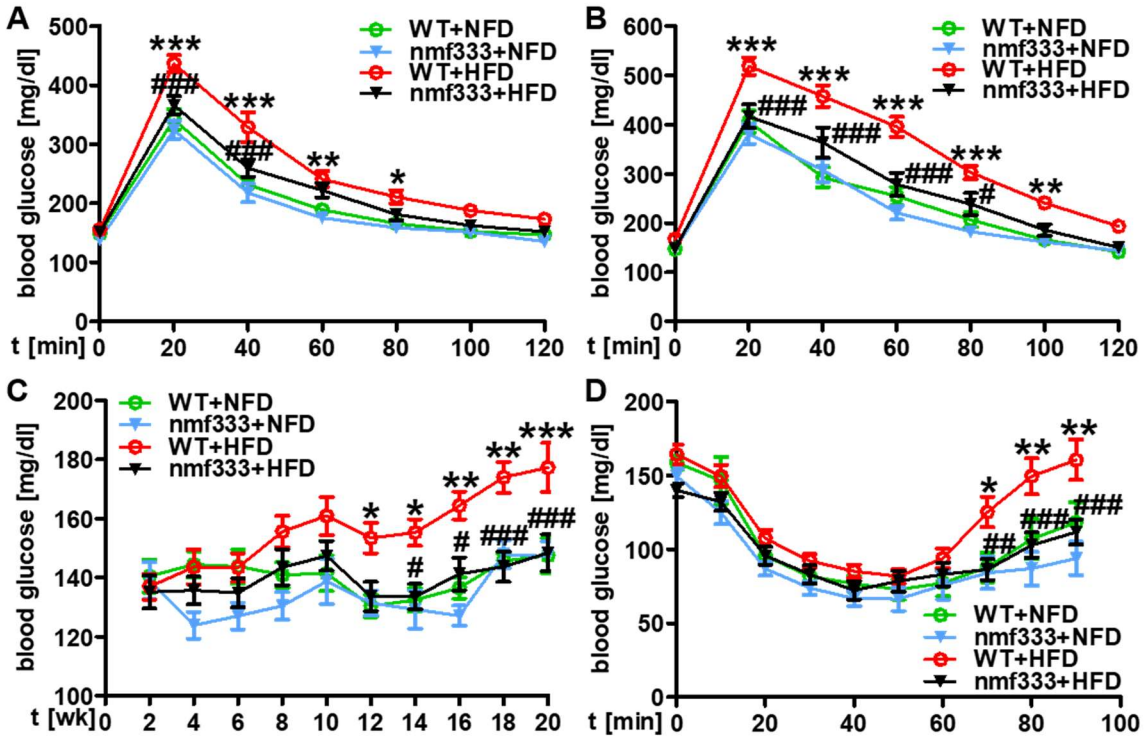

Figure 6. p22phox promotes HFD-induced glucose intolerance and insulin resistance [1]. **(A-D)** 5-weeks-old WT and nmf333 mice were fed a HFD for 20 weeks. Dietary control mice received NFD. **(A/B)** Intraperitoneal glucose tolerance tests (ipGTTs) were performed at **(A)** 10 and **(B)** 20 weeks of HFD after 6 h of fasting. **(C)** Intrinsic blood glucose levels were measured after 6 h of fasting bi-weekly starting from 2 weeks of HFD. **(D)** Intraperitoneal insulin tolerance test (ipITT) was performed at 18 weeks of HFD. Mice were fasted for 4 h. Data are means ± s.e.m., n = 20-23, *p < 0.05, **p < 0.01, ***p < 0.001 WTNFD vs. WTHFD, #p < 0.05, ##p < 0.01, ###p < 0.001 WTHFD vs. nmf333HFD by two-way ANOVA and Bonferroni posttest.

7.2. Effects of high-fat diet on pregnant mice

7.2.1. p22phox promotes high-fat diet-induced glucose intolerance in pregnant mice

Following 20 weeks of HFD (or NFD) 25-weeks old female mice were mated with age-matched males of the same genotype (Fig. 7) [1]. It took on average 3-5 weeks to achieve pregnancy; having, hence, experimental end-points at approximately 28-30 weeks of age (Fig. 7).

As shown in Fig. 5 and 6, WT HFD mice had by week 20 of feeding an increased BMI and elevated Lee's index of obesity, increased glucose intolerance and insulin resistance, showing a fully developed T2DM clinical picture [1].

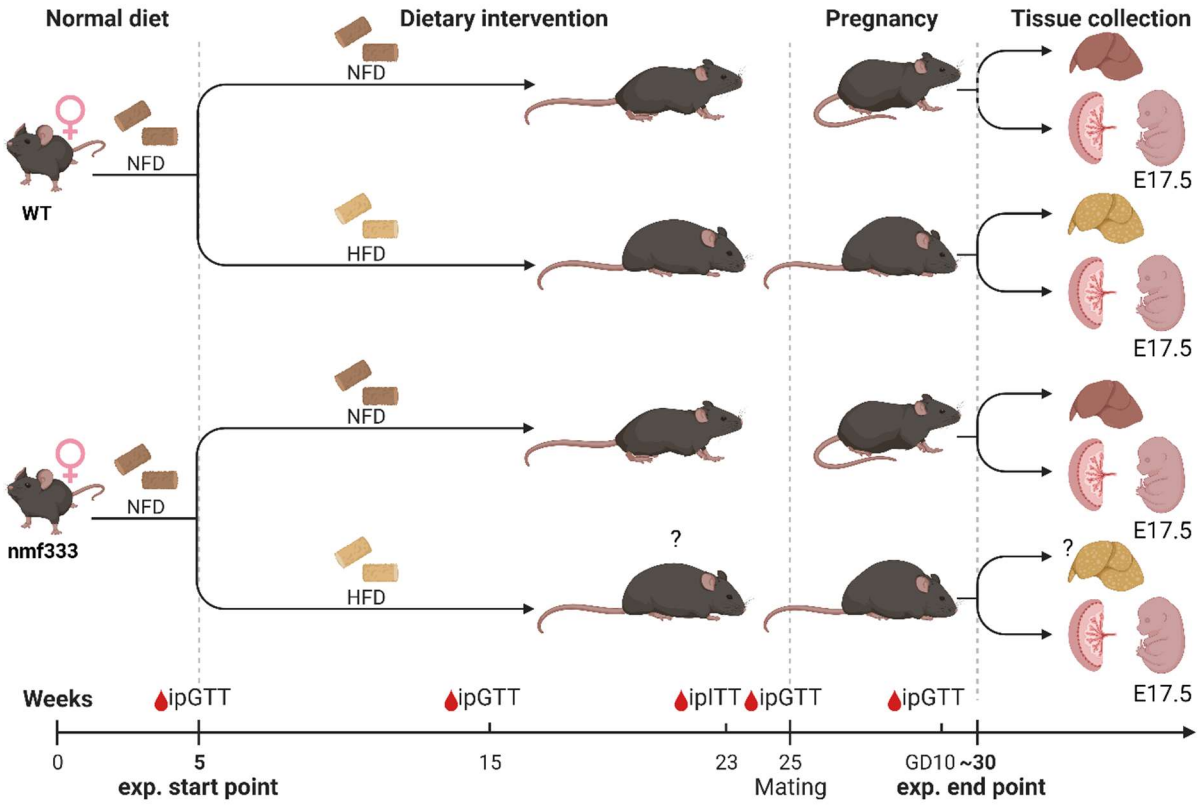

Figure 7. Experimental design [1].
5-weeks-old female WT and nmf333 mice were put on a HFD for 20 weeks. Dietary control mice received NFD. Over the course of the diet metabolic measurements were performed at different time points. At age 25 weeks mice were mated and kept on continuous diet during pregnancy. Mice were dissected at GD17.5 and organs were retrieved. Created with Biorender.com.

Therefore, we analyzed glucose intolerance during pregnancy by means of ipGTT at GD10 [1]. Similar to the situation before pregnancy, glucose intolerance was significantly higher in WT HFD mice compared to WT NFD, but also to nmf333 HFD (Fig. 8A). Compared to the ipGTT performed at 20 weeks of HFD before pregnancy, glucose tolerance was not significantly different at GD10 in any of the groups (Fig. 8B/C).

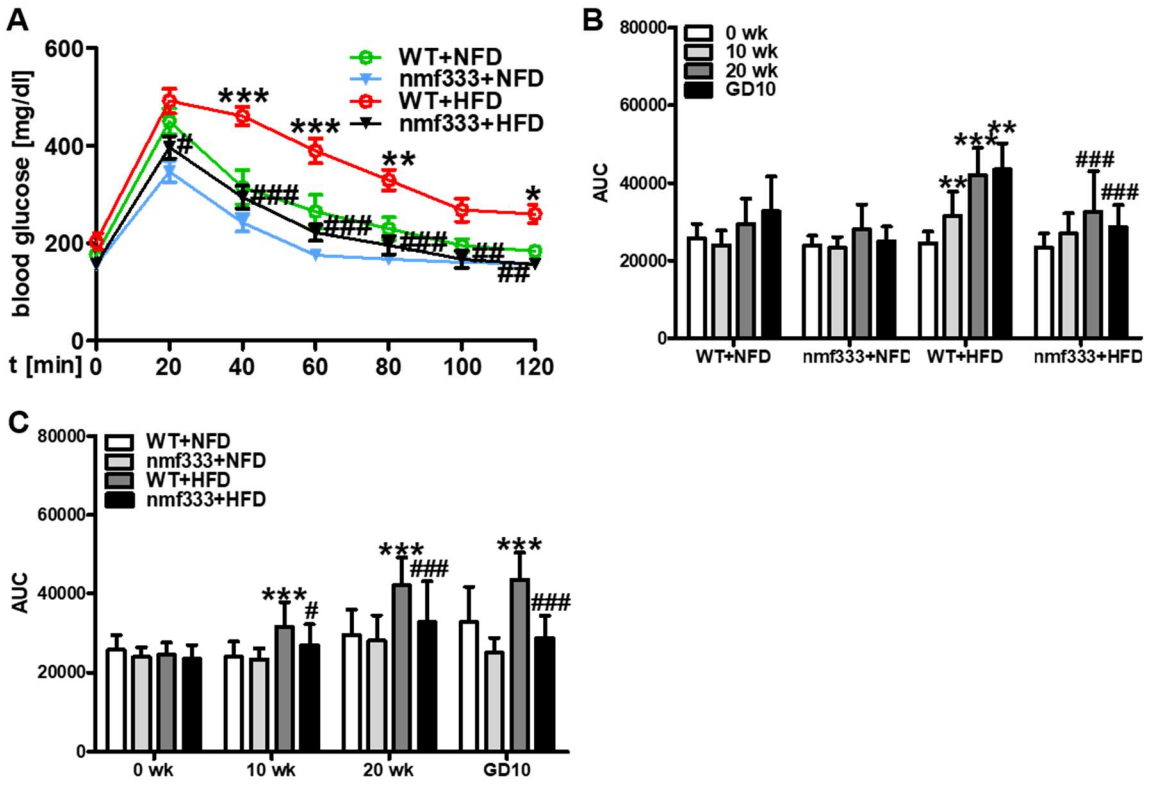

Figure 8. p22phox sustains HFD-induced impaired glucose tolerance during pregnancy [1]. **(A-C)** 5-weeks-old WT and nmf333 mice were fed a HFD for 20 weeks. Dietary controls were fed with NFD. Mice were mated starting from 25 weeks age and kept on continuous diet during the course of pregnancy. **(A)** ipGTTs were performed at gestational day 10 (GD10) after 6 h of fasting. **(B/C)** Area under the curve (AUC) values are displayed. Data are means ± s.d., n = 8-11, *p < 0.05, **p < 0.01, ***p < 0.001 WTNFD vs. WTHFD, #p < 0.05, ##p < 0.01, ###p < 0.001 WTHFD vs. nmf333HFD by two-way ANOVA and Bonferroni posttest test.

7.2.2. p22phox induces white fat deposition, liver and spleen enlargement in response to high-fat diet

When organ masses were evaluated, visceral white adipose tissue showed increased accumulation in pregnant (GD17.5) WT HFD mice compared to NFD controls, but partial reduction in HFD fed nmf333 mice (Fig. 9A) [1]. Furthermore, livers of WT HFD mice were significantly heavier than those of NFD mice and nmf333 HFD mice (Fig. 9C) [1].

The following paragraph has not been submitted for publication, thus contains new data.

The amount of brown adipose tissue retrieved from the interscapular spine did not differ between the groups (Fig. 9B). Pancreas masses seemed to be decreased in HFD fed WT mice, however, this difference was not significant (Fig. 9D). No significant differences in kidney masses could be observed between the groups (Fig. 9E). Interestingly, spleens were significantly heavier both in the nmf333 NFD and WT HFD group (Fig. 9F).

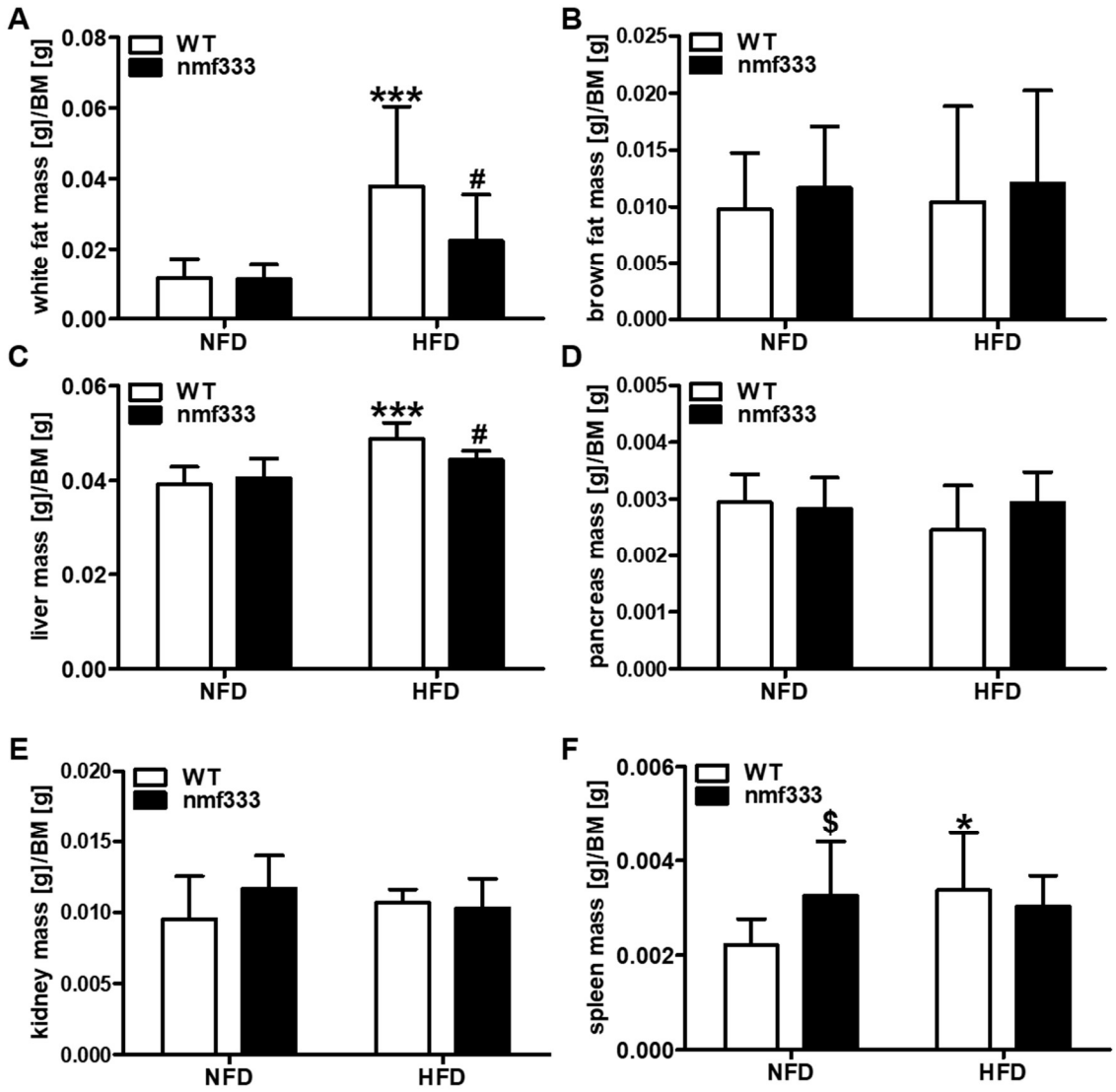

Figure 9. p22phox induces white fat deposition, liver and spleen enlargement in response to HFD. (A-F) 5-weeks-old WT and nmf333 mice were HFD fed for 20 weeks. Dietary controls received NFD. 25-weeks old mice were mated and kept on continuous diet during the course of pregnancy. Mice were dissected at GD17.5. Organs were retrieved and weighed. The organ to body mass ratio was calculated for white adipose tissue and liver [1], brown adipose tissue, pancreas, kidney and spleen. Data are means ± s.d., n = 11-13, $p < 0.05 WTNFD vs. nmf333NFD, *p < 0.05, ***p < 0.001 WTNFD vs. WTHFD, #p < 0.05 WTHFD vs. nmf333HFD by one-way ANOVA and Tukey's multiple-comparisons test.

7.2.3. p22phox promotes fatty liver disease in pregnancy

As obesity is associated with fatty liver disease [144], a histological evaluation of the liver was performed on formalin fixed paraffin embedded (FFPE) liver cross sections [1]. Periodic acid-Schiff (PAS) staining showed decreased glycogen storage in livers of HFD fed WT mice in contrast to NFD controls, while glycogen levels remained unchanged in nmf333 HFD fed mice (Fig. 10A/B). In line, immunostaining with the murine macrophage marker F4/80 (Fig. 10C/D) showed significantly increased numbers of macrophages in WT HFD livers compared to livers

from WT NFD mice, while this increase was significantly lower in nmf333 HFD dams. Staining with Haematoxylin and Eosin (H&E) showed a significantly higher amount of lipid droplets in livers from WT HFD dams compared to livers from NFD controls. This HFD-induced increase in lipid droplets was significantly lower in nmf333 HFD mice, without significant difference compared to the WT NFD group (Fig. 11A/B). Livers from WT HFD dams additionally showed increased accumulation of necrotic spots compared to NFD fed WT dams while this response was not observed in nmf333 HFD mice (Fig. 11C). Furthermore, upon histological examination livers of WT HFD mice presented signs for hepatocyte ballooning, which was less pronounced in nmf333 HFD mice and not present in WT NFD mice (data not shown).

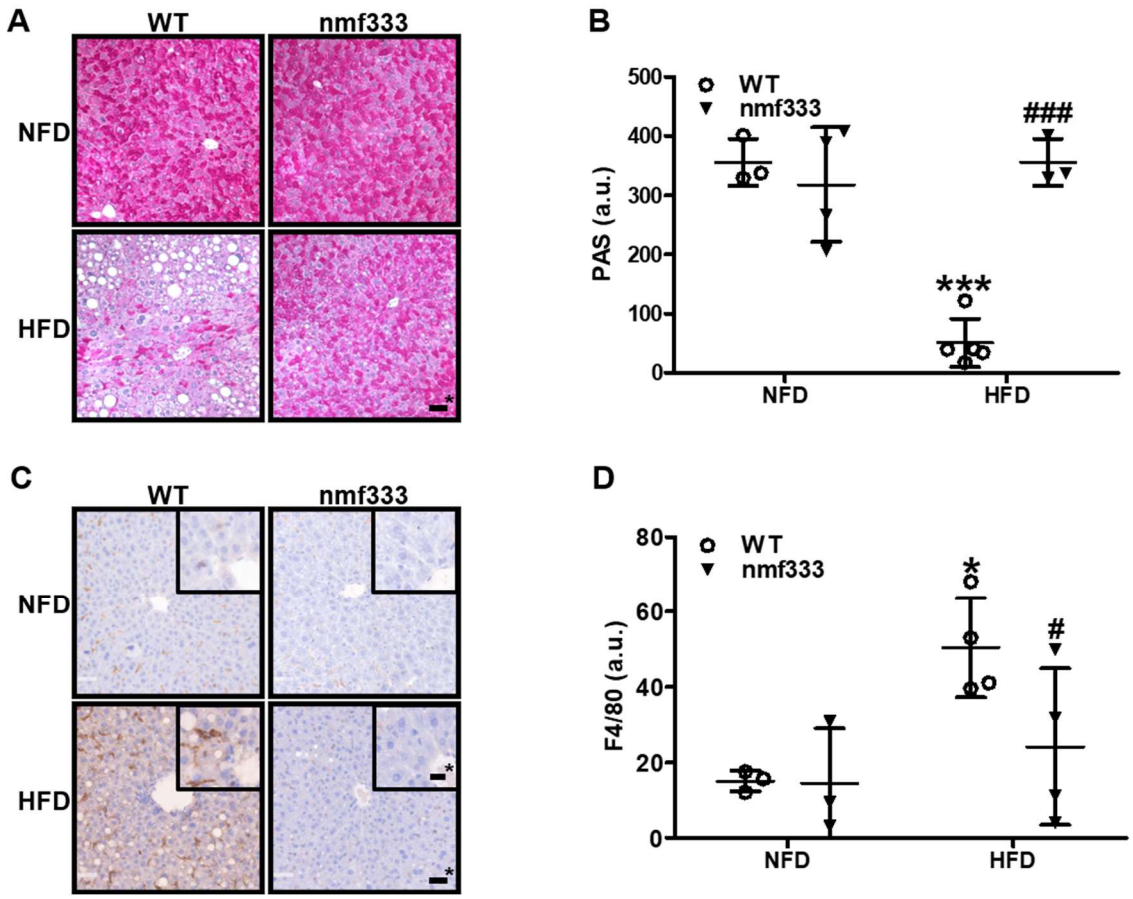

Figure 10. p22phox alters hepatic glycogen storage and inflammation in response to HFD [1]. **(A-D)** 5-weeks old WT and nmf333 mice were fed a HFD for 20 weeks. Dietary controls received NFD. 25-weeks-old mice were mated and kept on continuous diet during the course of pregnancy. Mice were dissected at GD17.5. **(A/B)** Formalin-fixed paraffin embedded (FFPE) sections of the liver were stained with Periodic acid-Schiff (PAS). **(A)** Representative stainings in 20x magnifications are shown. *Scale bar, 50 µm. **(B)** PAS-positive area was determined in 10 high-power fields per liver section. **(C/D)** FFPE liver sections were stained with an antibody against F4/80. Antibody-bound antigens were visualized by 3,3'-diaminobenzidine. Counterstaining was performed with Mayer's Haematoxylin. **(C)** Representative stainings in 20x and 40x magnifications are shown. *Scale bars, 50 µm. **(D)** $F4/80^{+}$ area was measured in 10 high-power fields per liver section. Data are means ± s.d., n = 3-5, *$p < 0.05$, ***$p < 0.01$ WTNFD vs. WTHFD, #$p < 0.05$, ###$p < 0.001$ WTHFD vs. nmf333HFD) by one-way ANOVA and Tukey's multiple-comparisons test.

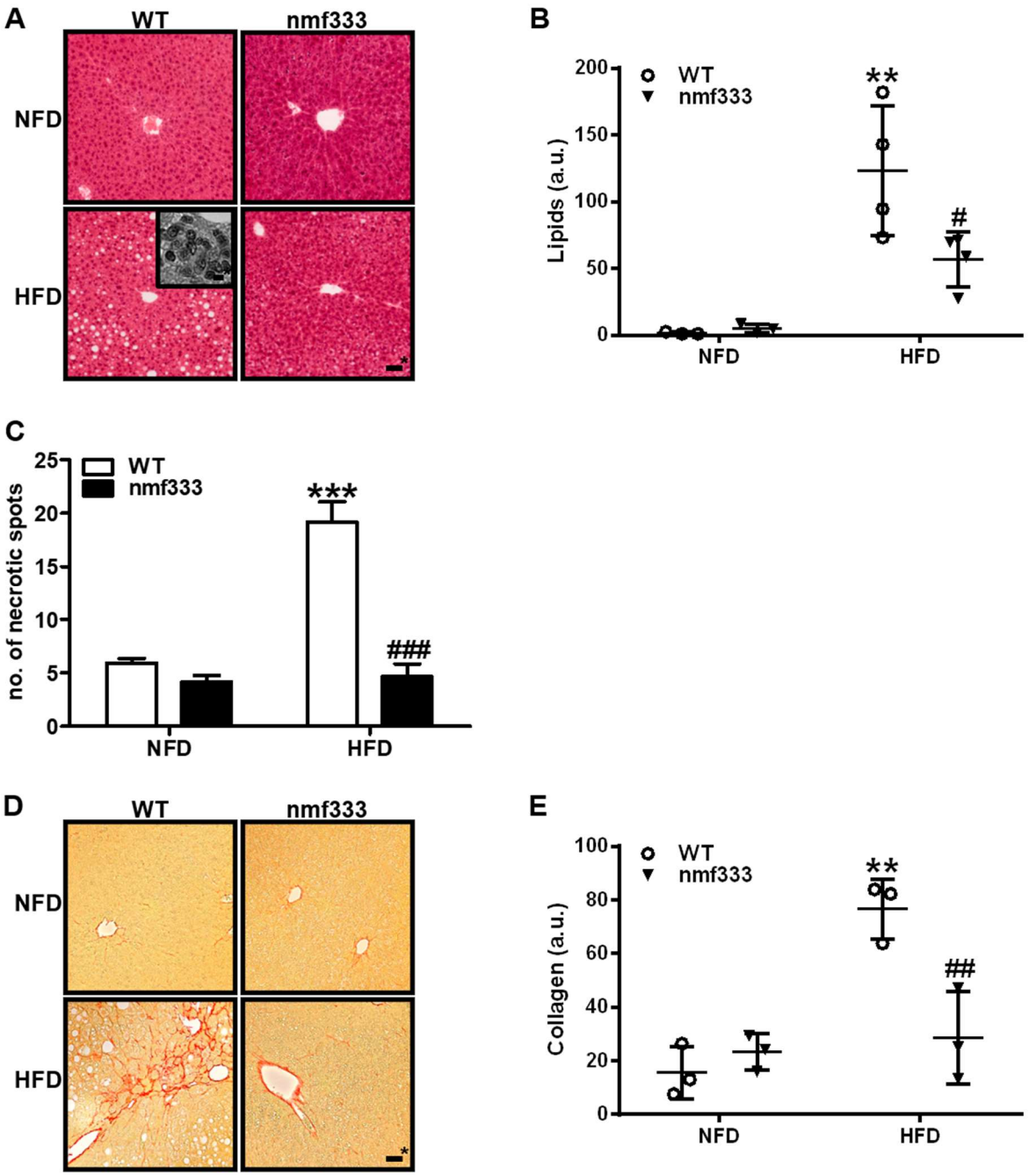

Figure 11. p22phox induces liver fatty degeneration, necrosis and fibrosis in response to HFD [1]. **(A-E)** WT and nmf333 mice were HFD fed for 20 weeks starting from 5 weeks age. Dietary controls were fed with NFD. 25-weeks-old mice were mated and kept on continuous diet during the course of pregnancy. Mice were dissected at GD17.5. **(A-C)** FFPE liver sections were stained with Hematoxylin and Eosin (H&E). **(A)** Representative stainings in 20x and 100x magnifications are shown. Black arrow points to necrosis. *Scale bars, 50 µm and 10 µm in higher magnification. **(B)** Amount of lipid droplets was calculated in 10 high-power fields per liver section. *Scale bar, 50 µm. Number of necrotic areas **(C)** was calculated in 10 high-power fields per liver section. **(D/E)** FFPE sections from the liver were stained with Picrosirius Red. **(D)** Representative stainings in 20x magnifications are shown. **(E)** Amount of collagen fibers were quantified in 10 high-power fields per liver section. Data are means ± s.d., n = 3-4, **p < 0.01, ***p < 0.001 WTNFD vs. WTHFD, #p < 0.05, ##p < 0.01, ###p < 0.001 WTHFD vs. nmf333HFD by one-way ANOVA and Tukey's multiple-comparisons test.

Picrosirius Red staining (Fig. 11D/E) showed a significant increase in collagen fibers in WT HFD dams compared to WT NFD controls, clearly pointing to the presence of fibrosis in WT HFD livers. This response was not observed in nmf333 HFD mice, exhibiting a similar collagen density to WT NFD mice. Taken together, the presence of hepatic steatosis, hepatocyte ballooning, inflammation and fibrosis point to a clear role of p22phox in the development of NAFLD in transition to NASH in obesity-induced T2DM [1].

7.2.4. p22phox induces oxidative stress in livers in response to high-fat diet

In order to assess DNA damage and oxidative stress, FFPE liver sections were stained with an antibody against 8-hydroxy-2'-deoxyguanosine (8-OHdG) [1], a widely recognized surrogate marker for oxidative DNA/RNA damage [145]. DNA damage was assessed by analysis of nuclei intensities. Livers of WT HFD fed dams had significantly more 8-OHdG positive nuclei compared to WT NFD controls, indicating increased levels of ROS load and oxidative stress, while this increase was not present in nmf333 HFD mice as 8-OHdG levels were not significantly different compared to WT NFD mice (Fig. 12).

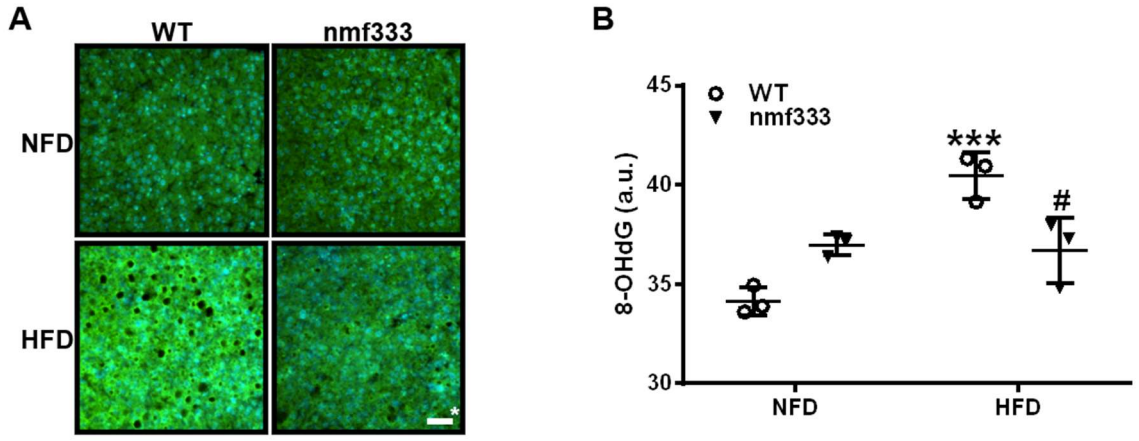

Figure 12. p22phox promotes oxidative DNA damage in the liver in response to HFD [1].
(A-B) WT and nmf333 mice were fed a HFD for 20 weeks starting from 5 weeks age. Dietary controls were fed with NFD. 25-weeks-old mice were mated and kept on continuous diet during the course of pregnancy. Mice were dissected at GD17.5. **(A/B)** FFPE sections of the liver were stained with an antibody against 8-OHdG. Nuclei were visualized with Hoechst 33342**. (A)** Representative stainings in 20x magnifications are shown. *Scale bar, 50 µm. **(B)** Fluorescence intensity was measured in 5 high-power fields per liver section. Data are means ± s.d., n = 3, ***p < 0.001 WTNFD vs. WTHFD, #p < 0.05 WTHFD vs. nmf333HFD by one-way ANOVA and Tukey's multiple-comparisons test.

7.3. Effects of high-fat diet on fetus and placenta

7.3.1. p22phox affects fetal survival in response to high-fat diet

Next, the effects of HFD-induced obesity and T2DM on pregnancy outcomes was evaluated, to this end, pregnancy was terminated at GD17.5 and fetal offspring and placentas were examined [1].

Overall, the litter size comprised 7-8 fetuses in utero in both WT and nmf333 NFD pregnancies and HFD WT and nmf333 pregnancies (data not shown) [1].

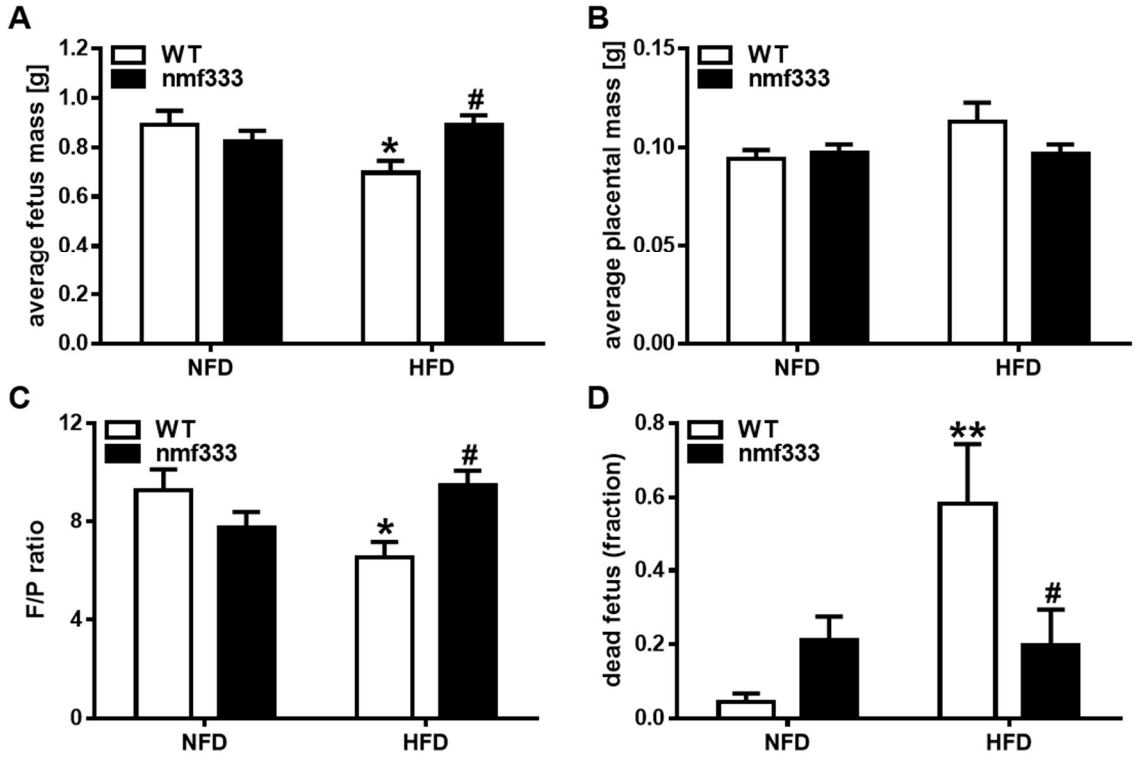

Figure 13. p22phox impairs fetal survival in response to HFD [1].
(A-D) 5-weeks-old WT and nmf333 mice were fed a HFD for 20 weeks. Dietary controls received NFD. 25-weeks-old mice were mated and kept on continuous diet during the course of pregnancy. Mice were dissected at GD17.5. **(A/B)** Placentas and fetuses were dissected at GD17.5 and weighed. **(C)** The fetal to placental mass ratio (F/P ratio) was calculated. (**(D)** The ratio of dead to living fetuses was calculated per mother. Data are means ± s.e.m., n = 11-13, *p < 0.05, **p < 0.01 WTNFD vs. WTHFD, #p < 0.05 WTHFD vs. nmf333HFD by one-way ANOVA and Tukey's multiple-comparisons test.

Fetal mass was significantly lower in offspring from WT HFD dams compared to NFD controls (Fig. 13A). Remarkably, fetal mass from nmf333 HFD offspring was not significantly different from WT and nmf333 NFD fetal mass. Furthermore, while there was a tendency of higher placenta mass in HFD WT dams, this did not reach significance (Fig. 13B). In line, the fetal to placental mass ratio (F/P ratio) was significantly lower in WT HFD pregnancies compared to

WT NFD pregnancies, while it was restored in the nmf333 HFD group (Fig. 13C). Moreover, the fraction of dead fetuses was notably higher in the WT HFD group compared to WT NFD controls (Fig. 13D). Surprisingly, the fraction of dead fetuses was not significantly different in HFD nmf333 dams compared to NFD WT and nmf333 pregnancies (Fig. 13D).

As the F/P ratio has been considered as a marker for placental efficiency [146] and maternal obesity has been shown to affect labyrinthine vascularization [147], morphology and vascular integrity of the placenta were evaluated [1]. H&E staining of placenta tissue sections showed that placentas from HFD WT dams exhibited signs of vascular congestion and blood coagulation in the placental labyrinth, indicated by large quantities of erythrocytes in the maternal blood lacunae, while this finding was not observed in placentas from all the other groups (Fig. 14A).

Maternal obesity has also been shown to affect blood vessel density and maturity [147]. Therefore, we investigated whether p22phox would alter placental vascularization [1]. To evaluate the quantity of mature vessels, placentas were stained with an antibody against α-SMA. Compared to WT NFD placentas, HFD feeding decreased α-SMA staining in WT placenta, although these data were not significant (Fig. 14B). Immunostaining for CD31 illustrated a significant decrease in the number of $CD31^+$ vessels in WT HFD placentas compared to NFD control placentas, while the number of $CD31^+$ vessels was significantly higher in nmf333 HFD placentas (Fig. 14C/D). However, placentas of WT HFD mice exhibited a significant decrease in CD31/α-SMA ratio indicating a reduced vessel maturity, while vessels in WT NFD placentas were more mature (Fig. 14E). Interestingly, the CD31/α-SMA ratio of nmf333 HFD placentas was significantly higher in comparison to placentas of WT HFD dams, however, vessels were still significantly less mature than those of WT NFD placentas (Fig. 14E).

The following paragraph has not been submitted for publication, thus contains new data.

As the amount of lectins in human placental trophoblasts and endothelial cells has been associated with intrauterine growth retardation [148], N-acetyl-D-glucosamine (WGA) disposition as a representative for lectin was evaluated in placental labyrinthic tissue. However, no significant changes in WGA distribution could be observed between the groups (Fig. 15 A/B).

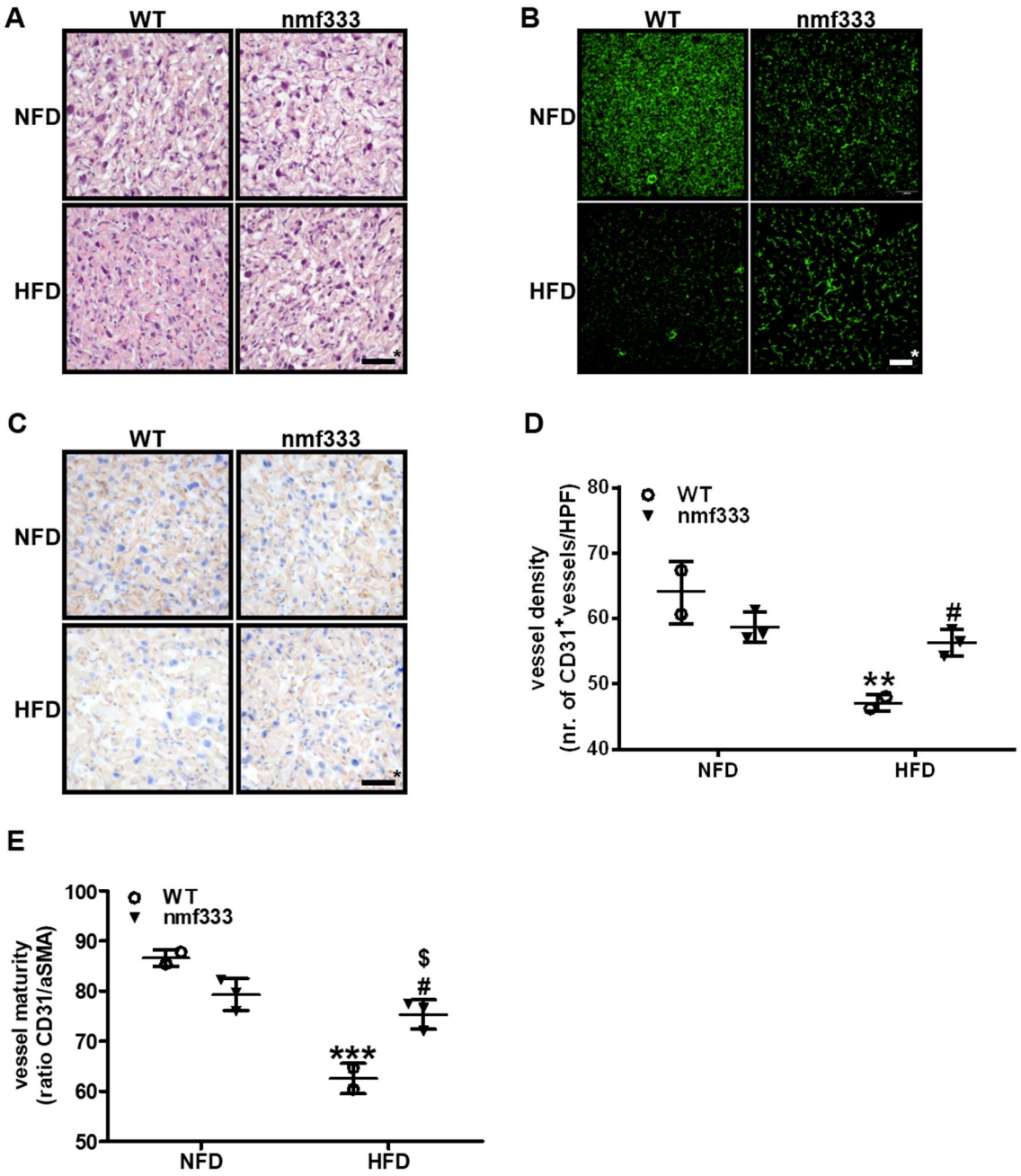

Figure 14. p22phox induces placental vascular congestion and decreases vessel density and maturity in response to HFD [1].

(A-E) WT and nmf333 mice were fed a HFD for 20 weeks starting from 5 weeks age. Dietary controls received NFD. 25-weeks-old mice were mated and kept on continuous diet during the course of pregnancy. Mice were dissected at GD17.5. **(A)** FFPE placenta sections were stained with H&E. Representative stainings of the placental labyrinth in 40x magnifications are shown. *Scale bar, 50 µm. **(B)** FFPE placenta sections were stained with an antibody against alpha smooth muscle actin (α-SMA). Representative stainings of the placental labyrinth in 10x magnifications are shown. **(C/D)** FFPE placenta sections were stained for CD31. Antibody-bound antigens were visualized by 3,3'-diaminobenzidine. Counterstaining was performed with Mayer's Haematoxylin. **(C)** Representative stainings in 40x magnifications are shown. *Scale bar, 50 µm. **(D)** Number of $CD31^+$ blood vessels were counted in 4-5 high-power fields per placenta section. **(E)** Vessel maturity was calculated by determining ratio between CD31 and α-SMA. Data are means ± s.d., n = 2-3, **p < 0.01, ***p < 0.001 WTNFD vs. WTHFD, $p < 0.05 WTNFD vs. nmf333HFD, #p < 0.05 WTHFD vs. nmf333HFD by one-way ANOVA and Tukey's multiple-comparisons test.

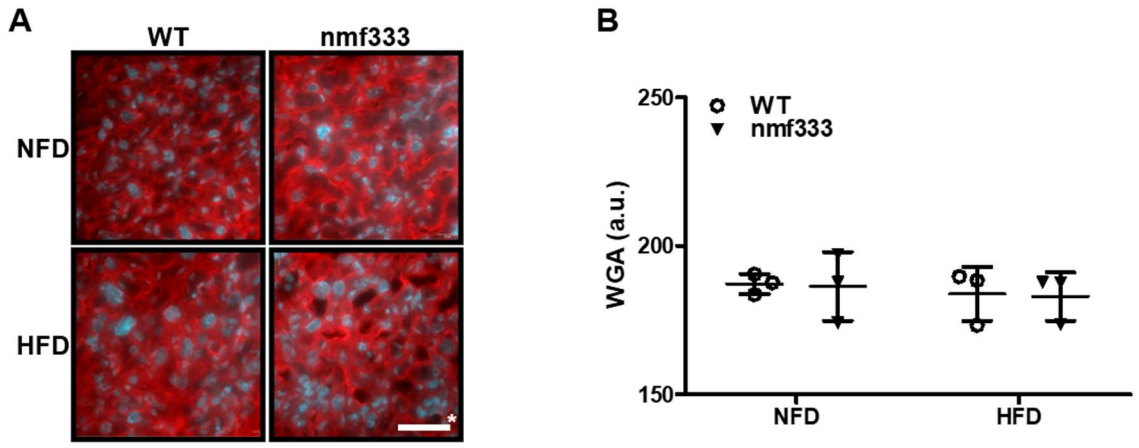

Figure 15: p22phox does not affect N-acetyl-D-glucosamine distribution in the placental labyrinth. **(A-B)** WT and nmf333 mice were fed a HFD for 20 weeks starting from 5 weeks age. Dietary controls were fed with NFD. 25-weeks-old mice were mated and kept on continuous diet during the course of pregnancy. Mice were dissected at GD17.5. **(A/B)** FFPE placenta sections were stained with wheat germ agglutinin (WGA). Nuclei were visualized with Hoechst 33342. **(A)** Representative stainings in 40x magnifications are shown. *Scale bar, 50 µm. **(B)** Fluorescence intensity was measured in 4 high-power fields per placenta section. Data are means ± s.d., n = 3, $p < 0.05$ was regarded as significant.

7.3.2. p22phox promotes high-fat diet-induced lipid accumulation and glycogen deposition in the placenta

In order to assess whether p22phox has an impact on placental metabolism under HFD, we investigated placental lipid deposition [1]. Oil Red O staining of placenta cryo-sections demonstrated a significant increase in lipid accumulation in WT HFD placentas compared to NFD control placentas both in the maternal (decidua basalis) and fetal (labyrinth) part, the increase in the latter being even more distinct, while HFD fed nmf333 littermates did not show changes in lipid accumulation (Fig. 16A-D).

Interestingly, changes in placental glycogen deposition have been linked to pregnancy complications, particularly those associated with altered fetal growth [149, 150]. One hypothesis suggests that, in diabetic pregnancies, the placenta stores excess glucose as glycogen to protect the fetus from hyperglycemia, thus limiting fetal overgrowth [151].

Thus, glycogen deposition was evaluated by staining placental FFPE sections with PAS [1]. Glycogen deposition was markedly elevated in placentas derived from WT HFD dams compared to all other groups (Fig. 16E/F).

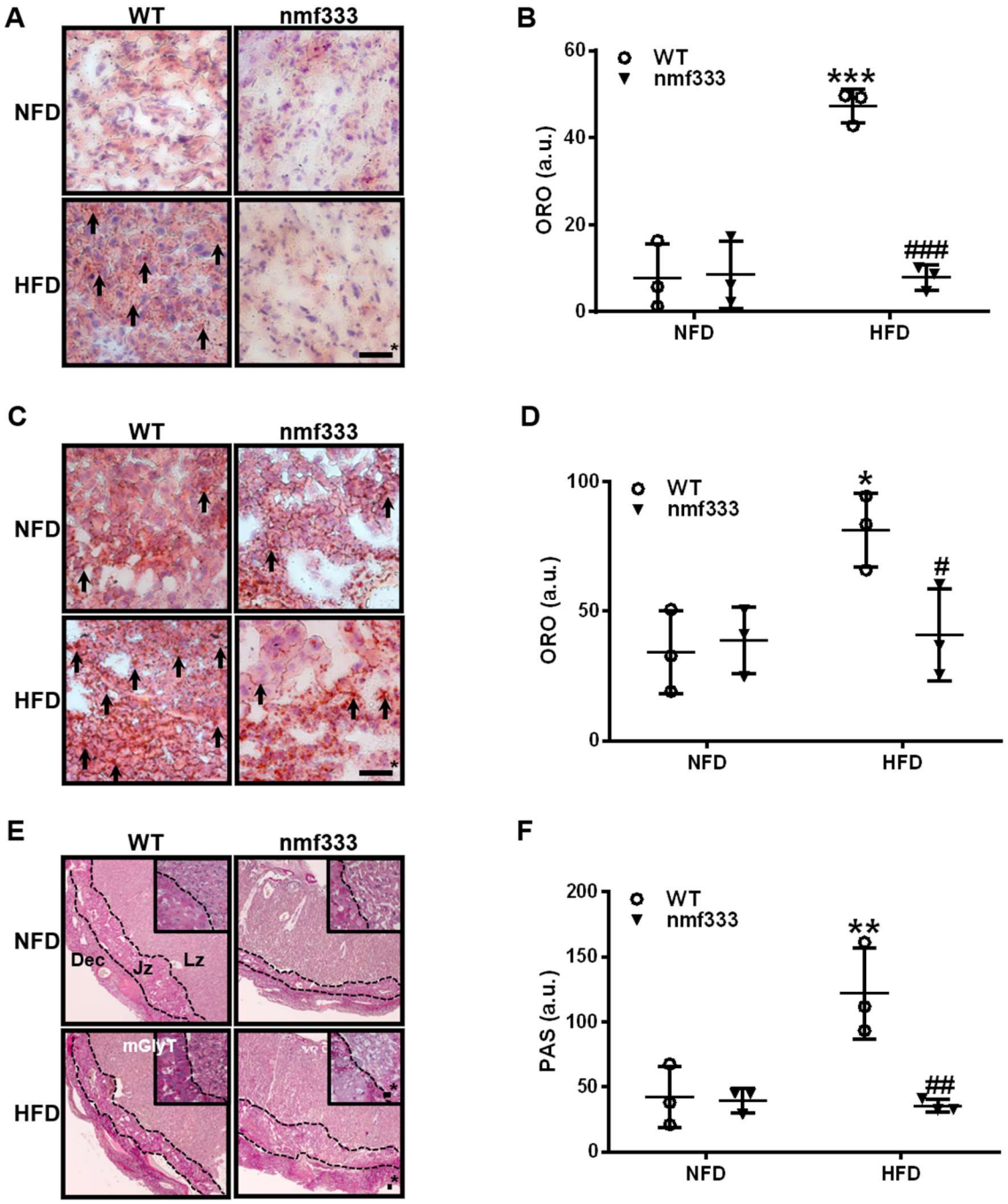

Figure 16. p22phox promotes HFD-induced lipid accumulation and glycogen storage in the placenta [1].

(A-F) 5-weeks-old WT and nmf333 mice were fed a HFD for 20 weeks. Dietary controls received NFD. 25-weeks-old mice were mated and kept on continuous diet during the course of pregnancy. Mice were dissected at GD17.5. **(A/B/C/D)** Cryofixed placenta sections were stained with Oil Red O. Counterstaining was performed with Mayer's hematoxylin. **(A/C)** Representative stainings of the labyrinth **(A)** and decidua **(C)** in 40x magnifications are shown. Lipid droplets are exemplary highlighted by black arrows. *Scale bars, 50 µm. **(B/D)** Amount of lipids were quantified in 10 high-power fields per placenta section. **(E/F)** FFPE placenta sections were stained with PAS. **(E)** Representative stainings in 5x and 20x magnifications are shown. *Scale bars, 50 µm. **(F)** Amount of glycogen was measured in 10 high-power fields per placenta section. Data are means ± s.d., n = 3, *p < 0.05, **p < 0.01, ***p < 0.001 WTNFD vs. WTHFD, #p < 0.05, ##p < 0.01, ###p < 0.001 WTHFD vs. nmf333HFD by one-way ANOVA and Tukey's multiple-comparisons test.

7.3.3. p22phox drives high-fat diet-induced oxidative stress in the placenta

Next, we examined possible DNA damage and oxidative stress in HFD-induced obese and diabetic placentas [1]. FFPE sections were therefore stained with 8-OHdG. Indeed, placentas of WT HFD fed mice presented clearly elevated levels of oxidative DNA damage both in maternal (decidua basalis) and fetal (labyrinth) tissue compared to WT NFD placentas, while placentas of HFD fed nmf333 mice showed significantly lower levels of oxidative stress (Fig. 17A-D).

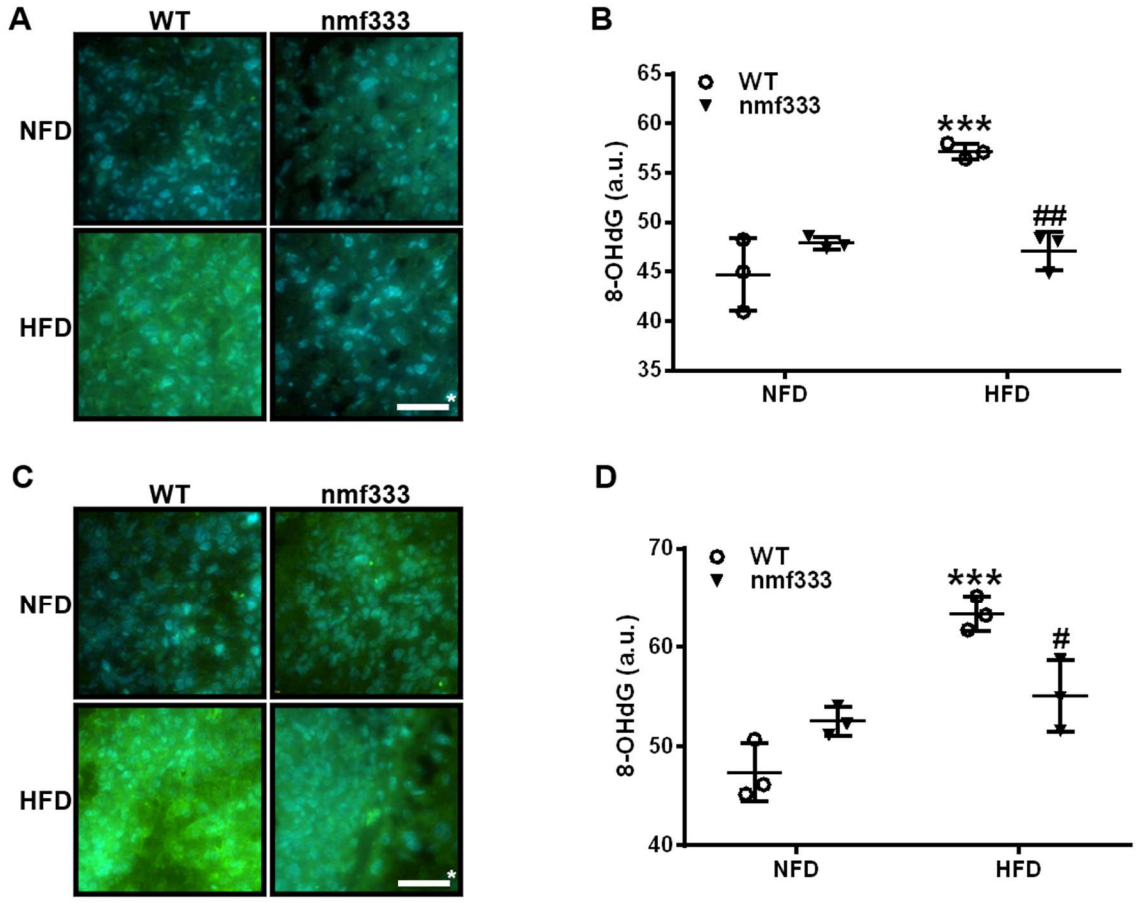

Figure 17. p22phox drives HFD-induced oxidative DNA damage in the placenta [1].
(A-D) 5-weeks-old WT and nmf333 mice were HFD fed for 20 weeks. Dietary controls received NFD. 25-weeks-old mice were mated and kept on continuous diet during the course of pregnancy. Mice were dissected at GD17.5. **(A/B/C/D)** FFPE placenta sections were stained with an antibody against 8-OHdG. Nuclei were visualized with Hoechst 33342. **(A/C)** Representative stainings of the labyrinth **(A)** and decidua **(C)** in 40x magnifications are shown. *Scale bars, 50 µm. **(B/D)** Fluorescence intensity was measured in 4 high-power fields per placenta section. Data are means ± s.d., n = 3, ***p < 0.001 WTNFD vs. WTHFD, #p < 0.05, ##p < 0.01 WTHFD vs. nmf333HFD by one-way ANOVA and Tukey's multiple-comparisons test.

7.3.4. p22phox promotes high-fat diet-induced lipid accumulation and oxidative stress in fetal livers

In consideration of the fact that p22phox alters placental metabolism and promotes oxidative DNA damage, we investigated possible changes in the fetal organism [1]. Besides being the first organ to be passed by the nutrient-rich maternal blood, the fetal liver is also a target of environmental changes through epigenetic mechanisms which could be the cause for metabolic diseases in adulthood [152].

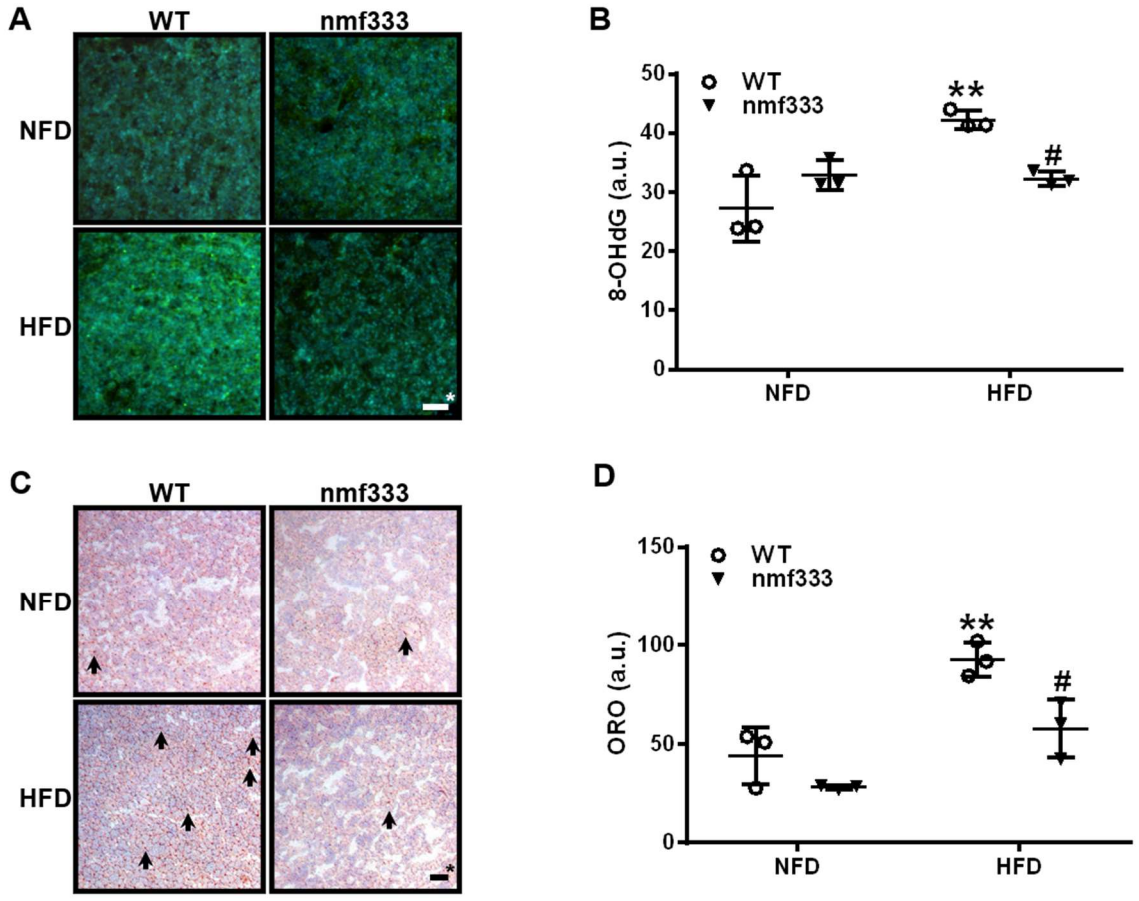

Figure 18. p22phox promotes HFD-induced oxidative stress and lipid accumulation in fetal livers [1].
(A-D) 5-weeks-old WT and nmf333 mice were HFD fed for 20 weeks. Dietary controls received NFD. 25-weeks-old mice were mated and kept on continuous diet during the course of pregnancy. Mice were dissected at GD17.5. **(A/B)** FFPE sections of E17.5 old fetuses were stained with an antibody against 8-OHdG. Nuclei were visualized with Hoechst 33342. **(A)** Representative stainings of the fetal liver in 20x magnifications are shown. *Scale bars, 50µm. **(B)** Fluorescence intensity was measured in 5 high-power fields per fetal liver section. **(C/D)** Cryofixed fetus sections were stained with Oil Red O. Counterstaining was performed with Mayer's hematoxylin. **(C)** Representative stainings of fetal livers in 20x magnifications are shown. *Scale bars, 50µm. **(D)** Amount of lipids were quantified in 10 high-power fields per fetal liver section. Data are means ± s.d., n = 3, **p < 0.01 WTNFD vs. WTHFD, #p < 0.05 WTHFD vs. nmf333HFD by one-way ANOVA and Tukey's multiple-comparisons test.

To test whether oxidative stress is also present in fetal livers of HFD fed dams, FFPE sections of the fetus (E17.5) were stained for 8-OHdG. In livers from WT HFD fetuses nuclear 8-OHdG levels were significantly higher compared to the NFD groups, while this increase was not observed in livers from HFD fed nmf333 fetuses (Fig. 18A/B).

When lipid deposition was assessed by Oil Red O staining, fetal livers from the WT HFD group exhibited significantly increased diffuse accumulation of lipid droplets in contrast to offspring from WT NFD dams, however, lipid deposition was substantially lower in livers from HFD nmf333 fetuses (Fig. 18C/D).

These data clearly point to a role of p22phox in promoting HFD-induced oxidative damage and lipid deposition in fetal livers [1].

8. Discussion

Parts and contents of this chapter and the following subchapters have been submitted for publication [1].

High-fat diet has been shown to induce obesity in various animal models, especially in mice [153-155]. A chronic HFD regime has also been associated with obesity-related metabolic complications, such as the metabolic syndrome [156, 157] and T2DM [158, 159]. In this study, the role of p22phox-dependent NADPH oxidases in the development of HFD-induced obesity and glucose intolerance was investigated, and their function in the genesis of metabolic complications during pregnancy was evaluated [1]. For this purpose, an animal model with mutant nmf333 mice lacking functional p22phox due to a point mutation in the CYBA gene [128] was used and exposed to fat-derived calories before and during pregnancy [1].

This study shows that p22phox under HFD mediates: a) obesity and white fat deposition; b) glucose intolerance and insulin resistance; c) intrauterine growth retardation and fetal death; and d) ROS-mediated placental lipotoxicity and vascular remodeling [1].

8.1. p22phox promotes high-fat diet-induced obesity, glucose intolerance and insulin resistance

Data in this study demonstrated that mice with a functional p22phox protein developed obesity and visceral white fat accumulation in response to HFD feeding, whereas mice lacking functional p22phox remained relatively unscathed, suggesting that p22phox mediates obesity development under HFD [1].

Evidence suggests that HFD fed mice overexpressing p22phox in vascular smooth muscle exhibited augmented obesity, reduced HDL cholesterol, increased levels of leptin and the proinflammatory chemokine MCP-1 as well as excessive ROS production [1, 160]. Indeed, NADPH oxidases have been shown to be systemically upregulated in vascular, adipose and kidney tissues in a rat model of diet-induced obesity [1, 161]. In addition, Furukawa et al. have reported augmented NADPH oxidase expression and increased ROS production in adipose tissue of obese mice, suggesting a link between NADPH oxidases and obesity-related metabolic disorders [1, 109]. In line, a previous study with NOX2 knockout (NOX2KO) mice has shown a reduction of visceral fat accumulation (inguinal fat depot) in HFD fed NOX2KO mice compared to WT mice under HFD [162].

Results of this study support the notion that p22phox, an important NOX stabilizer and obligatory subunit essential for the activation of several NOX isoforms, is a driving force in the development of obesity and obesity-related diseases. We could show that p22phox induced glucose intolerance and insulin resistance in a HFD regime [1].

These results are consistent with previous reports suggesting ROS to be the initial key trigger for HFD-induced insulin resistance [1, 163]. Furthermore, monocytes of patients with T2DM have shown increased expression of p22phox, indicating that a state of hyperglycemia promotes oxidative stress by activation of NADPH oxidases [1, 164]. In line, studies on Zucker diabetic fatty (ZDF) rats, a widely used animal model for type 2 diabetes [165], have also presented higher levels of NADPH oxidase activity and ROS generation in obese diabetic rats than in lean controls [1, 166, 167]. Similar results were found in the NOX2KO HFD mouse model showing a significant increase in intrinsic blood glucose levels and glucose intolerance measured with OGTT in WT HFD compared to HFD fed NOX2KO mouse [162].

However, our results did not show a significant increase in glucose intolerance in HFD fed pregnant WT mice compared to non-pregnant HFD fed WT mice, whereas nmf333 HFD mice exhibited unharmed glucose tolerance even during pregnancy, suggesting that p22phox indeed promotes HFD-induced glucose intolerance in mice which is maintained during pregnancy, but does not necessarily induce GDM [1].

These findings may be in conflict with previous evidence showing the presence of increased placental oxidative stress in women with GDM [1, 168]. Nevertheless, to this day not much has been published about the exact role of the NOX family in the evolution of GDM, requiring further studies to reveal the underlying mechanisms of NADPH oxidases and ROS in the development of GDM [1].

8.2. p22phox induces NAFLD/NASH and oxidative stress under high-fat diet in maternal livers

Western diet consumption has been demonstrated to upregulate the expression of some NOX isoforms in the liver, thereby inducing impaired insulin responses and oxidative stress [169]. In particular, it has been observed that a diet rich in fructose can upregulate the expression of both NOX2 and NOX4 in the liver and adipose tissue [170].

NADPH oxidases were shown to play an important role in sustaining the progression of various chronic liver diseases, such as non-alcoholic fatty liver disease (NAFLD), but also more serious liver diseases like non-alcoholic steatohepatitis (NASH), liver fibrosis and cirrhosis [1, 171-175]. A recent study investigated the existence of single-nucleotide polymorphisms (SNPs) in the genes coding for NOX4 (NOX4) and p22phox (CYBA) and observed an association between the rs3017887 SNP of NOX4 and higher liver enzyme concentration in NAFLD patients, and also between the CYBA-675 T/A CYBA polymorphism and higher triglyceride levels in NASH patients [1, 176].

On this account, this study examined the role of p22phox in the development of NAFLD/NASH in pregnant mice fed with HFD. Indeed, we could show that p22phox promoted hepatic steatosis, accumulation of liver necrosis and fibrosis in pregnant mice under HFD, producing a state of NAFLD in transition to NASH [1].

Concomitantly, recent evidence has pointed to increased expression of NOX1 in livers of NASH patients but also in HFD fed mice [177]. In addition, NOX1 deficiency attenuated HFD-induced liver injury and suppressed the accumulation of protein nitrotyrosine adducts in hepatic sinusoids [177]. In accordance to our study, these data suggest the important role of NOX1 and NADPH oxidases in the progression of NAFLD. In support, it has previously been demonstrated that progression of NAFLD is associated with NOX2-dependent ROS generation [1, 178, 179].

This study indicates that HFD-induced obesity and impaired glucose tolerance provoked by p22phox is associated with NAFLD/NASH in pregnancy [1].

The following paragraphs have not been submitted for publication, unless otherwise stated.

Previous studies have shown a clear link between NAFLD and metabolic diseases such as glucose intolerance/T2DM and the metabolic syndrome in non-pregnant patients [180, 181]. Recent evidence points out that the incidence of NAFLD in early gestation is involved in the development of GDM in later stages of pregnancy [182], clearly highlighting the link between NAFLD and impaired glucose homeostasis in pregnancy. Interestingly, several studies reported disconcordant findings, suggesting no link between NAFLD and glucose intolerance. Sattari et al. reported that sonographic evidence of NAFLD during later gestational stages were not concomitant with impaired glucose tolerance during and after pregnancy [183]. Likewise, it has been stated that though NAFLD is prevalent in women with prior GDM, it is not associated

with glucose intolerance but with increasing insulin resistance and larger waist circumference [184]. This discrepancy might relate to a multifactorial pathogenesis of NAFLD in pregnancy.

It is known that T2DM is associated with elevated levels of liver glycogen both in fasting and non-fasting conditions [185, 186]. Recent evidence suggests that in diabetic livers glycogen, which under healthy conditions consists of α-particles that are made by multiple β-particles, is composed of more fragile α-particles. In fasting conditions, diabetic glycogen was found to degrade more quickly and form smaller-sized particles than in non-fasting conditions [187]. However, this is not the case in livers with steatosis, such as in NAFLD/NASH. In comparison to patients with T2DM, NAFLD patients have been shown to have lower basal hepatic glucose production [181]. In db/db mice hepatic steatosis was already accompanied by reduced glycogen storage [188]. The shrinking capacity of glycogen production and storage is even more amplified with the increase of fibrosis as seen in liver cirrhosis [189].

Interestingly, in this study, a significant reduction of glycogen in livers of pregnant HFD fed WT mice was shown. These livers exhibited signs of hepatic steatosis and fibrosis consistent with NAFLD/NASH. Taken together, these data further support the observation that p22phox induces NAFLD/NASH under HFD in pregnant mice.

Kupffer cells, resident hepatic macrophages located in liver sinusoids, are critical mediators of hepatic response to liver injury and inflammation, but they also contribute to different liver pathologies such as metabolic liver diseases [190]. These cells were shown as major contributors in the progression of NAFLD/NASH and insulin resistance [191-193]. As a member of the mononuclear cells, Kupffer cells have been shown to express F4/80 [194].

This study reports a significant increase in F4/80-positive cells in the liver of HFD fed pregnant WT and their relative decrease in HFD nmf333 mice, indicating that p22phox under HFD conditions increases the number of hepatic macrophages [1].

This is in accordance to previous findings that showed increased ROS generation by hepatic macrophages via NOX2 activation in NAFLD [179]. In support, NADPH oxidases have been reported to contribute to the evolution of liver fibrosis. Elevated NOX4 levels were shown in patients with NASH compared to healthy controls [175]. Furthermore, mice with hepatocyte-specific NOX4-deficiency exhibited attenuated oxidative stress and liver fibrosis under HFD-induced steatohepatitis [175].

Data in the present study clearly demonstrated the presence of oxidative stress and DNA damage in HFD fed WT mouse livers, indicating that functional p22phox induces oxidative

stress in maternal livers under HFD and thus plays a critical role in the development of HFD-induced NAFLD/NASH [1].

These results support and specify previous findings showing that NADPH oxidase deficiency protects mice from oxidative phosphorylation dysfunction, oxidative DNA damage and NASH caused by HFD [195]. In support, studies have shown development of oxidative stress in patients with NAFLD, which is even aggravated when progression to NASH occurs [196]. Concomitantly, previous studies demonstrated that the presence of ROS leads to lipid accumulation in hepatocytes and thus contributes to the genesis of NAFLD/NASH, even though the proposed pathways differed [197, 198].

8.3. p22phox promotes intrauterine growth restriction and intrauterine fetal death under high-fat diet

Maternal obesity has been associated with adverse pregnancy outcomes such as preeclampsia, GDM and cesarean section, but also with fetal complications like congenital anomalies and macrosomia [1, 199, 200]. Similarly, diabetes in pregnancy is accompanied with high risks both for mother and fetus with higher incidence of hypertensive disorders, cardiovascular complications, congenital malformations and stillbirth [1, 201].

The present study investigated the effect of p22phox in pregnancies of HFD-induced obese and (pre)diabetic dams. We could show that in our mouse model p22phox promoted intrauterine growth restriction (IUGR) as indicated by significantly lower fetal mass, a decreased fetal to placental mass ratio (F/P ratio) and most importantly a significant increase in intrauterine fetal deaths, illustrated by a fraction of dead fetuses of approximately 50% [1]. Since no studies about the relationship between p22phox, obesity/diabetes and pregnancy have yet been performed, our study provides novel data in this field.

Chronic HFD regime before and during pregnancy has been reported to affect fetal growth [1]. Previous evidence has shown that fetuses of mothers fed HFD prior to and during pregnancy exhibited significantly lower fetal weights [1, 202]. In line, maternal HFD in non-human primate models was accompanied with a significantly increased rate of stillbirth in HFD groups compared to controls [1, 203].

Studies on the reproduction of diabetic rats have reported significantly increased resorptions and embryonic losses, smaller litter sizes, a reduced number of living fetuses, and smaller

fetuses for gestational age [1, 204, 205]. But adverse pregnancy outcomes associated with diabetes also comprise diverse fetal malformations [204]. Interestingly, apart from lower fetus weights, diabetic female rats also presented higher placental weights, higher levels of placental oxidative stress markers and ROS production, as well as increased levels of nitric oxide end products and 8-OHdG in the placenta [206].

The following paragraphs have not been submitted for publication.

The risk of perinatal death has been shown to be dependent on the F/P ratio, with perinatal deaths occurring the fewest when the F/P ratio was appropriate (balanced growth of placenta and infant) [146].

Similarly, the decrease in F/P ratio in our WT HFD mice might be related to the increased incidence of fetal deaths in this group. On the contrary, pregnancies of nmf333 HFD mice exhibited an appropriate F/P ratio comparable to that of NFD controls, possibly explaining the less frequent fetal deaths in this group.

However, the exact reasons behind the stronger occurrence of IUGR and fetal deaths in obese and diabetic dams are not well understood.

8.4. p22phox promotes high-fat diet-induced lipotoxicity in placentas and fetal livers

Pregnancy complications such as preeclampsia and IUGR have often been associated with the occurrence of oxidative stress and lipid peroxidation [1, 207, 208]. Therefore, we hypothesized that NADPH oxidases and especially p22phox play a critical role in HFD-induced lipotoxicity. Hence, we investigated the possible presence of lipotoxicity in the placenta which as a mediator between mother and fetus could have deleterious effects for the fetus when affected.

Indeed, we could show that placentas and fetal livers of the WT HFD group presented significantly increased lipid accumulation compared to the respective p22phox-deficient nmf333 group [1].

So far, studies have reported that placentas of obese and HFD fed dams presented increased placental fatty acid transporter expression and fatty acid oxidation, and also uptake of chylomicron lipids [1, 209, 210]. Maternal obesity has also been associated with a lipotoxic placental environment, prone to impair angiogenesis and increase inflammation and oxidative stress [211].

Currently, the relationship between NADPH oxidases, placental lipotoxicity and glucose intolerance/T2DM has not been properly explored. It was previously demonstrated that placentas of patients with T2DM exhibited lipid overaccumulation, increased lipid peroxidation and NO overproduction [1, 212]. This was confirmed by data illustrating that placentas of obese women with GDM revealed a greater number of notably larger lipid droplets [213]. Besides, previous evidence has shown that NADPH oxidases are accountable for increased lipid peroxidation in human placental microsomes and mitochondria [1, 214-216]. Matsubara et al. have histochemically demonstrated NADPH oxidase activity in syncytial microvillous membranes of the human placenta and therefore presumed that these enzymes may play a role in placental lipid peroxidation [217]. Furthermore, lipid peroxidation has previously been associated with pregnancy complications such as preeclampsia. Studies have reported increased placental lipid peroxidation and decreased antioxidant enzyme activity in preeclamptic pregnancies [218, 219].

In line, in the present study, we could show that under HFD and diabetic conditions NADPH oxidases and in particular p22phox indeed contributed to placental lipid peroxidation [1].

Accumulating evidence suggests that impaired maternal lipid metabolism also alters fetal metabolism [1, 220]. It was shown that fetuses of obese dams exhibited elevated blood triglyceride levels [210]. Previous studies have reported lipotoxicity in livers of fetuses from HFD fed mothers with increased levels of liver triglycerides and hepatic oxidative stress [1, 221]. Increased levels of triglycerides were also depicted by Oil Red O staining, illustrating diffuse accumulation of lipid droplets in fetal livers from HFD mothers [222]. In line, in a primate model of maternal obesity, signs of increased lipid accumulation and severe steatosis were found in fetal livers [223]. Additionally, oxidative damage markers were significantly increased in livers of offspring from obese dams [1, 224].

Our data support these findings by showing p22phox-dependent accumulation of lipid droplets and signs for oxidative damage in fetal livers under HFD conditions which might illustrate the impact of placental lipotoxicity on the fetus [1].

8.5. p22phox induces reactive oxygen species-mediated vasculopathy in high-fat diet placentas

The majority of the following paragraphs have not been submitted for publication, unless otherwise stated.

Discussion

Diabetes and obesity have been associated with an imbalance between the maternal oxidative and anti-oxidative defense system, resulting in extensive oxidative stress levels [225]. Similar studies with diabetic rats reported that maternal diabetes significantly increased levels of oxidative stress and 8-OHdG in the placenta [206, 226]. Oxidative stress in the placenta can lead to severe pregnancy complications such as preeclampsia and fetal growth restriction [227-229] as well as GDM [229]. However, there are not many studies examining the role of NADPH oxidases, in particular that of p22phox, in the formation of placental oxidative stress under HFD conditions.

In the present study it was shown that p22phox-dependent NADPH oxidases promoted oxidative damage both in the decidua and in the placental labyrinth under HFD [1].

Previous studies have demonstrated that NADPH oxidases are the major source of placental superoxide production in early pregnancy [230]. Evidence pointed to the isoform NOX1 as a major source of increased ROS levels in preeclamptic placentas [231]. Other studies have identified elevated endothelial NOX2 expression in women with preeclampsia and demonstrated that apocynin, an unspecific inhibitor of NADPH oxidases [232], prevented negative effects of NOX2-mediated oxidative stress [233]. In addition, higher NOX4 protein levels were demonstrated in human placentas with preeclampsia [234].

In contrast, growing evidence suggests that ROS are not necessarily detrimental, but can also play an important role in initial stages of pregnancy. For instance, it was demonstrated that trophoblast cells expressed main subunits of NADPH oxidases, thus enabling them to produce ROS and thereby contribute to implantation and placentation [235]. In line, it was shown that ROS, when primarily generated by p22phox/NOX4 complex activation, play a crucial role in initiating decidualization [236].

However, our study results indicate that ROS-mediated oxidative stress generated by functional NADPH oxidases in placentas contribute to impaired fetal survival under HFD and T2DM conditions [1].

Nonhuman primate models have demonstrated that HFD disturbs uterine and placental hemodynamics by reducing both uterine and fetal volume blood flow, consequently leading to increased frequency of placental infarctions [1, 203]. Furthermore, recent evidence links maternal obesity to impaired labyrinthine vasculature, suggesting reduced placental nutrient transport from the maternal circulation to be the underlying cause for fetal growth restriction [1, 34].

Our data support and extend these findings by showing massive vascular congestion in HFD fed WT placentas whereas HFD fed nmf333 mice were not affected, indicating that p22phox is a major contributor to HFD-induced placental vasculopathy.

In C57BL/6 mice it was also demonstrated that HFD before and during pregnancy resulted in impaired glucose metabolism, insulin resistance and increased levels of placental oxidative stress [237]. There is evidence suggesting that the latter plays a critical role in placental vascular dysfunction associated with IUGR [1, 238]. Oxidative stress was additionally shown to contribute to endothelial necrosis, accompanied by reduced endothelial cell marker (CD31), pointing to oxidative stress-mediated placental vascular damage under HFD [1, 237]. Similar results were reported in C57BL/6N mice which presented downregulated expression of CD31 on both mRNA and protein level under HFD, indicating impaired vascularization in the labyrinth zone of the placenta [239].

Disturbed vascularization was also demonstrated by Hayes et al., although a 2-fold increase of $CD31^+$ and a 30% decrease in αSMA-stained blood vessels was shown, pointing to the presence of more, but immature blood vessels [147]. In line, several studies reported placental hypoxia in HFD fed mice with likewise increased CD31 immunostaining [240, 241]. These data seem difficult to reconcile with the reduction of $CD31^+$ vessels mentioned before, but in fact, under hypoxic conditions increased VEGF expression stimulates angiogenesis [242, 243] and as a result promotes the development of immature blood vessels and increase in CD31 staining [240]. This evidence of placental hypoxia coincides with the previously mentioned reduction of uteroplacental blood flow under HFD conditions [203]. These controversial findings may refer to different stages of placental damage under HFD: while in the beginning oxidative stress-induced endothelial necrosis and reduction of blood vessels (decreasing CD31 staining) predominate, reduced placental blood flow in later stages might lead to placental infarctions and consequently placental hypoxia, promoting angiogenesis via hypoxia-inducible factors [244]. However, the exact mechanistic sequences are not yet fully understood.

Our results show decreased vessel density, demonstrated by CD31 immunostaining as well as reduced vessel maturity in HFD fed WT placentas and thereby support and augment the evidence of impaired vascularization in the placenta [1]. Since mutant nmf333 mice under HFD were not affected, our data indicate that p22phox plays a critical role in the development of HFD-induced placental vascular dysfunction [1]. In addition, we observed a reduction of α-SMA^+ vessels in the placental labyrinth of HFD fed WT mice, however, these data were not

significant. Nevertheless, this finding may reflect the dominance of immature blood vessels in these placentas.

Taken together, in placentas of WT HFD dams vascular dysfunction in terms of vascular congestion and damage, provoked by p22phox-dependent NADPH oxidases, could additionally contribute to the higher incidence of IUGR and intrauterine fetal deaths in this group [1].

8.6. Conclusion

Contents of this chapter have been submitted for publication [1].

This study could show for the first time that p22phox as a key subunit of NADPH oxidases plays a crucial role in the development of obesity and T2DM. Mice with p22phox-dependent NADPH oxidases exhibited an obese phenotype and developed glucose intolerance and insulin resistance under HFD in contrast to littermates with p22phox-deficiency.

p22phox was involved in the sustainment of obesity and glucose intolerance also during pregnancy. In addition, pregnant HFD mice with p22phox-dependent NADPH oxidases presented characteristics of NAFLD in transition to NASH with increased necrosis, higher number of macrophages, liver fibrosis and oxidative stress.

Our results demonstrated that the reproduction performance of female mice with p22phox-dependent NADPH oxidases was severely impaired under HFD conditions since this group showed a significant reduction in fetal mass (IUGR) and F/P ratio, but also a massive increase in intrauterine fetal deaths.

Moreover, p22phox contributed to increased ROS-mediated oxidative damage and lipotoxicity as well as vascular dysfunction in placentas of HFD fed pregnant dams which in the combination might be the underlying reason for its major impact on fetal survival.

Taken together, findings in this study point to a significant role of p22phox in pregnancy complications and adverse fetal outcomes associated with obesity and T2DM, which may provide a fundament for future therapeutic approaches.

8.7. Limitations of the study

Since the nmf333 mutant mouse strain carries a single point mutation in the CYBA gene which causes instability of the p22phox protein, it is a good model for p22phox-deficiency. However, mRNA levels of p22phox are preserved. Hence, more studies should be carried out on mice with a complete knockout of p22phox, in order to more specifically evaluate the role of p22phox in the pathogenesis of obesity and diabetes-related disorders.

9. List of figures

10. References

[1] Li L., Petry A., Görlach A., and Kračun D., "Maternal obesity-induced type II diabetes promotes ROS-dependent non-alcoholic fatty liver disease, placental pathology and fetal death", [Manuscript submitted for publication in Journal of Biological Chemistry], Department of Medicine, Technical University of Munich, 2023.

[2] World Obesity Federation. "Prevalence of obesity." https://www.worldobesity.org/about/about-obesity/prevalence-of-obesity (accessed June 30th, 2020).

[3] Haslam D. W. and James W. P., "Obesity," (in eng), *Lancet,* vol. 366, no. 9492, pp. 1197-209, Oct 1 2005, doi: 10.1016/s0140-6736(05)67483-1.

[4] World Health Organization. "Obesity and overweight." https://www.who.int/news-room/fact-sheets/detail/obesity-and-overweight (accessed June 30th, 2020).

[5] Engin A., "The Definition and Prevalence of Obesity and Metabolic Syndrome," in *Obesity and Lipotoxicity*, A. B. Engin and A. Engin Eds. Cham: Springer International Publishing, 2017, pp. 1-17.

[6] McCracken E., Monaghan M., and Sreenivasan S., "Pathophysiology of the metabolic syndrome," (in eng), *Clin Dermatol,* vol. 36, no. 1, pp. 14-20, Jan-Feb 2018, doi: 10.1016/j.clindermatol.2017.09.004.

[7] Grundy S. M., "Metabolic syndrome update," (in eng), *Trends Cardiovasc Med,* vol. 26, no. 4, pp. 364-73, May 2016, doi: 10.1016/j.tcm.2015.10.004.

[8] Saklayen M. G., "The Global Epidemic of the Metabolic Syndrome," (in eng), *Curr Hypertens Rep,* vol. 20, no. 2, p. 12, Feb 26 2018, doi: 10.1007/s11906-018-0812-z.

[9] Tuomi T., Santoro N., Caprio S., Cai M., Weng J., and Groop L., "The many faces of diabetes: a disease with increasing heterogeneity," (in eng), *Lancet,* vol. 383, no. 9922, pp. 1084-94, Mar 22 2014, doi: 10.1016/s0140-6736(13)62219-9.

[10] Zimmet P., Alberti K. G., Magliano D. J., and Bennett P. H., "Diabetes mellitus statistics on prevalence and mortality: facts and fallacies," *Nature Reviews Endocrinology,* vol. 12, no. 10, pp. 616-622, 2016/10/01 2016, doi: 10.1038/nrendo.2016.105.

[11] Zheng Y., Ley S. H., and Hu F. B., "Global aetiology and epidemiology of type 2 diabetes mellitus and its complications," *Nature Reviews Endocrinology,* vol. 14, no. 2, pp. 88-98, 2018/02/01 2018, doi: 10.1038/nrendo.2017.151.

[12] World Health Organization, *Classification of diabetes mellitus*. 2019, p. 4.

[13] Flannick J., Johansson S., and Njølstad P. R., "Common and rare forms of diabetes mellitus: towards a continuum of diabetes subtypes," *Nature Reviews Endocrinology,* vol. 12, no. 7, pp. 394-406, 2016/07/01 2016, doi: 10.1038/nrendo.2016.50.

[14] Abdul-Ghani M. A. and DeFronzo R. A., "Plasma glucose concentration and prediction of future risk of type 2 diabetes," (in eng), *Diabetes care,* vol. 32 Suppl 2, no. Suppl 2, pp. S194-S198, 2009, doi: 10.2337/dc09-S309.

[15] Kahn S. E., Cooper M. E., and Del Prato S., "Pathophysiology and treatment of type 2 diabetes: perspectives on the past, present, and future," (in eng), *Lancet (London, England),* vol. 383, no. 9922, pp. 1068-1083, 2014, doi: 10.1016/S0140-6736(13)62154-6.

[16] Roden M. and Shulman G. I., "The integrative biology of type 2 diabetes," *Nature,* vol. 576, no. 7785, pp. 51-60, 2019/12/01 2019, doi: 10.1038/s41586-019-1797-8.

[17] American Diabetes Association, "2. Classification and Diagnosis of Diabetes: Standards of Medical Care in Diabetes-2020," (in eng), *Diabetes Care,* vol. 43, no. Suppl 1, pp. S14-s31, Jan 2020, doi: 10.2337/dc20-S002.

[18] Wheeler E., Leong A., Liu C.-T., Hivert M.-F., Strawbridge R. J., Podmore C., Li M., Yao J., Sim X., Hong J., Chu A. Y., Zhang W., Wang X., Chen P., Maruthur N. M.,

Porneala B. C., Sharp S. J., Jia Y., Kabagambe E. K., Chang L.-C., Chen W.-M., Elks C. E., Evans D. S., Fan Q., Giulianini F., Go M. J., Hottenga J.-J., Hu Y., Jackson A. U., Kanoni S., Kim Y. J., Kleber M. E., Ladenvall C., Lecoeur C., Lim S.-H., Lu Y., Mahajan A., Marzi C., Nalls M. A., Navarro P., Nolte I. M., Rose L. M., Rybin D. V., Sanna S., Shi Y., Stram D. O., Takeuchi F., Tan S. P., van der Most P. J., Van Vliet-Ostaptchouk J. V., Wong A., Yengo L., Zhao W., Goel A., Martinez Larrad M. T., Radke D., Salo P., Tanaka T., van Iperen E. P. A., Abecasis G., Afaq S., Alizadeh B. Z., Bertoni A. G., Bonnefond A., Böttcher Y., Bottinger E. P., Campbell H., Carlson O. D., Chen C.-H., Cho Y. S., Garvey W. T., Gieger C., Goodarzi M. O., Grallert H., Hamsten A., Hartman C. A., Herder C., Hsiung C. A., Huang J., Igase M., Isono M., Katsuya T., Khor C.-C., Kiess W., Kohara K., Kovacs P., Lee J., Lee W.-J., Lehne B., Li H., Liu J., Lobbens S., Luan J. a., Lyssenko V., Meitinger T., Miki T., Miljkovic I., Moon S., Mulas A., Müller G., Müller-Nurasyid M., Nagaraja R., Nauck M., Pankow J. S., Polasek O., Prokopenko I., Ramos P. S., Rasmussen-Torvik L., Rathmann W., Rich S. S., Robertson N. R., Roden M., Roussel R., Rudan I., Scott R. A., Scott W. R., Sennblad B., Siscovick D. S., Strauch K., Sun L., Swertz M., Tajuddin S. M., Taylor K. D., Teo Y.-Y., Tham Y. C., Tönjes A., Wareham N. J., Willemsen G., Wilsgaard T., Hingorani A. D., Consortium E.-C., Consortium E. P.-I., Lifelines Cohort S., Egan J., Ferrucci L., Hovingh G. K., Jula A., Kivimaki M., Kumari M., Njølstad I., Palmer C. N. A., Serrano Ríos M., Stumvoll M., Watkins H., Aung T., Blüher M., Boehnke M., Boomsma D. I., Bornstein S. R., Chambers J. C., Chasman D. I., Chen Y.-D. I., Chen Y.-T., Cheng C.-Y., Cucca F., de Geus E. J. C., Deloukas P., Evans M. K., Fornage M., Friedlander Y., Froguel P., Groop L., Gross M. D., Harris T. B., Hayward C., Heng C.-K., Ingelsson E., Kato N., Kim B.-J., Koh W.-P., Kooner J. S., Körner A., Kuh D., Kuusisto J., Laakso M., Lin X., Liu Y., Loos R. J. F., Magnusson P. K. E., März W., McCarthy M. I., Oldehinkel A. J., Ong K. K., Pedersen N. L., Pereira M. A., Peters A., Ridker P. M., Sabanayagam C., Sale M., Saleheen D., Saltevo J., Schwarz P. E., Sheu W. H. H., Snieder H., Spector T. D., Tabara Y., Tuomilehto J., van Dam R. M., Wilson J. G., Wilson J. F., Wolffenbuttel B. H. R., Wong T. Y., Wu J.-Y., Yuan J.-M., Zonderman A. B., Soranzo N., Guo X., Roberts D. J., Florez J. C., Sladek R., Dupuis J., Morris A. P., Tai E. S., Selvin E., Rotter J. I., Langenberg C., Barroso I. and Meigs J. B., "Impact of common genetic determinants of Hemoglobin A1c on type 2 diabetes risk and diagnosis in ancestrally diverse populations: A transethnic genome-wide meta-analysis," (in eng), *PLoS Med,* vol. 14, no. 9, pp. e1002383-e1002383, 2017, doi: 10.1371/journal.pmed.1002383.

[19] World Health Organization. "Diabetes." https://www.who.int/news-room/fact-sheets/detail/diabetes (accessed July 4th, 2020).

[20] McIntyre H. D., Catalano P., Zhang C., Desoye G., Mathiesen E. R., and Damm P., "Gestational diabetes mellitus," *Nature Reviews Disease Primers,* vol. 5, no. 1, p. 47, 2019/07/11 2019, doi: 10.1038/s41572-019-0098-8.

[21] Younossi Z. M., Koenig A. B., Abdelatif D., Fazel Y., Henry L., and Wymer M., "Global epidemiology of nonalcoholic fatty liver disease-Meta-analytic assessment of prevalence, incidence, and outcomes," (in eng), *Hepatology,* vol. 64, no. 1, pp. 73-84, Jul 2016, doi: 10.1002/hep.28431.

[22] Younossi Z., Anstee Q. M., Marietti M., Hardy T., Henry L., Eslam M., George J., and Bugianesi E., "Global burden of NAFLD and NASH: trends, predictions, risk factors and prevention," (in eng), *Nat Rev Gastroenterol Hepatol,* vol. 15, no. 1, pp. 11-20, Jan 2018, doi: 10.1038/nrgastro.2017.109.

[23] Estes C., Razavi H., Loomba R., Younossi Z., and Sanyal A. J., "Modeling the epidemic of nonalcoholic fatty liver disease demonstrates an exponential increase in burden of disease," (in eng), *Hepatology (Baltimore, Md.),* vol. 67, no. 1, pp. 123-133, 2018, doi: 10.1002/hep.29466.

References

[24] Chalasani N., Younossi Z., Lavine J. E., Diehl A. M., Brunt E. M., Cusi K., Charlton M., and Sanyal A. J., "The diagnosis and management of non-alcoholic fatty liver disease: practice guideline by the American Gastroenterological Association, American Association for the Study of Liver Diseases, and American College of Gastroenterology," (in eng), *Gastroenterology,* vol. 142, no. 7, pp. 1592-609, Jun 2012, doi: 10.1053/j.gastro.2012.04.001.

[25] Friedman S. L., Neuschwander-Tetri B. A., Rinella M., and Sanyal A. J., "Mechanisms of NAFLD development and therapeutic strategies," (in eng), *Nature medicine,* vol. 24, no. 7, pp. 908-922, 2018, doi: 10.1038/s41591-018-0104-9.

[26] Wainwright P. and Byrne C. D., "Bidirectional Relationships and Disconnects between NAFLD and Features of the Metabolic Syndrome," (in eng), *Int J Mol Sci,* vol. 17, no. 3, p. 367, Mar 11 2016, doi: 10.3390/ijms17030367.

[27] Kwok R., Choi K. C., Wong G. L., Zhang Y., Chan H. L., Luk A. O., Shu S. S., Chan A. W., Yeung M. W., Chan J. C., Kong A. P., and Wong V. W., "Screening diabetic patients for non-alcoholic fatty liver disease with controlled attenuation parameter and liver stiffness measurements: a prospective cohort study," (in eng), *Gut,* vol. 65, no. 8, pp. 1359-68, Aug 2016, doi: 10.1136/gutjnl-2015-309265.

[28] Portillo-Sanchez P., Bril F., Maximos M., Lomonaco R., Biernacki D., Orsak B., Subbarayan S., Webb A., Hecht J., and Cusi K., "High Prevalence of Nonalcoholic Fatty Liver Disease in Patients With Type 2 Diabetes Mellitus and Normal Plasma Aminotransferase Levels," (in eng), *The Journal of clinical endocrinology and metabolism,* vol. 100, no. 6, pp. 2231-2238, 2015, doi: 10.1210/jc.2015-1966.

[29] Younossi Z. M., Golabi P., de Avila L., Paik J. M., Srishord M., Fukui N., Qiu Y., Burns L., Afendy A., and Nader F., "The global epidemiology of NAFLD and NASH in patients with type 2 diabetes: A systematic review and meta-analysis," (in eng), *J Hepatol,* vol. 71, no. 4, pp. 793-801, Oct 2019, doi: 10.1016/j.jhep.2019.06.021.

[30] Mantovani A., Byrne C. D., Bonora E., and Targher G., "Nonalcoholic Fatty Liver Disease and Risk of Incident Type 2 Diabetes: A Meta-analysis," (in eng), *Diabetes Care,* vol. 41, no. 2, pp. 372-382, Feb 2018, doi: 10.2337/dc17-1902.

[31] Bian H., Zhu X., Xia M., Yan H., Chang X., Hu X., Pan B., Guo W., Li X., and Gao X., "Impact of type 2 diabetes on nonalcoholic steatohepatitis and advanced fibrosis in patients with nonalcoholic fatty liver disease," (in eng), *Endocr Pract,* vol. 26, no. 4, pp. 444-453, Apr 2020, doi: 10.4158/ep-2019-0342.

[32] Gupte P., Amarapurkar D., Agal S., Baijal R., Kulshrestha P., Pramanik S., Patel N., Madan A., Amarapurkar A., and Hafeezunnisa, "Non-alcoholic steatohepatitis in type 2 diabetes mellitus," (in eng), *J Gastroenterol Hepatol,* vol. 19, no. 8, pp. 854-8, Aug 2004, doi: 10.1111/j.1440-1746.2004.03312.x.

[33] Marchi J., Berg M., Dencker A., Olander E. K., and Begley C., "Risks associated with obesity in pregnancy, for the mother and baby: a systematic review of reviews," (in eng), *Obes Rev,* vol. 16, no. 8, pp. 621-38, Aug 2015, doi: 10.1111/obr.12288.

[34] de Barros Mucci D., Kusinski L. C., Wilsmore P., Loche E., Pantaleão L. C., Ashmore T. J., Blackmore H. L., Fernandez-Twinn D. S., Carmo M. d. G. T. d., and Ozanne S. E., "Impact of maternal obesity on placental transcriptome and morphology associated with fetal growth restriction in mice," *International Journal of Obesity,* vol. 44, no. 5, pp. 1087-1096, 2020/05/01 2020, doi: 10.1038/s41366-020-0561-3.

[35] Catalano P. M. and Shankar K., "Obesity and pregnancy: mechanisms of short term and long term adverse consequences for mother and child," (in eng), *BMJ,* vol. 356, pp. j1-j1, 2017, doi: 10.1136/bmj.j1.

[36] Christians J. K., Lennie K. I., Wild L. K., and Garcha R., "Effects of high-fat diets on fetal growth in rodents: a systematic review," (in eng), *Reprod Biol Endocrinol,* vol. 17, no. 1, pp. 39-39, 2019, doi: 10.1186/s12958-019-0482-y.

References

[37] Wankhade U. D., Thakali K. M., and Shankar K., "Persistent influence of maternal obesity on offspring health: Mechanisms from animal models and clinical studies," (in eng), *Molecular and cellular endocrinology,* vol. 435, pp. 7-19, Nov 5 2016, doi: 10.1016/j.mce.2016.07.001.

[38] Ye W., Luo C., Huang J., Li C., Liu Z., and Liu F., "Gestational diabetes mellitus and adverse pregnancy outcomes: systematic review and meta-analysis," (in eng), *BMJ,* vol. 377, p. e067946, May 25 2022, doi: 10.1136/bmj-2021-067946.

[39] Yu Y., Soohoo M., Sørensen H. T., Li J., and Arah O. A., "Gestational Diabetes Mellitus and the Risks of Overall and Type-Specific Cardiovascular Diseases: A Population- and Sibling-Matched Cohort Study," *Diabetes Care,* vol. 45, no. 1, pp. 151-159, 2021, doi: 10.2337/dc21-1018.

[40] Bellamy L., Casas J.-P., Hingorani A. D., and Williams D., "Type 2 diabetes mellitus after gestational diabetes: a systematic review and meta-analysis," *The Lancet,* vol. 373, no. 9677, pp. 1773-1779, 2009, doi: 10.1016/S0140-6736(09)60731-5.

[41] Weissgerber T. L. and Mudd L. M., "Preeclampsia and diabetes," (in eng), *Curr Diab Rep,* vol. 15, no. 3, p. 9, Mar 2015, doi: 10.1007/s11892-015-0579-4.

[42] Murphy H. R., Howgate C., O'Keefe J., Myers J., Morgan M., Coleman M. A., Jolly M., Valabhji J., Scott E. M., Knighton P., Young B., Lewis-Barned N., Anglioni E., Barron E., Bell R., Berry A., Cartright C., Colling S., Curley M., Duggan A., Draper L., Fargher L., Flanagan M., Hawdon J., Holt R., Kurinczuk J., Maresh M., Pinnock A., Shonegeval L., Todd D., and Tomkins N., "Characteristics and outcomes of pregnant women with type 1 or type 2 diabetes: a 5-year national population-based cohort study," *The Lancet Diabetes & Endocrinology,* vol. 9, no. 3, pp. 153-164, 2021, doi: 10.1016/S2213-8587(20)30406-X.

[43] Øyen N., Diaz L. J., Leirgul E., Boyd H. A., Priest J., Mathiesen E. R., Quertermous T., Wohlfahrt J., and Melbye M., "Prepregnancy Diabetes and Offspring Risk of Congenital Heart Disease: A Nationwide Cohort Study," (in eng), *Circulation,* vol. 133, no. 23, pp. 2243-53, Jun 7 2016, doi: 10.1161/circulationaha.115.017465.

[44] Ornoy A., Reece E. A., Pavlinkova G., Kappen C., and Miller R. K., "Effect of maternal diabetes on the embryo, fetus, and children: Congenital anomalies, genetic and epigenetic changes and developmental outcomes," *Birth Defects Research Part C: Embryo Today: Reviews,* vol. 105, no. 1, pp. 53-72, 2015, doi: 10.1002/bdrc.21090.

[45] The HAPO Study Cooperative Research Group, "Hyperglycemia and Adverse Pregnancy Outcomes," *New England Journal of Medicine,* vol. 358, no. 19, pp. 1991-2002, 2008/05/08 2008, doi: 10.1056/NEJMoa0707943.

[46] Gutierrez J. C., Hrubec T. C., Prater M. R., Smith B. J., Freeman L. E., and Holladay S. D., "Aortic and ventricular dilation and myocardial reduction in gestation day 17 ICR mouse fetuses of diabetic mothers," (in eng), *Birth defects research. Part A, Clinical and molecular teratology,* vol. 79, no. 6, pp. 459-64, Jun 2007, doi: 10.1002/bdra.20357.

[47] Morgan S. C., Relaix F., Sandell L. L., and Loeken M. R., "Oxidative stress during diabetic pregnancy disrupts cardiac neural crest migration and causes outflow tract defects," (in eng), *Birth defects research. Part A, Clinical and molecular teratology,* vol. 82, no. 6, pp. 453-63, Jun 2008, doi: 10.1002/bdra.20457.

[48] Kumar S. D., Dheen S. T., and Tay S. S., "Maternal diabetes induces congenital heart defects in mice by altering the expression of genes involved in cardiovascular development," (in eng), *Cardiovascular diabetology,* vol. 6, p. 34, Oct 30 2007, doi: 10.1186/1475-2840-6-34.

[49] Toboła-Wróbel K., Pietryga M., Dydowicz P., Napierała M., Brązert J., and Florek E., "Association of Oxidative Stress on Pregnancy," (in eng), *Oxid Med Cell Longev,* vol. 2020, p. 6398520, 2020, doi: 10.1155/2020/6398520.

References

[50] McMurray F., Patten D. A., and Harper M. E., "Reactive Oxygen Species and Oxidative Stress in Obesity-Recent Findings and Empirical Approaches," (in eng), *Obesity (Silver Spring),* vol. 24, no. 11, pp. 2301-2310, Nov 2016, doi: 10.1002/oby.21654.

[51] Volpe C. M. O., Villar-Delfino P. H., dos Anjos P. M. F., and Nogueira-Machado J. A., "Cellular death, reactive oxygen species (ROS) and diabetic complications," *Cell Death & Disease,* vol. 9, no. 2, p. 119, 2018/01/25 2018, doi: 10.1038/s41419-017-0135-z.

[52] Joo E. H., Kim Y. R., Kim N., Jung J. E., Han S. H., and Cho H. Y., "Effect of Endogenic and Exogenic Oxidative Stress Triggers on Adverse Pregnancy Outcomes: Preeclampsia, Fetal Growth Restriction, Gestational Diabetes Mellitus and Preterm Birth," (in eng), *Int J Mol Sci,* vol. 22, no. 18, Sep 19 2021, doi: 10.3390/ijms221810122.

[53] Chiarello D. I., Abad C., Rojas D., Toledo F., Vázquez C. M., Mate A., Sobrevia L., and Marín R., "Oxidative stress: Normal pregnancy versus preeclampsia," *Biochimica et Biophysica Acta (BBA) - Molecular Basis of Disease,* vol. 1866, no. 2, p. 165354, 2020/02/01/ 2020, doi: https://doi.org/10.1016/j.bbadis.2018.12.005.

[54] Forrester S. J., Kikuchi D. S., Hernandes M. S., Xu Q., and Griendling K. K., "Reactive Oxygen Species in Metabolic and Inflammatory Signaling," (in eng), *Circ Res,* vol. 122, no. 6, pp. 877-902, 2018, doi: 10.1161/CIRCRESAHA.117.311401.

[55] Buvelot H., Jaquet V., and Krause K. H., "Mammalian NADPH Oxidases," (in eng), *Methods Mol Biol,* vol. 1982, pp. 17-36, 2019, doi: 10.1007/978-1-4939-9424-3_2.

[56] Ray P. D., Huang B.-W., and Tsuji Y., "Reactive oxygen species (ROS) homeostasis and redox regulation in cellular signaling," (in eng), *Cell Signal,* vol. 24, no. 5, pp. 981-990, 2012, doi: 10.1016/j.cellsig.2012.01.008.

[57] Yang Y., Bazhin A. V., Werner J., and Karakhanova S., "Reactive oxygen species in the immune system," (in eng), *Int Rev Immunol,* vol. 32, no. 3, pp. 249-70, Jun 2013, doi: 10.3109/08830185.2012.755176.

[58] Villalpando-Rodriguez G. E. and Gibson S. B., "Reactive Oxygen Species (ROS) Regulates Different Types of Cell Death by Acting as a Rheostat," (in eng), *Oxid Med Cell Longev,* vol. 2021, p. 9912436, 2021, doi: 10.1155/2021/9912436.

[59] Kehrer J. P., "The Haber-Weiss reaction and mechanisms of toxicity," *Toxicology,* vol. 149, no. 1, pp. 43-50, Aug 14 2000. [Online]. Available: http://www.ncbi.nlm.nih.gov/pubmed/10963860.

[60] Haber F. W. J., "Über die Katalyse des Hydroperoxydes " *Naturwissenschaften,* vol. 20, no. 51, pp. 948-950, 1932.

[61] Droge W., "Free radicals in the physiological control of cell function," *Physiological reviews,* vol. 82, no. 1, pp. 47-95, Jan 2002, doi: 10.1152/physrev.00018.2001.

[62] Fenton H. J. H., "Oxidation of tartaric acid in presence of iron," *Journal of the Chemical Society, Transactions,* vol. 65, pp. 899-910, 1894.

[63] Bedard K. and Krause K. H., "The NOX family of ROS-generating NADPH oxidases: physiology and pathophysiology," (in eng), *Physiol Rev,* vol. 87, no. 1, pp. 245-313, Jan 2007, doi: 10.1152/physrev.00044.2005.

[64] Babior B. M., Kipnes R. S., and Curnutte J. T., "Biological defense mechanisms. The production by leukocytes of superoxide, a potential bactericidal agent," (in eng), *J Clin Invest,* vol. 52, no. 3, pp. 741-4, Mar 1973, doi: 10.1172/jci107236.

[65] Petry A., Weitnauer M., and Görlach A., "Receptor activation of NADPH oxidases," (in eng), *Antioxid Redox Signal,* vol. 13, no. 4, pp. 467-87, Aug 15 2010, doi: 10.1089/ars.2009.3026.

[66] Groemping Y. and Rittinger K., "Activation and assembly of the NADPH oxidase: a structural perspective," (in eng), *Biochem J,* vol. 386, no. Pt 3, pp. 401-16, Mar 15 2005, doi: 10.1042/bj20041835.

[67] Suh Y. A., Arnold R. S., Lassegue B., Shi J., Xu X., Sorescu D., Chung A. B., Griendling K. K., and Lambeth J. D., "Cell transformation by the superoxide-generating oxidase Mox1," (in eng), *Nature,* vol. 401, no. 6748, pp. 79-82, Sep 2 1999, doi: 10.1038/43459.

[68] Cheng G., Cao Z., Xu X., van Meir E. G., and Lambeth J. D., "Homologs of gp91phox: cloning and tissue expression of Nox3, Nox4, and Nox5," (in eng), *Gene,* vol. 269, no. 1-2, pp. 131-40, May 16 2001, doi: 10.1016/s0378-1119(01)00449-8.

[69] De Deken X., Wang D., Many M. C., Costagliola S., Libert F., Vassart G., Dumont J. E., and Miot F., "Cloning of two human thyroid cDNAs encoding new members of the NADPH oxidase family," (in eng), *J Biol Chem,* vol. 275, no. 30, pp. 23227-33, Jul 28 2000, doi: 10.1074/jbc.M000916200.

[70] Petry A., "Characterization of novel NADPH oxidases in endothelial cells under basal and stress conditions," Fakultät für Chemie und Pharmazie der Ludwig-Maximilians-Universität München, LMU Munich, 2009. [Online]. Available: http://nbn-resolving.de/urn:nbn:de:bvb:19-108225

[71] Weaver J. R. and Taylor-Fishwick D. A., "Role of NADPH Oxidase in Beta Cell Dysfunction," in *Islets of Langerhans, 2. ed.*, M. S. Islam Ed. Dordrecht: Springer Netherlands, 2013, pp. 1-29.

[72] Heyworth P. G., Cross A. R., and Curnutte J. T., "Chronic granulomatous disease," (in eng), *Curr Opin Immunol,* vol. 15, no. 5, pp. 578-84, Oct 2003, doi: 10.1016/s0952-7915(03)00109-2.

[73] Takeya R., Ueno N., Kami K., Taura M., Kohjima M., Izaki T., Nunoi H., and Sumimoto H., "Novel human homologues of p47phox and p67phox participate in activation of superoxide-producing NADPH oxidases," (in eng), *J Biol Chem,* vol. 278, no. 27, pp. 25234-46, Jul 4 2003, doi: 10.1074/jbc.M212856200.

[74] Bánfi B., Malgrange B., Knisz J., Steger K., Dubois-Dauphin M., and Krause K. H., "NOX3, a superoxide-generating NADPH oxidase of the inner ear," (in eng), *J Biol Chem,* vol. 279, no. 44, pp. 46065-72, Oct 29 2004, doi: 10.1074/jbc.M403046200.

[75] Paffenholz R., Bergstrom R. A., Pasutto F., Wabnitz P., Munroe R. J., Jagla W., Heinzmann U., Marquardt A., Bareiss A., Laufs J., Russ A., Stumm G., Schimenti J. C., and Bergstrom D. E., "Vestibular defects in head-tilt mice result from mutations in Nox3, encoding an NADPH oxidase," (in eng), *Genes Dev,* vol. 18, no. 5, pp. 486-91, Mar 1 2004, doi: 10.1101/gad.1172504.

[76] Geiszt M., Kopp J. B., Várnai P., and Leto T. L., "Identification of renox, an NAD(P)H oxidase in kidney," (in eng), *Proc Natl Acad Sci U S A,* vol. 97, no. 14, pp. 8010-4, Jul 5 2000, doi: 10.1073/pnas.130135897.

[77] Shiose A., Kuroda J., Tsuruya K., Hirai M., Hirakata H., Naito S., Hattori M., Sakaki Y., and Sumimoto H., "A novel superoxide-producing NAD(P)H oxidase in kidney," (in eng), *J Biol Chem,* vol. 276, no. 2, pp. 1417-23, Jan 12 2001, doi: 10.1074/jbc.M007597200.

[78] Nisimoto Y., Diebold B. A., Cosentino-Gomes D., and Lambeth J. D., "Nox4: a hydrogen peroxide-generating oxygen sensor," (in eng), *Biochemistry,* vol. 53, no. 31, pp. 5111-20, Aug 12 2014, doi: 10.1021/bi500331y.

[79] Bánfi B., Molnár G., Maturana A., Steger K., Hegedûs B., Demaurex N., and Krause K. H., "A Ca(2+)-activated NADPH oxidase in testis, spleen, and lymph nodes," (in eng), *J Biol Chem,* vol. 276, no. 40, pp. 37594-601, Oct 5 2001, doi: 10.1074/jbc.M103034200.

[80] Fulton D. J., "Nox5 and the regulation of cellular function," (in eng), *Antioxid Redox Signal,* vol. 11, no. 10, pp. 2443-52, Oct 2009, doi: 10.1089/ars.2009.2587.

[81] Bánfi B., Tirone F., Durussel I., Knisz J., Moskwa P., Molnár G. Z., Krause K. H., and Cox J. A., "Mechanism of Ca2+ activation of the NADPH oxidase 5 (NOX5)," (in eng), *J Biol Chem,* vol. 279, no. 18, pp. 18583-91, Apr 30 2004, doi: 10.1074/jbc.M310268200.

[82] BelAiba R. S., Djordjevic T., Petry A., Diemer K., Bonello S., Banfi B., Hess J., Pogrebniak A., Bickel C., and Görlach A., "NOX5 variants are functionally active in

endothelial cells," (in eng), *Free Radic Biol Med,* vol. 42, no. 4, pp. 446-59, Feb 15 2007, doi: 10.1016/j.freeradbiomed.2006.10.054.

[83] Lambeth J. D., Kawahara T., and Diebold B., "Regulation of Nox and Duox enzymatic activity and expression," (in eng), *Free Radic Biol Med,* vol. 43, no. 3, pp. 319-31, Aug 1 2007, doi: 10.1016/j.freeradbiomed.2007.03.028.

[84] Wang D., De Deken X., Milenkovic M., Song Y., Pirson I., Dumont J. E., and Miot F., "Identification of a novel partner of duox: EFP1, a thioredoxin-related protein," (in eng), *J Biol Chem,* vol. 280, no. 4, pp. 3096-103, Jan 28 2005, doi: 10.1074/jbc.M407709200.

[85] Dupuy C., Kaniewski J., Dème D., Pommier J., and Virion A., "NADPH-dependent H2O2 generation catalyzed by thyroid plasma membranes. Studies with electron scavengers," (in eng), *Eur J Biochem,* vol. 185, no. 3, pp. 597-603, Nov 20 1989, doi: 10.1111/j.1432-1033.1989.tb15155.x.

[86] Forteza R., Salathe M., Miot F., Forteza R., and Conner G. E., "Regulated hydrogen peroxide production by Duox in human airway epithelial cells," (in eng), *Am J Respir Cell Mol Biol,* vol. 32, no. 5, pp. 462-9, May 2005, doi: 10.1165/rcmb.2004-0302OC.

[87] Kawahara T., Ritsick D., Cheng G., and Lambeth J. D., "Point mutations in the proline-rich region of p22phox are dominant inhibitors of Nox1- and Nox2-dependent reactive oxygen generation," (in eng), *J Biol Chem,* vol. 280, no. 36, pp. 31859-69, Sep 9 2005, doi: 10.1074/jbc.M501882200.

[88] Ambasta R. K., Kumar P., Griendling K. K., Schmidt H. H., Busse R., and Brandes R. P., "Direct interaction of the novel Nox proteins with p22phox is required for the formation of a functionally active NADPH oxidase," (in eng), *J Biol Chem,* vol. 279, no. 44, pp. 45935-41, Oct 29 2004, doi: 10.1074/jbc.M406486200.

[89] Martyn K. D., Frederick L. M., von Loehneysen K., Dinauer M. C., and Knaus U. G., "Functional analysis of Nox4 reveals unique characteristics compared to other NADPH oxidases," (in eng), *Cell Signal,* vol. 18, no. 1, pp. 69-82, Jan 2006, doi: 10.1016/j.cellsig.2005.03.023.

[90] Prior K.-K., Leisegang M. S., Josipovic I., Löwe O., Shah A. M., Weissmann N., Schröder K., and Brandes R. P., "CRISPR/Cas9-mediated knockout of p22phox leads to loss of Nox1 and Nox4, but not Nox5 activity," *Redox Biology,* vol. 9, pp. 287-295, 2016/10/01/ 2016, doi: https://doi.org/10.1016/j.redox.2016.08.013.

[91] Huang J., Hitt N. D., and Kleinberg M. E., "Stoichiometry of p22-phox and gp91-phox in phagocyte cytochrome b558," (in eng), *Biochemistry,* vol. 34, no. 51, pp. 16753-7, Dec 26 1995, doi: 10.1021/bi00051a024.

[92] Dinauer M. C., Pierce E. A., Bruns G. A., Curnutte J. T., and Orkin S. H., "Human neutrophil cytochrome b light chain (p22-phox). Gene structure, chromosomal location, and mutations in cytochrome-negative autosomal recessive chronic granulomatous disease," (in eng), *J Clin Invest,* vol. 86, no. 5, pp. 1729-37, Nov 1990, doi: 10.1172/jci114898.

[93] Parkos C. A., Dinauer M. C., Walker L. E., Allen R. A., Jesaitis A. J., and Orkin S. H., "Primary structure and unique expression of the 22-kilodalton light chain of human neutrophil cytochrome b," (in eng), *Proceedings of the National Academy of Sciences of the United States of America,* vol. 85, no. 10, pp. 3319-3323, 1988, doi: 10.1073/pnas.85.10.3319.

[94] Azumi H., Inoue N., Takeshita S., Rikitake Y., Kawashima S., Hayashi Y., Itoh H., and Yokoyama M., "Expression of NADH/NADPH oxidase p22phox in human coronary arteries," (in eng), *Circulation,* vol. 100, no. 14, pp. 1494-8, Oct 5 1999, doi: 10.1161/01.cir.100.14.1494.

[95] Wu J. S., Tsai H. D., Cheung W. M., Hsu C. Y., and Lin T. N., "PPAR-γ Ameliorates Neuronal Apoptosis and Ischemic Brain Injury via Suppressing NF-κB-Driven p22phox

Transcription," (in eng), *Mol Neurobiol,* vol. 53, no. 6, pp. 3626-3645, Aug 2016, doi: 10.1007/s12035-015-9294-z.

[96] Ameziane-El-Hassani R., Morand S., Boucher J. L., Frapart Y. M., Apostolou D., Agnandji D., Gnidehou S., Ohayon R., Noël-Hudson M. S., Francon J., Lalaoui K., Virion A., and Dupuy C., "Dual oxidase-2 has an intrinsic Ca2+-dependent H2O2-generating activity," (in eng), *J Biol Chem,* vol. 280, no. 34, pp. 30046-54, Aug 26 2005, doi: 10.1074/jbc.M500516200.

[97] De Deken X., Wang D., Dumont J. E., and Miot F., "Characterization of ThOX proteins as components of the thyroid H(2)O(2)-generating system," (in eng), *Exp Cell Res,* vol. 273, no. 2, pp. 187-96, Feb 15 2002, doi: 10.1006/excr.2001.5444.

[98] Turrens J. F., "Mitochondrial formation of reactive oxygen species," (in eng), *J Physiol,* vol. 552, no. Pt 2, pp. 335-44, Oct 15 2003, doi: 10.1113/jphysiol.2003.049478.

[99] Addabbo F., Montagnani M., and Goligorsky M. S., "Mitochondria and reactive oxygen species," (in eng), *Hypertension,* vol. 53, no. 6, pp. 885-892, 2009, doi: 10.1161/HYPERTENSIONAHA.109.130054.

[100] Wang W., Fang H., Groom L., Cheng A., Zhang W., Liu J., Wang X., Li K., Han P., Zheng M., Yin J., Wang W., Mattson M. P., Kao J. P., Lakatta E. G., Sheu S. S., Ouyang K., Chen J., Dirksen R. T., and Cheng H., "Superoxide flashes in single mitochondria," (in eng), *Cell,* vol. 134, no. 2, pp. 279-90, Jul 25 2008, doi: 10.1016/j.cell.2008.06.017.

[101] Lenaz G., "Mitochondria and reactive oxygen species. Which role in physiology and pathology?," (in eng), *Adv Exp Med Biol,* vol. 942, pp. 93-136, 2012, doi: 10.1007/978-94-007-2869-1_5.

[102] Lambert A. J. and Brand M. D., "Reactive oxygen species production by mitochondria," (in eng), *Methods Mol Biol,* vol. 554, pp. 165-81, 2009, doi: 10.1007/978-1-59745-521-3_11.

[103] Görlach A., Dimova E. Y., Petry A., Martínez-Ruiz A., Hernansanz-Agustín P., Rolo A. P., Palmeira C. M., and Kietzmann T., "Reactive oxygen species, nutrition, hypoxia and diseases: Problems solved?," (in eng), *Redox Biol,* vol. 6, pp. 372-385, Dec 2015, doi: 10.1016/j.redox.2015.08.016.

[104] Poderoso J. J., Carreras M. C., Lisdero C., Riobó N., Schöpfer F., and Boveris A., "Nitric oxide inhibits electron transfer and increases superoxide radical production in rat heart mitochondria and submitochondrial particles," (in eng), *Arch Biochem Biophys,* vol. 328, no. 1, pp. 85-92, Apr 1 1996, doi: 10.1006/abbi.1996.0146.

[105] Quinlan C. L., Goncalves R. L. S., Hey-Mogensen M., Yadava N., Bunik V. I., and Brand M. D., "The 2-oxoacid dehydrogenase complexes in mitochondria can produce superoxide/hydrogen peroxide at much higher rates than complex I," (in eng), *The Journal of biological chemistry,* vol. 289, no. 12, pp. 8312-8325, 2014, doi: 10.1074/jbc.M113.545301.

[106] Tretter L. and Adam-Vizi V., "Generation of reactive oxygen species in the reaction catalyzed by alpha-ketoglutarate dehydrogenase," (in eng), *J Neurosci,* vol. 24, no. 36, pp. 7771-7778, 2004, doi: 10.1523/JNEUROSCI.1842-04.2004.

[107] Kaludercic N., Deshwal S., and Di Lisa F., "Reactive oxygen species and redox compartmentalization," (in eng), *Front Physiol,* vol. 5, pp. 285-285, 2014, doi: 10.3389/fphys.2014.00285.

[108] Elsner M., Gehrmann W., and Lenzen S., "Peroxisome-generated hydrogen peroxide as important mediator of lipotoxicity in insulin-producing cells," (in eng), *Diabetes,* vol. 60, no. 1, pp. 200-8, Jan 2011, doi: 10.2337/db09-1401.

[109] Furukawa S., Fujita T., Shimabukuro M., Iwaki M., Yamada Y., Nakajima Y., Nakayama O., Makishima M., Matsuda M., and Shimomura I., "Increased oxidative stress in obesity and its impact on metabolic syndrome," (in eng), *The Journal of clinical investigation,* vol. 114, no. 12, pp. 1752-1761, 2004, doi: 10.1172/JCI21625.

[110] Giacco F. and Brownlee M., "Oxidative stress and diabetic complications," (in eng), *Circ Res,* vol. 107, no. 9, pp. 1058-70, Oct 29 2010, doi: 10.1161/circresaha.110.223545.
[111] Förstermann U., "Oxidative stress in vascular disease: causes, defense mechanisms and potential therapies," *Nature Clinical Practice Cardiovascular Medicine,* vol. 5, no. 6, pp. 338-349, 2008/06/01 2008, doi: 10.1038/ncpcardio1211.
[112] de Mello A. H., Costa A. B., Engel J. D. G., and Rezin G. T., "Mitochondrial dysfunction in obesity," (in eng), *Life Sci,* vol. 192, pp. 26-32, Jan 1 2018, doi: 10.1016/j.lfs.2017.11.019.
[113] Bonnard C., Durand A., Peyrol S., Chanseaume E., Chauvin M. A., Morio B., Vidal H., and Rieusset J., "Mitochondrial dysfunction results from oxidative stress in the skeletal muscle of diet-induced insulin-resistant mice," (in eng), *J Clin Invest,* vol. 118, no. 2, pp. 789-800, Feb 2008, doi: 10.1172/jci32601.
[114] Hastie R. and Lappas M., "The effect of pre-existing maternal obesity and diabetes on placental mitochondrial content and electron transport chain activity," (in eng), *Placenta,* vol. 35, no. 9, pp. 673-83, Sep 2014, doi: 10.1016/j.placenta.2014.06.368.
[115] Chen J. X. and Stinnett A., "Critical role of the NADPH oxidase subunit p47phox on vascular TLR expression and neointimal lesion formation in high-fat diet-induced obesity," (in eng), *Lab Invest,* vol. 88, no. 12, pp. 1316-28, Dec 2008, doi: 10.1038/labinvest.2008.92.
[116] Marchesi C., Ebrahimian T., Angulo O., Paradis P., and Schiffrin E. L., "Endothelial nitric oxide synthase uncoupling and perivascular adipose oxidative stress and inflammation contribute to vascular dysfunction in a rodent model of metabolic syndrome," (in eng), *Hypertension,* vol. 54, no. 6, pp. 1384-92, Dec 2009, doi: 10.1161/hypertensionaha.109.138305.
[117] Diano S., Liu Z. W., Jeong J. K., Dietrich M. O., Ruan H. B., Kim E., Suyama S., Kelly K., Gyengesi E., Arbiser J. L., Belsham D. D., Sarruf D. A., Schwartz M. W., Bennett A. M., Shanabrough M., Mobbs C. V., Yang X., Gao X. B., and Horvath T. L., "Peroxisome proliferation-associated control of reactive oxygen species sets melanocortin tone and feeding in diet-induced obesity," (in eng), *Nat Med,* vol. 17, no. 9, pp. 1121-7, Aug 28 2011, doi: 10.1038/nm.2421.
[118] Evans J. L., Goldfine I. D., Maddux B. A., and Grodsky G. M., "Oxidative stress and stress-activated signaling pathways: a unifying hypothesis of type 2 diabetes," (in eng), *Endocr Rev,* vol. 23, no. 5, pp. 599-622, Oct 2002, doi: 10.1210/er.2001-0039.
[119] Houstis N., Rosen E. D., and Lander E. S., "Reactive oxygen species have a causal role in multiple forms of insulin resistance," (in eng), *Nature,* vol. 440, no. 7086, pp. 944-8, Apr 13 2006, doi: 10.1038/nature04634.
[120] Kaneto H., Katakami N., Matsuhisa M., and Matsuoka T.-a., "Role of reactive oxygen species in the progression of type 2 diabetes and atherosclerosis," (in eng), *Mediators Inflamm,* vol. 2010, pp. 453892-453892, 2010, doi: 10.1155/2010/453892.
[121] Gerber P. A. and Rutter G. A., "The Role of Oxidative Stress and Hypoxia in Pancreatic Beta-Cell Dysfunction in Diabetes Mellitus," (in eng), *Antioxidants & redox signaling,* vol. 26, no. 10, pp. 501-518, 2017, doi: 10.1089/ars.2016.6755.
[122] Robertson R. P., "Chronic oxidative stress as a central mechanism for glucose toxicity in pancreatic islet beta cells in diabetes," (in eng), *J Biol Chem,* vol. 279, no. 41, pp. 42351-4, Oct 8 2004, doi: 10.1074/jbc.R400019200.
[123] Robertson R. P., Harmon J., Tran P. O., Tanaka Y., and Takahashi H., "Glucose toxicity in beta-cells: type 2 diabetes, good radicals gone bad, and the glutathione connection," (in eng), *Diabetes,* vol. 52, no. 3, pp. 581-7, Mar 2003, doi: 10.2337/diabetes.52.3.581.
[124] Ihara Y., Toyokuni S., Uchida K., Odaka H., Tanaka T., Ikeda H., Hiai H., Seino Y., and Yamada Y., "Hyperglycemia causes oxidative stress in pancreatic beta-cells of GK rats,

a model of type 2 diabetes," (in eng), *Diabetes,* vol. 48, no. 4, pp. 927-32, Apr 1999, doi: 10.2337/diabetes.48.4.927.

[125] Carlsson C., Borg L. A., and Welsh N., "Sodium palmitate induces partial mitochondrial uncoupling and reactive oxygen species in rat pancreatic islets in vitro," (in eng), *Endocrinology,* vol. 140, no. 8, pp. 3422-8, Aug 1999, doi: 10.1210/endo.140.8.6908.

[126] Joseph J. W., Koshkin V., Saleh M. C., Sivitz W. I., Zhang C. Y., Lowell B. B., Chan C. B., and Wheeler M. B., "Free fatty acid-induced beta-cell defects are dependent on uncoupling protein 2 expression," (in eng), *J Biol Chem,* vol. 279, no. 49, pp. 51049-56, Dec 3 2004, doi: 10.1074/jbc.M409189200.

[127] Wang X., Li H., De Leo D., Guo W., Koshkin V., Fantus I. G., Giacca A., Chan C. B., Der S., and Wheeler M. B., "Gene and protein kinase expression profiling of reactive oxygen species-associated lipotoxicity in the pancreatic beta-cell line MIN6," (in eng), *Diabetes,* vol. 53, no. 1, pp. 129-40, Jan 2004, doi: 10.2337/diabetes.53.1.129.

[128] Nakano Y., Longo-Guess C. M., Bergstrom D. E., Nauseef W. M., Jones S. M., and Banfi B., "Mutation of the Cyba gene encoding p22phox causes vestibular and immune defects in mice," *J Clin Invest,* vol. 118, no. 3, pp. 1176-85, Mar 2008, doi: 10.1172/JCI33835.

[129] Simson E. L. and Gold R. M., "The lee obesity index vindicated?," *Physiology & Behavior,* vol. 29, no. 2, pp. 371-376, 1982/08/01/ 1982, doi: https://doi.org/10.1016/0031-9384(82)90028-2.

[130] Mouse Metabolic Phenotyping Centers. "Intraperitoneal Insulin Tolerance Test." https://mmpc.org/shared/document.aspx?id=84&doctype=Protocol (accessed April 19, 2020).

[131] Mahany E. B., Han X., Borges B. C., da Silveira Cruz-Machado S., Allen S. J., Garcia-Galiano D., Hoenerhoff M. J., Bellefontaine N. H., and Elias C. F., "Obesity and High-Fat Diet Induce Distinct Changes in Placental Gene Expression and Pregnancy Outcome," (in eng), *Endocrinology,* vol. 159, no. 4, pp. 1718-1733, Apr 1 2018, doi: 10.1210/en.2017-03053.

[132] Lowe J. S. and Anderson P. G., "Chapter 1 - Histology," in *Stevens & Lowe's Human Histology (Fourth Edition) (Fourth Edition)*, J. S. Lowe and P. G. Anderson Eds. Philadelphia: Mosby, 2015, pp. 1-10.

[133] Nakata T. and Suzuki N., "Chromogen-based immunohistochemical method for elucidation of the coexpression of two antigens using antibodies from the same species," (in eng), *The journal of histochemistry and cytochemistry : official journal of the Histochemistry Society,* vol. 60, no. 8, pp. 611-619, 2012, doi: 10.1369/0022155412449348.

[134] Guirado R., Carceller H., Castillo-Gómez E., Castrén E., and Nacher J., "Automated analysis of images for molecular quantification in immunohistochemistry," (in eng), *Heliyon,* vol. 4, no. 6, pp. e00669-e00669, 2018, doi: 10.1016/j.heliyon.2018.e00669.

[135] Kracun D., Riess F., Kanchev I., Gawaz M., and Gorlach A., "The beta3-integrin binding protein beta3-endonexin is a novel negative regulator of hypoxia-inducible factor-1," *Antioxidants & redox signaling,* vol. 20, no. 13, pp. 1964-76, May 01 2014, doi: 10.1089/ars.2013.5286.

[136] Chan J. K., "The wonderful colors of the hematoxylin-eosin stain in diagnostic surgical pathology," (in eng), *Int J Surg Pathol,* vol. 22, no. 1, pp. 12-32, Feb 2014, doi: 10.1177/1066896913517939.

[137] Junqueira L. C., Bignolas G., and Brentani R. R., "Picrosirius staining plus polarization microscopy, a specific method for collagen detection in tissue sections," (in eng), *Histochem J,* vol. 11, no. 4, pp. 447-55, Jul 1979, doi: 10.1007/bf01002772.

[138] Adamo C. "PicroSirius Red Stain for Collagen." https://med.emory.edu/departments/medicine/divisions/cardiology/research/labs/micros

copy-in-medicine/_documents/picrosirius-red-stain-collagen.pdf (accessed April 18, 2020).

[139] Mehlem A., Hagberg C., Muhl L., and Falkevall A., "Imaging of neutral lipids by oil red O for analyzing the metabolic status in health and disease," *Nature protocols,* vol. 8, pp. 1149-1154, 05/23 2013, doi: 10.1038/nprot.2013.055.

[140] Heydemann A., "An Overview of Murine High Fat Diet as a Model for Type 2 Diabetes Mellitus," (in eng), *J Diabetes Res,* vol. 2016, pp. 2902351-2902351, 2016, doi: 10.1155/2016/2902351.

[141] Small L., Brandon A. E., Turner N., and Cooney G. J., "Modeling insulin resistance in rodents by alterations in diet: what have high-fat and high-calorie diets revealed?," (in eng), *Am J Physiol Endocrinol Metab,* vol. 314, no. 3, pp. E251-e265, Mar 1 2018, doi: 10.1152/ajpendo.00337.2017.

[142] Islam M. S. and Loots du T., "Experimental rodent models of type 2 diabetes: a review," (in eng), *Methods Find Exp Clin Pharmacol,* vol. 31, no. 4, pp. 249-61, May 2009, doi: 10.1358/mf.2009.31.4.1362513.

[143] Jannasch F., Kröger J., and Schulze M. B., "Dietary Patterns and Type 2 Diabetes: A Systematic Literature Review and Meta-Analysis of Prospective Studies," (in eng), *J Nutr,* vol. 147, no. 6, pp. 1174-1182, Jun 2017, doi: 10.3945/jn.116.242552.

[144] Chang Y., Jung H.-S., Cho J., Zhang Y., Yun K. E., Lazo M., Pastor-Barriuso R., Ahn J., Kim C.-W., Rampal S., Cainzos-Achirica M., Zhao D., Chung E. C., Shin H., Guallar E., and Ryu S., "Metabolically Healthy Obesity and the Development of Nonalcoholic Fatty Liver Disease," *Official journal of the American College of Gastroenterology | ACG,* vol. 111, no. 8, 2016. [Online]. Available: https://journals.lww.com/ajg/Fulltext/2016/08000/Metabolically_Healthy_Obesity_and_the_Development.19.aspx.

[145] Kasai H., "Analysis of a form of oxidative DNA damage, 8-hydroxy-2′-deoxyguanosine, as a marker of cellular oxidative stress during carcinogenesis," *Mutation Research/Reviews in Mutation Research,* vol. 387, no. 3, pp. 147-163, 1997/12/01/ 1997, doi: https://doi.org/10.1016/S1383-5742(97)00035-5.

[146] Matsuda Y., Itoh T., Itoh H., Ogawa M., Sasaki K., Kanayama N., and Matsubara S., "Impact of placental weight and fetal/placental weight ratio Z score on fetal growth and the perinatal outcome," (in eng), *Int J Med Sci,* vol. 15, no. 5, pp. 484-491, 2018, doi: 10.7150/ijms.23107.

[147] Hayes E. K., Lechowicz A., Petrik J. J., Storozhuk Y., Paez-Parent S., Dai Q., Samjoo I. A., Mansell M., Gruslin A., Holloway A. C., and Raha S., "Adverse fetal and neonatal outcomes associated with a life-long high fat diet: role of altered development of the placental vasculature," (in eng), *PLoS One,* vol. 7, no. 3, p. e33370, 2012, doi: 10.1371/journal.pone.0033370.

[148] Sgambati E., Biagiotti R., Marini M., and Brizzi E., "Lectin Histochemistry in the Human Placenta of Pregnancies Complicated by Intrauterine Growth Retardation Based on Absent or Reversed Diastolic Flow," *Placenta,* vol. 23, no. 6, pp. 503-515, 2002/07/01/ 2002, doi: https://doi.org/10.1053/plac.2002.0793.

[149] Akison L. K., Nitert M. D., Clifton V. L., Moritz K. M., and Simmons D. G., "Review: Alterations in placental glycogen deposition in complicated pregnancies: Current preclinical and clinical evidence," *Placenta,* vol. 54, pp. 52-58, 2017/06/01/ 2017, doi: https://doi.org/10.1016/j.placenta.2017.01.114.

[150] Tunster S. J., Watson E. D., Fowden A. L., and Burton G. J., "Placental glycogen stores and fetal growth: insights from genetic mouse models," (in eng), *Reproduction,* vol. 159, no. 6, pp. R213-r235, Jun 2020, doi: 10.1530/rep-20-0007.

[151] Desoye G., Korgun E. T., Ghaffari-Tabrizi N., and Hahn T., "Is fetal macrosomia in adequately controlled diabetic women the result of a placental defect?--a hypothesis," (in

eng), *J Matern Fetal Neonatal Med,* vol. 11, no. 4, pp. 258-61, Apr 2002, doi: 10.1080/jmf.11.4.258.261.

[152] Gruppuso P. A. and Sanders J. A., "Regulation of liver development: implications for liver biology across the lifespan," (in eng), *J Mol Endocrinol,* vol. 56, no. 3, pp. R115-25, Apr 2016, doi: 10.1530/jme-15-0313.

[153] Gregoire F. M., Zhang Q., Smith S. J., Tong C., Ross D., Lopez H., and West D. B., "Diet-induced obesity and hepatic gene expression alterations in C57BL/6J and ICAM-1-deficient mice," (in eng), *Am J Physiol Endocrinol Metab,* vol. 282, no. 3, pp. E703-13, Mar 2002, doi: 10.1152/ajpendo.00072.2001.

[154] Podrini C., Cambridge E. L., Lelliott C. J., Carragher D. M., Estabel J., Gerdin A. K., Karp N. A., Scudamore C. L., Ramirez-Solis R., and White J. K., "High-fat feeding rapidly induces obesity and lipid derangements in C57BL/6N mice," (in eng), *Mamm Genome,* vol. 24, no. 5-6, pp. 240-51, Jun 2013, doi: 10.1007/s00335-013-9456-0.

[155] West D. B., Boozer C. N., Moody D. L., and Atkinson R. L., "Dietary obesity in nine inbred mouse strains," (in eng), *Am J Physiol,* vol. 262, no. 6 Pt 2, pp. R1025-32, Jun 1992, doi: 10.1152/ajpregu.1992.262.6.R1025.

[156] Vuguin P. M., Hartil K., Kruse M., Kaur H., Lin C. L., Fiallo A., Glenn A. S., Patel A., Williams L., Seki Y., Katz E. B., and Charron M. J., "Shared effects of genetic and intrauterine and perinatal environment on the development of metabolic syndrome," (in eng), *PLoS One,* vol. 8, no. 5, p. e63021, 2013, doi: 10.1371/journal.pone.0063021.

[157] Hartil K., Vuguin P. M., Kruse M., Schmuel E., Fiallo A., Vargas C., Warner M. J., Durand J. L., Jelicks L. A., and Charron M. J., "Maternal substrate utilization programs the development of the metabolic syndrome in male mice exposed to high fat in utero," (in eng), *Pediatr Res,* vol. 66, no. 4, pp. 368-73, Oct 2009, doi: 10.1203/PDR.0b013e3181b33375.

[158] Wu Y., Wu T., Wu J., Zhao L., Li Q., Varghese Z., Moorhead J. F., Powis S. H., Chen Y., and Ruan X. Z., "Chronic inflammation exacerbates glucose metabolism disorders in C57BL/6J mice fed with high-fat diet," (in eng), *J Endocrinol,* vol. 219, no. 3, pp. 195-204, Dec 2013, doi: 10.1530/joe-13-0160.

[159] Winzell M. S. and Ahrén B., "The high-fat diet-fed mouse: a model for studying mechanisms and treatment of impaired glucose tolerance and type 2 diabetes," (in eng), *Diabetes,* vol. 53 Suppl 3, pp. S215-9, Dec 2004, doi: 10.2337/diabetes.53.suppl_3.s215.

[160] Youn J. Y., Siu K. L., Lob H. E., Itani H., Harrison D. G., and Cai H., "Role of vascular oxidative stress in obesity and metabolic syndrome," (in eng), *Diabetes,* vol. 63, no. 7, pp. 2344-55, Jul 2014, doi: 10.2337/db13-0719.

[161] Jiang F., Lim H. K., Morris M. J., Prior L., Velkoska E., Wu X., and Dusting G. J., "Systemic upregulation of NADPH oxidase in diet-induced obesity in rats," *Redox Report,* vol. 16, no. 6, pp. 223-229, 2011/11/01 2011, doi: 10.1179/174329211X13049558293713.

[162] Pepping J. K., "The Role of NADPH oxidase 2 (NOX2) in High-Fat Diet-Induced Adiposopathy and Brain Dysfunction in a Mouse Model," LSU Master's Theses, 1329, 2016.

[163] Matsuzawa-Nagata N., Takamura T., Ando H., Nakamura S., Kurita S., Misu H., Ota T., Yokoyama M., Honda M., Miyamoto K., and Kaneko S., "Increased oxidative stress precedes the onset of high-fat diet-induced insulin resistance and obesity," (in eng), *Metabolism,* vol. 57, no. 8, pp. 1071-7, Aug 2008, doi: 10.1016/j.metabol.2008.03.010.

[164] Huang X., Sun M., Li D., Liu J., Guo H., Dong Y., Jiang L., Pan Q., Man Y., Wang S., and Li J., "Augmented NADPH oxidase activity and p22phox expression in monocytes underlie oxidative stress of patients with type 2 diabetes mellitus," (in eng), *Diabetes Res Clin Pract,* vol. 91, no. 3, pp. 371-80, Mar 2011, doi: 10.1016/j.diabres.2010.12.026.

[165] Szabadfi K., Pinter E., Reglodi D., and Gabriel R., "Chapter One - Neuropeptides, Trophic Factors, and Other Substances Providing Morphofunctional and Metabolic

Protection in Experimental Models of Diabetic Retinopathy," in *International Review of Cell and Molecular Biology*, vol. 311, K. W. Jeon Ed.: Academic Press, 2014, pp. 1-121.

[166] Syed I., Kyathanahalli C. N., Jayaram B., Govind S., Rhodes C. J., Kowluru R. A., and Kowluru A., "Increased phagocyte-like NADPH oxidase and ROS generation in type 2 diabetic ZDF rat and human islets: role of Rac1-JNK1/2 signaling pathway in mitochondrial dysregulation in the diabetic islet," (in eng), *Diabetes,* vol. 60, no. 11, pp. 2843-2852, 2011, doi: 10.2337/db11-0809.

[167] Chinen I., Shimabukuro M., Yamakawa K., Higa N., Matsuzaki T., Noguchi K., Ueda S., Sakanashi M., and Takasu N., "Vascular lipotoxicity: endothelial dysfunction via fatty-acid-induced reactive oxygen species overproduction in obese Zucker diabetic fatty rats," (in eng), *Endocrinology,* vol. 148, no. 1, pp. 160-5, Jan 2007, doi: 10.1210/en.2006-1132.

[168] Coughlan M. T., Vervaart P. P., Permezel M., Georgiou H. M., and Rice G. E., "Altered placental oxidative stress status in gestational diabetes mellitus," (in eng), *Placenta,* vol. 25, no. 1, pp. 78-84, Jan 2004, doi: 10.1016/s0143-4004(03)00183-8.

[169] Cremonini E. and Oteiza P. I., "(-)-Epicatechin and its metabolites prevent palmitate-induced NADPH oxidase upregulation, oxidative stress and insulin resistance in HepG2 cells," (in eng), *Arch Biochem Biophys,* vol. 646, pp. 55-63, May 15 2018, doi: 10.1016/j.abb.2018.03.027.

[170] Bettaieb A., Vazquez Prieto M. A., Rodriguez Lanzi C., Miatello R. M., Haj F. G., Fraga C. G., and Oteiza P. I., "(-)-Epicatechin mitigates high-fructose-associated insulin resistance by modulating redox signaling and endoplasmic reticulum stress," (in eng), *Free Radic Biol Med,* vol. 72, pp. 247-56, Jul 2014, doi: 10.1016/j.freeradbiomed.2014.04.011.

[171] Yoshida T., Murayama H., Kawashima M., Nagahara R., Kangawa Y., Mizukami S., Kimura M., Abe H., Hayashi S. M., and Shibutani M., "Apocynin and enzymatically modified isoquercitrin suppress the expression of a NADPH oxidase subunit p22phox in steatosis-related preneoplastic liver foci of rats," (in eng), *Exp Toxicol Pathol,* vol. 69, no. 1, pp. 9-16, Jan 2017, doi: 10.1016/j.etp.2016.10.003.

[172] García-Ruiz I., Solís-Muñoz P., Fernández-Moreira D., Grau M., Muñoz-Yagüe T., and Solís-Herruzo J. A., "NADPH oxidase is implicated in the pathogenesis of oxidative phosphorylation dysfunction in mice fed a high-fat diet," *Scientific Reports,* vol. 6, no. 1, p. 23664, 2016/05/13 2016, doi: 10.1038/srep23664.

[173] Das S., Alhasson F., Dattaroy D., Pourhoseini S., Seth R. K., Nagarkatti M., Nagarkatti P. S., Michelotti G. A., Diehl A. M., Kalyanaraman B., and Chatterjee S., "NADPH Oxidase–Derived Peroxynitrite Drives Inflammation in Mice and Human Nonalcoholic Steatohepatitis via TLR4-Lipid Raft Recruitment," *Am J Pathol,* vol. 185, no. 7, pp. 1944-1957, 2015/07/01/ 2015, doi: https://doi.org/10.1016/j.ajpath.2015.03.024.

[174] Sancho P., Mainez J., Crosas-Molist E., Roncero C., Fernández-Rodriguez C. M., Pinedo F., Huber H., Eferl R., Mikulits W., and Fabregat I., "NADPH Oxidase NOX4 Mediates Stellate Cell Activation and Hepatocyte Cell Death during Liver Fibrosis Development," *PLOS ONE,* vol. 7, no. 9, p. e45285, 2012, doi: 10.1371/journal.pone.0045285.

[175] Bettaieb A., Jiang J. X., Sasaki Y., Chao T. I., Kiss Z., Chen X., Tian J., Katsuyama M., Yabe-Nishimura C., Xi Y., Szyndralewiez C., Schröder K., Shah A., Brandes R. P., Haj F. G., and Török N. J., "Hepatocyte Nicotinamide Adenine Dinucleotide Phosphate Reduced Oxidase 4 Regulates Stress Signaling, Fibrosis, and Insulin Sensitivity During Development of Steatohepatitis in Mice," (in eng), *Gastroenterology,* vol. 149, no. 2, pp. 468-80.e10, Aug 2015, doi: 10.1053/j.gastro.2015.04.009.

[176] Rabelo F., Stefano J. T., Cavaleiro A. M., Lima R. V. C., de Campos Mazo D. F., Carrilho F. J., Correa-Giannella M. L., and Oliveira C. P., "Association between the CYBA and NOX4 genes of NADPH oxidase and its relationship with metabolic syndrome in non-

alcoholic fatty liver disease in Brazilian population," (in eng), *Hepatobiliary Pancreat Dis Int,* vol. 17, no. 4, pp. 330-335, Aug 2018, doi: 10.1016/j.hbpd.2018.06.005.

[177] Matsumoto M., Zhang J., Zhang X., Liu J., Jiang J. X., Yamaguchi K., Taruno A., Katsuyama M., Iwata K., Ibi M., Cui W., Matsuno K., Marunaka Y., Itoh Y., Torok N. J., and Yabe-Nishimura C., "The NOX1 isoform of NADPH oxidase is involved in dysfunction of liver sinusoids in nonalcoholic fatty liver disease," (in eng), *Free Radic Biol Med,* vol. 115, pp. 412-420, Feb 1 2018, doi: 10.1016/j.freeradbiomed.2017.12.019.

[178] Albadrani M., Seth R. K., Sarkar S., Kimono D., Mondal A., Bose D., Porter D. E., Scott G. I., Brooks B., Raychoudhury S., Nagarkatti M., Nagarkatti P., Jule Y., Diehl A. M., and Chatterjee S., "Exogenous PP2A inhibitor exacerbates the progression of nonalcoholic fatty liver disease via NOX2-dependent activation of miR21," (in eng), *Am J Physiol Gastrointest Liver Physiol,* vol. 317, no. 4, pp. G408-g428, Oct 1 2019, doi: 10.1152/ajpgi.00061.2019.

[179] Kim S. Y., Jeong J.-M., Kim S. J., Seo W., Kim M.-H., Choi W.-M., Yoo W., Lee J.-H., Shim Y.-R., Yi H.-S., Lee Y.-S., Eun H. S., Lee B. S., Chun K., Kang S.-J., Kim S. C., Gao B., Kunos G., Kim H. M., and Jeong W.-I., "Pro-inflammatory hepatic macrophages generate ROS through NADPH oxidase 2 via endocytosis of monomeric TLR4-MD2 complex," (in eng), *Nat Commun,* vol. 8, no. 1, pp. 2247-2247, 2017, doi: 10.1038/s41467-017-02325-2.

[180] Targher G., Bertolini L., Padovani R., Rodella S., Tessari R., Zenari L., Day C., and Arcaro G., "Prevalence of Nonalcoholic Fatty Liver Disease and Its Association With Cardiovascular Disease Among Type 2 Diabetic Patients," *Diabetes Care,* vol. 30, no. 5, p. 1212, 2007, doi: 10.2337/dc06-2247.

[181] Marchesini G., Brizi M., Bianchi G., Tomassetti S., Bugianesi E., Lenzi M., McCullough A. J., Natale S., Forlani G., and Melchionda N., "Nonalcoholic Fatty Liver Disease," *Diabetes,* vol. 50, no. 8, p. 1844, 2001, doi: 10.2337/diabetes.50.8.1844.

[182] Lee S. M., Kwak S. H., Koo J. N., Oh I. H., Kwon J. E., Kim B. J., Kim S. M., Kim S. Y., Kim G. M., Joo S. K., Koo B. K., Shin S., Vixay C., Norwitz E. R., Park C. W., Jun J. K., Kim W., and Park J. S., "Non-alcoholic fatty liver disease in the first trimester and subsequent development of gestational diabetes mellitus," (in eng), *Diabetologia,* vol. 62, no. 2, pp. 238-248, Feb 2019, doi: 10.1007/s00125-018-4779-8.

[183] Sattari M., Bril F., Egerman R., Kalavalapalli S., and Cusi K., "Relationship between non-alcoholic fatty liver disease during pregnancy and abnormal glucose metabolism during and after pregnancy," (in eng), *J Investig Med,* vol. 68, no. 3, pp. 743-747, Mar 2020, doi: 10.1136/jim-2019-001186.

[184] Foghsgaard S., Andreasen C., Vedtofte L., Andersen E. S., Bahne E., Strandberg C., Buhl T., Holst J. J., Svare J. A., Clausen T. D., Mathiesen E. R., Damm P., Gluud L. L., Knop F. K., and Vilsbøll T., "Nonalcoholic Fatty Liver Disease Is Prevalent in Women With Prior Gestational Diabetes Mellitus and Independently Associated With Insulin Resistance and Waist Circumference," (in eng), *Diabetes Care,* vol. 40, no. 1, pp. 109-116, Jan 2017, doi: 10.2337/dc16-1017.

[185] Sullivan M. A., Harcourt B. E., Xu P., Forbes J. M., and Gilbert R. G., "Impairment of Liver Glycogen Storage in the db/db Animal Model of Type 2 Diabetes: A Potential Target for Future Therapeutics?," (in eng), *Curr Drug Targets,* vol. 16, no. 10, pp. 1088-93, 2015, doi: 10.2174/1389450116666150727123115.

[186] Oliveira D. S. d., Amado C. A. B., Martini M. C., Suzuki-Kemmelmeier F., and Bracht A., "Glycogen levels and energy status of the liver of fasting rats with diabetes types 1 and 2," *Brazilian Archives of Biology and Technology,* vol. 50, pp. 785-791, 2007. [Online]. Available: http://www.scielo.br/scielo.php?script=sci_arttext&pid=S1516-89132007000500006&nrm=iso.

[187] Wang L., Liu Q., Wang M., Du Y., Tan X., Xu B., Cheung U., Li E., Gilbert R. G., and Tang D., "Effects of fasting on liver glycogen structure in rats with type 2 diabetes," (in eng), *Carbohydr Polym,* vol. 237, p. 116144, Jun 1 2020, doi: 10.1016/j.carbpol.2020.116144.

[188] Zhang W. Q., Zhao T. T., Gui D. K., Gao C. L., Gu J. L., Gan W. J., Huang W., Xu Y., Zhou H., Chen W. N., Liu Z. L., and Xu Y. H., "Sodium Butyrate Improves Liver Glycogen Metabolism in Type 2 Diabetes Mellitus," (in eng), *J Agric Food Chem,* vol. 67, no. 27, pp. 7694-7705, Jul 10 2019, doi: 10.1021/acs.jafc.9b02083.

[189] Krähenbühl L., Lang C., Lüdes S., Seiler C., Schäfer M., Zimmermann A., and Krähenbühl S., "Reduced hepatic glycogen stores in patients with liver cirrhosis," (in eng), *Liver Int,* vol. 23, no. 2, pp. 101-9, Apr 2003, doi: 10.1034/j.1600-0676.2003.00805.x.

[190] Dixon L. J., Barnes M., Tang H., Pritchard M. T., and Nagy L. E., "Kupffer cells in the liver," (in eng), *Compr Physiol,* vol. 3, no. 2, pp. 785-797, 2013, doi: 10.1002/cphy.c120026.

[191] Huang W., Metlakunta A., Dedousis N., Zhang P., Sipula I., Dube J. J., Scott D. K., and O'Doherty R. M., "Depletion of liver Kupffer cells prevents the development of diet-induced hepatic steatosis and insulin resistance," (in eng), *Diabetes,* vol. 59, no. 2, pp. 347-57, Feb 2010, doi: 10.2337/db09-0016.

[192] Lanthier N., Molendi-Coste O., Cani P. D., van Rooijen N., Horsmans Y., and Leclercq I. A., "Kupffer cell depletion prevents but has no therapeutic effect on metabolic and inflammatory changes induced by a high-fat diet," (in eng), *Faseb j,* vol. 25, no. 12, pp. 4301-11, Dec 2011, doi: 10.1096/fj.11-189472.

[193] Stienstra R., Saudale F., Duval C., Keshtkar S., Groener J. E., van Rooijen N., Staels B., Kersten S., and Müller M., "Kupffer cells promote hepatic steatosis via interleukin-1beta-dependent suppression of peroxisome proliferator-activated receptor alpha activity," (in eng), *Hepatology,* vol. 51, no. 2, pp. 511-22, Feb 2010, doi: 10.1002/hep.23337.

[194] Kinoshita M., Uchida T., Sato A., Nakashima M., Nakashima H., Shono S., Habu Y., Miyazaki H., Hiroi S., and Seki S., "Characterization of two F4/80-positive Kupffer cell subsets by their function and phenotype in mice," (in eng), *J Hepatol,* vol. 53, no. 5, pp. 903-10, Nov 2010, doi: 10.1016/j.jhep.2010.04.037.

[195] García-Ruiz I., Solís-Muñoz P., Fernández-Moreira D., Grau M., Muñoz-Yagüe T., and Solís-Herruzo J. A., "NADPH oxidase is implicated in the pathogenesis of oxidative phosphorylation dysfunction in mice fed a high-fat diet," (in eng), *Sci Rep,* vol. 6, p. 23664, May 13 2016, doi: 10.1038/srep23664.

[196] Videla L. A., Rodrigo R., Orellana M., Fernandez V., Tapia G., Quiñones L., Varela N., Contreras J., Lazarte R., Csendes A., Rojas J., Maluenda F., Burdiles P., Diaz J. C., Smok G., Thielemann L., and Poniachik J., "Oxidative stress-related parameters in the liver of non-alcoholic fatty liver disease patients," (in eng), *Clin Sci (Lond),* vol. 106, no. 3, pp. 261-8, Mar 2004, doi: 10.1042/cs20030285.

[197] Jin Y., Tan Y., Chen L., Liu Y., and Ren Z., "Reactive Oxygen Species Induces Lipid Droplet Accumulation in HepG2 Cells by Increasing Perilipin 2 Expression," (in eng), *Int J Mol Sci,* vol. 19, no. 11, Nov 2 2018, doi: 10.3390/ijms19113445.

[198] Sekiya M., Hiraishi A., Touyama M., and Sakamoto K., "Oxidative stress induced lipid accumulation via SREBP1c activation in HepG2 cells," (in eng), *Biochem Biophys Res Commun,* vol. 375, no. 4, pp. 602-7, Oct 31 2008, doi: 10.1016/j.bbrc.2008.08.068.

[199] Stothard K. J., Tennant P. W., Bell R., and Rankin J., "Maternal overweight and obesity and the risk of congenital anomalies: a systematic review and meta-analysis," (in eng), *Jama,* vol. 301, no. 6, pp. 636-50, Feb 11 2009, doi: 10.1001/jama.2009.113.

[200] Rubens M., Ramamoorthy V., Saxena A., McGranaghan P., Veledar E., and Hernandez A., "Obstetric outcomes during delivery hospitalizations among obese pregnant women

in the United States," *Scientific Reports,* vol. 12, no. 1, p. 6862, 2022/04/27 2022, doi: 10.1038/s41598-022-10786-9.

[201] McCance D. R., "Diabetes in pregnancy," (in eng), *Best Pract Res Clin Obstet Gynaecol,* vol. 29, no. 5, pp. 685-99, Jul 2015, doi: 10.1016/j.bpobgyn.2015.04.009.

[202] Song Y. P., Chen Y. H., Gao L., Wang P., Wang X. L., Luo B., Li J., and Xu D. X., "Differential effects of high-fat diets before pregnancy and/or during pregnancy on fetal growth development," (in eng), *Life Sci,* vol. 212, pp. 241-250, Nov 1 2018, doi: 10.1016/j.lfs.2018.10.008.

[203] Frias A. E., Morgan T. K., Evans A. E., Rasanen J., Oh K. Y., Thornburg K. L., and Grove K. L., "Maternal high-fat diet disturbs uteroplacental hemodynamics and increases the frequency of stillbirth in a nonhuman primate model of excess nutrition," (in eng), *Endocrinology,* vol. 152, no. 6, pp. 2456-64, Jun 2011, doi: 10.1210/en.2010-1332.

[204] Wentzel P., Eriksson U. J., and Herrera E., "High-fat diet in pregnant rats and adverse fetal outcome," (in eng), *Ups J Med Sci,* vol. 124, no. 2, pp. 125-134, Apr 2019, doi: 10.1080/03009734.2019.1604588.

[205] Bequer L., Gómez T., Molina J. L., Álvarez A., Chaviano C., and Clapés S., "Experimental diabetes impairs maternal reproductive performance in pregnant Wistar rats and their offspring," (in eng), *Syst Biol Reprod Med,* vol. 64, no. 1, pp. 60-70, Feb 2018, doi: 10.1080/19396368.2017.1395928.

[206] Saad M. I., Abdelkhalek T. M., Saleh M. M., Haiba M. M., Tawfik S. H., and Kamel M. A., "Maternal diabetes impairs oxidative and inflammatory response in murine placenta," (in eng), *Springerplus,* vol. 5, pp. 532-532, 2016, doi: 10.1186/s40064-016-2180-y.

[207] Chapple S. J., Cheng X., and Mann G. E., "Effects of 4-hydroxynonenal on vascular endothelial and smooth muscle cell redox signaling and function in health and disease," *Redox Biology,* vol. 1, no. 1, pp. 319-331, 2013/01/01/ 2013, doi: https://doi.org/10.1016/j.redox.2013.04.001.

[208] Guerby P., Swiader A., Tasta O., Pont F., Rodriguez F., Parant O., Vayssière C., Shibata T., Uchida K., Salvayre R., and Negre-Salvayre A., "Modification of endothelial nitric oxide synthase by 4-oxo-2(E)-nonenal(ONE) in preeclamptic placentas," *Free Radical Biology and Medicine,* vol. 141, pp. 416-425, 2019/09/01/ 2019, doi: https://doi.org/10.1016/j.freeradbiomed.2019.07.015.

[209] Rebholz S. L., Burke K. T., Yang Q., Tso P., and Woollett L. A., "Dietary fat impacts fetal growth and metabolism: uptake of chylomicron remnant core lipids by the placenta," (in eng), *Am J Physiol Endocrinol Metab,* vol. 301, no. 2, pp. E416-25, Aug 2011, doi: 10.1152/ajpendo.00619.2010.

[210] Zhu M. J., Ma Y., Long N. M., Du M., and Ford S. P., "Maternal obesity markedly increases placental fatty acid transporter expression and fetal blood triglycerides at midgestation in the ewe," (in eng), *Am J Physiol Regul Integr Comp Physiol,* vol. 299, no. 5, pp. R1224-31, Nov 2010, doi: 10.1152/ajpregu.00309.2010.

[211] Saben J., Lindsey F., Zhong Y., Thakali K., Badger T. M., Andres A., Gomez-Acevedo H., and Shankar K., "Maternal obesity is associated with a lipotoxic placental environment," (in eng), *Placenta,* vol. 35, no. 3, pp. 171-7, Mar 2014, doi: 10.1016/j.placenta.2014.01.003.

[212] Capobianco E., Martínez N., Fornes D., Higa R., Di Marco I., Basualdo M. N., Faingold M. C., and Jawerbaum A., "PPAR activation as a regulator of lipid metabolism, nitric oxide production and lipid peroxidation in the placenta from type 2 diabetic patients," (in eng), *Molecular and cellular endocrinology,* vol. 377, no. 1-2, pp. 7-15, Sep 5 2013, doi: 10.1016/j.mce.2013.06.027.

[213] Mandò C., Anelli G. M., Novielli C., Panina-Bordignon P., Massari M., Mazzocco M. I., and Cetin I., "Impact of Obesity and Hyperglycemia on Placental Mitochondria," (in eng), *Oxid Med Cell Longev,* vol. 2018, p. 2378189, 2018, doi: 10.1155/2018/2378189.

[214] Milczarek R., Sokolowska E., Hallmann A., and Klimek J., "The NADPH- and iron-dependent lipid peroxidation in human placental microsomes," (in eng), *Mol Cell Biochem,* vol. 295, no. 1-2, pp. 105-11, Jan 2007, doi: 10.1007/s11010-006-9279-3.

[215] Klimek J., "Cytochrome P-450 involvement in the NADPH-dependent lipid peroxidation in human placental mitochondria," (in eng), *Biochim Biophys Acta,* vol. 1044, no. 1, pp. 158-64, May 1 1990, doi: 10.1016/0005-2760(90)90231-l.

[216] Kulkarni A. P. and Kenel M. F., "Human placental lipid peroxidation. Some characteristics of the NADPH-supported microsomal reaction," (in eng), *Gen Pharmacol,* vol. 18, no. 5, pp. 491-6, 1987, doi: 10.1016/0306-3623(87)90068-1.

[217] Matsubara S. and Sato I., "Enzyme histochemically detectable NAD(P)H oxidase in human placental trophoblasts: normal, preeclamptic, and fetal growth restriction-complicated pregnancy," (in eng), *Histochem Cell Biol,* vol. 116, no. 1, pp. 1-7, Jul 2001, doi: 10.1007/s004180100301.

[218] Poranen A. K., Ekblad U., Uotila P., and Ahotupa M., "Lipid peroxidation and antioxidants in normal and pre-eclamptic pregnancies," (in eng), *Placenta,* vol. 17, no. 7, pp. 401-5, Sep 1996, doi: 10.1016/s0143-4004(96)90021-1.

[219] Serdar Z., Gür E., Develioğlu O., Colakoğullari M., and Dirican M., "Placental and decidual lipid peroxidation and antioxidant defenses in preeclampsia. Lipid peroxidation in preeclampsia," (in eng), *Pathophysiology,* vol. 9, no. 1, p. 21, Oct 2002, doi: 10.1016/s0928-4680(02)00052-4.

[220] Bowman C. E., Selen Alpergin E. S., Cavagnini K., Smith D. M., Scafidi S., and Wolfgang M. J., "Maternal Lipid Metabolism Directs Fetal Liver Programming following Nutrient Stress," *Cell Reports,* vol. 29, no. 5, pp. 1299-1310.e3, 2019/10/29/ 2019, doi: https://doi.org/10.1016/j.celrep.2019.09.053.

[221] McCurdy C. E., Bishop J. M., Williams S. M., Grayson B. E., Smith M. S., Friedman J. E., and Grove K. L., "Maternal high-fat diet triggers lipotoxicity in the fetal livers of nonhuman primates," (in eng), *J Clin Invest,* vol. 119, no. 2, pp. 323-35, Feb 2009, doi: 10.1172/jci32661.

[222] Heerwagen M. J., Stewart M. S., de la Houssaye B. A., Janssen R. C., and Friedman J. E., "Transgenic increase in N-3/n-6 Fatty Acid ratio reduces maternal obesity-associated inflammation and limits adverse developmental programming in mice," (in eng), *PLoS One,* vol. 8, no. 6, p. e67791, 2013, doi: 10.1371/journal.pone.0067791.

[223] Puppala S., Li C., Glenn J. P., Saxena R., Gawrieh S., Quinn A., Palarczyk J., Dick E. J., Jr., Nathanielsz P. W., and Cox L. A., "Primate fetal hepatic responses to maternal obesity: epigenetic signalling pathways and lipid accumulation," (in eng), *J Physiol,* vol. 596, no. 23, pp. 5823-5837, Dec 2018, doi: 10.1113/jp275422.

[224] Alfaradhi M. Z., Fernandez-Twinn D. S., Martin-Gronert M. S., Musial B., Fowden A., and Ozanne S. E., "Oxidative stress and altered lipid homeostasis in the programming of offspring fatty liver by maternal obesity," (in eng), *Am J Physiol Regul Integr Comp Physiol,* vol. 307, no. 1, pp. R26-34, Jul 1 2014, doi: 10.1152/ajpregu.00049.2014.

[225] Hoch D., Gauster M., Hauguel-de Mouzon S., and Desoye G., "Diabesity-associated oxidative and inflammatory stress signalling in the early human placenta," (in eng), *Mol Aspects Med,* vol. 66, pp. 21-30, Apr 2019, doi: 10.1016/j.mam.2018.11.002.

[226] Spada A. P., Damasceno D. C., Sinzato Y. K., Campos K. E., Faria P. A., Dallaqua B., Calderon I. M., Rudge M. V., and Rodrigues T., "Oxidative Stress in Maternal Blood and Placenta From Mild Diabetic Rats," (in eng), *Reprod Sci,* vol. 21, no. 8, pp. 973-977, Aug 2014, doi: 10.1177/1933719113519175.

[227] Schoots M. H., Gordijn S. J., Scherjon S. A., van Goor H., and Hillebrands J. L., "Oxidative stress in placental pathology," (in eng), *Placenta,* vol. 69, pp. 153-161, Sep 2018, doi: 10.1016/j.placenta.2018.03.003.

[228] Burton G. J. and Jauniaux E., "Pathophysiology of placental-derived fetal growth restriction," (in eng), *Am J Obstet Gynecol,* vol. 218, no. 2s, pp. S745-s761, Feb 2018, doi: 10.1016/j.ajog.2017.11.577.

[229] Fisher J. J., Bartho L. A., Perkins A. V., and Holland O. J., "Placental mitochondria and reactive oxygen species in the physiology and pathophysiology of pregnancy," (in eng), *Clin Exp Pharmacol Physiol,* vol. 47, no. 1, pp. 176-184, Jan 2020, doi: 10.1111/1440-1681.13172.

[230] Hernandez I., Fournier T., Chissey A., Therond P., Slama A., Beaudeux J. L., and Zerrad-Saadi A., "NADPH oxidase is the major source of placental superoxide in early pregnancy: association with MAPK pathway activation," (in eng), *Sci Rep,* vol. 9, no. 1, p. 13962, Sep 27 2019, doi: 10.1038/s41598-019-50417-4.

[231] Cui X. L., Brockman D., Campos B., and Myatt L., "Expression of NADPH oxidase isoform 1 (Nox1) in human placenta: involvement in preeclampsia," (in eng), *Placenta,* vol. 27, no. 4-5, pp. 422-431, Apr-May 2006, doi: 10.1016/j.placenta.2005.04.004.

[232] Petrônio M. S., Zeraik M. L., Fonseca L. M. d., and Ximenes V. F., "Apocynin: chemical and biophysical properties of a NADPH oxidase inhibitor," (in eng), *Molecules,* vol. 18, no. 3, pp. 2821-2839, 2013, doi: 10.3390/molecules18032821.

[233] Lim R., Acharya R., Delpachitra P., Hobson S., Sobey C. G., Drummond G. R., and Wallace E. M., "Activin and NADPH-oxidase in preeclampsia: insights from in vitro and murine studies," (in eng), *Am J Obstet Gynecol,* vol. 212, no. 1, pp. 86.e1-12, Jan 2015, doi: 10.1016/j.ajog.2014.07.021.

[234] Scaife P. J., Simpson A., Kurlak L. O., Briggs L. V., Gardner D. S., Broughton Pipkin F., Jones C. J. P., and Mistry H. D., "Increased Placental Cell Senescence and Oxidative Stress in Women with Pre-Eclampsia and Normotensive Post-Term Pregnancies," (in eng), *Int J Mol Sci,* vol. 22, no. 14, Jul 7 2021, doi: 10.3390/ijms22147295.

[235] Gomes S. Z., Lorenzon A. R., Vieira J. S., Rocha C. R., Bandeira C., Hoshida M. S., Lopes L. R., and Bevilacqua E., "Expression of NADPH oxidase by trophoblast cells: potential implications for the postimplanting mouse embryo," (in eng), *Biol Reprod,* vol. 86, no. 2, p. 56, Feb 2012, doi: 10.1095/biolreprod.111.094748.

[236] Al-Sabbagh M., Fusi L., Higham J., Lee Y., Lei K., Hanyaloglu A. C., Lam E. W., Christian M., and Brosens J. J., "NADPH oxidase-derived reactive oxygen species mediate decidualization of human endometrial stromal cells in response to cyclic AMP signaling," (in eng), *Endocrinology,* vol. 152, no. 2, pp. 730-40, Feb 2011, doi: 10.1210/en.2010-0899.

[237] Liang C., DeCourcy K., and Prater M. R., "High-saturated-fat diet induces gestational diabetes and placental vasculopathy in C57BL/6 mice," (in eng), *Metabolism,* vol. 59, no. 7, pp. 943-50, Jul 2010, doi: 10.1016/j.metabol.2009.10.015.

[238] Schneider D., Hernández C., Farías M., Uauy R., Krause B. J., and Casanello P., "Oxidative stress as common trait of endothelial dysfunction in chorionic arteries from fetuses with IUGR and LGA," (in eng), *Placenta,* vol. 36, no. 5, pp. 552-8, May 2015, doi: 10.1016/j.placenta.2015.02.003.

[239] Kretschmer T., Schulze-Edinghausen M., Turnwald E.-M., Janoschek R., Bae-Gartz I., Zentis P., Handwerk M., Wohlfarth M., Schauss A., Hucklenbruch-Rother E., Dötsch J., and Appel S., "Effect of Maternal Obesity in Mice on IL-6 Levels and Placental Endothelial Cell Homeostasis," (in eng), *Nutrients,* vol. 12, no. 2, p. 296, 2020, doi: 10.3390/nu12020296.

[240] Wallace J. G., Bellissimo C. J., Yeo E., Fei Xia Y., Petrik J. J., Surette M. G., Bowdish D. M. E., and Sloboda D. M., "Obesity during pregnancy results in maternal intestinal inflammation, placental hypoxia, and alters fetal glucose metabolism at mid-gestation," (in eng), *Sci Rep,* vol. 9, no. 1, p. 17621, Nov 26 2019, doi: 10.1038/s41598-019-54098-x.

[241] Gohir W., Kennedy K. M., Wallace J. G., Saoi M., Bellissimo C. J., Britz-McKibbin P., Petrik J. J., Surette M. G., and Sloboda D. M., "High-fat diet intake modulates maternal intestinal adaptations to pregnancy and results in placental hypoxia, as well as altered fetal gut barrier proteins and immune markers," (in eng), *J Physiol,* vol. 597, no. 12, pp. 3029-3051, Jun 2019, doi: 10.1113/jp277353.

[242] Marti H. J., Bernaudin M., Bellail A., Schoch H., Euler M., Petit E., and Risau W., "Hypoxia-induced vascular endothelial growth factor expression precedes neovascularization after cerebral ischemia," (in eng), *Am J Pathol,* vol. 156, no. 3, pp. 965-976, 2000, doi: 10.1016/S0002-9440(10)64964-4.

[243] Shweiki D., Itin A., Soffer D., and Keshet E., "Vascular endothelial growth factor induced by hypoxia may mediate hypoxia-initiated angiogenesis," (in eng), *Nature,* vol. 359, no. 6398, pp. 843-5, Oct 29 1992, doi: 10.1038/359843a0.

[244] Chen L., Endler A., and Shibasaki F., "Hypoxia and angiogenesis: regulation of hypoxia-inducible factors via novel binding factors," *Experimental & Molecular Medicine,* vol. 41, no. 12, pp. 849-857, 2009/12/01 2009, doi: 10.3858/emm.2009.41.12.103.

11. Appendix A – Automated image analysis using ImageJ

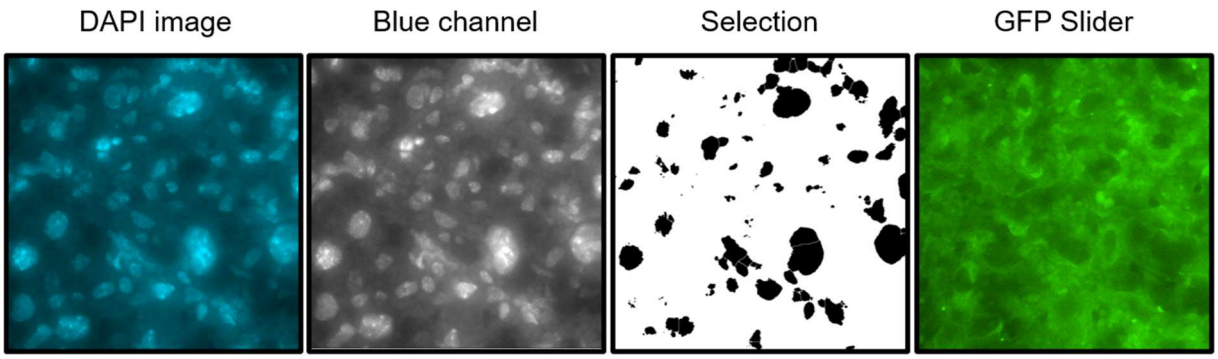

Appendix Figure 1: 8-OHdG staining quantification. An automated protocol according to Guirado et al. was implemented and adjusted [134]. DAPI image was split into color channels. 10% of the brightest pixels were selected on the blue channel to create a mask which was applied on the GFP Slider image to determine mean gray values.

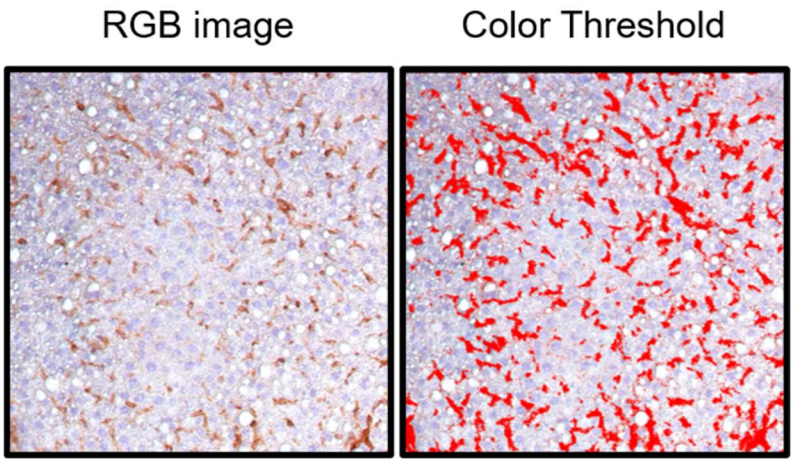

Appendix Figure 2: F4/80 staining quantification. Color threshold was set by adjusting hue, saturation and brightness according to the brown reaction sites.

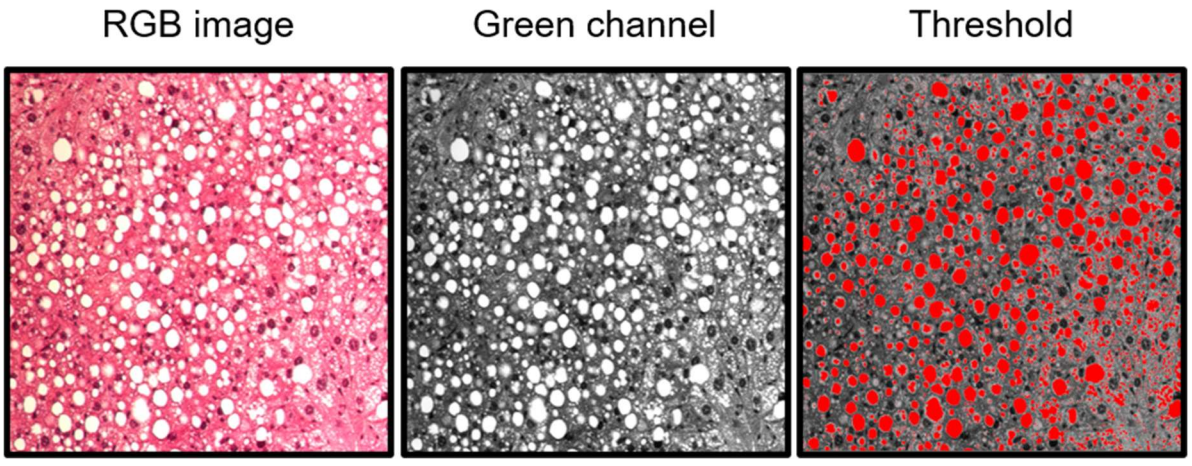

Appendix Figure 3: H&E staining quantification of lipid droplets. RGB image was split into color channels. Threshold was set on the green channel according to the extent of lipid droplets.

Appendix A – Automated image analysis using ImageJ

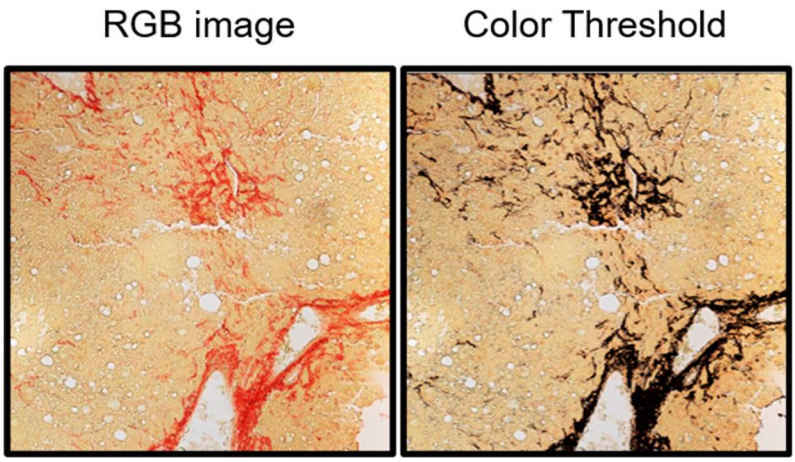

Appendix Figure 4: Picrosirius Red staining quantification of collagen. Color threshold was set by adjusting hue, saturation and brightness according to the red fibers.

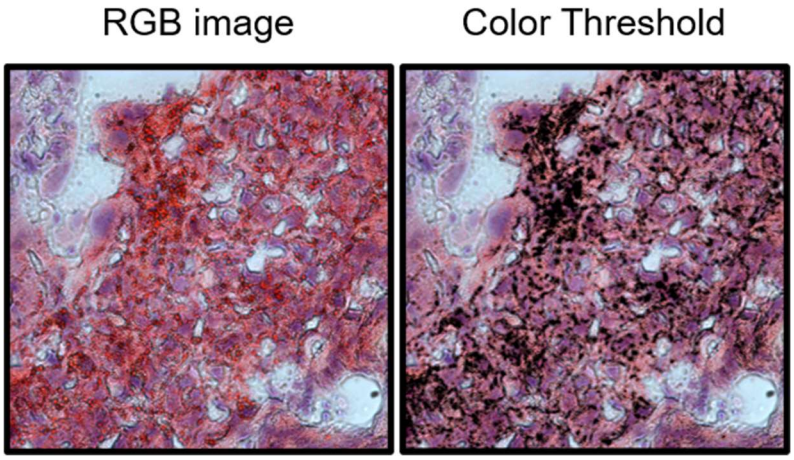

Appendix Figure 5: ORO staining quantification of lipids. Color threshold was set by adjusting hue, saturation and brightness according to the stained area.

12. Appendix B – Source code of automated image analysis

12.1. Split images in four equal parts

```
origen = getDirectory("Images to process");
lista = getFileList(origen);
File.makeDirectory(origen + "Split\\");
setBatchMode(true);
for (j = 0; j < lista.length; j++) {
    showProgress(j + 1, lista.length);
    open(origen + lista[j]);

    nombre = lista[j];
    n = 2;
    id = getImageID();
    title = getTitle();
    getLocationAndSize(locX, locY, sizeW, sizeH);
    width = getWidth();
    height = getHeight();
    tileWidth = width / n;
    tileHeight = height / n;

    for (y = 0; y < n; y++) {
        offsetY = y * height / n;
        for (x = 0; x < n; x++) {
            open(origen + lista[j]);
            offsetX = x * width / n;

            makeRectangle(offsetX, offsetY, tileWidth, tileHeight);
            run("Crop");

            saveAs("tiff", origen + "Split\\" + nombre + "-" + y + "-" + x);
        }
    }
}
```

12.2. Select nuclei on blue image and use selection on green image

```
origen = getDirectory("Images to process");
lista = getFileList(origen);
File.makeDirectory(origen +"Masks\\");
setBatchMode(true);
for (j = 0; j < lista.length; j++) {
    showProgress(j + 1, lista.length);
    open(origen + lista[j]);

    run("Next Slice [>]");
    run("Delete Slice");

    nombre = lista[j];
    setBackgroundColor(0, 0, 0);
    run("Duplicate...", "duplicate");
    run("Gaussian Blur...", "sigma=1");
    run("Split Channels");

    id = getImageID();
    selectImage(id + 0);

    run("Duplicate...", "duplicate");
    tissueThreshPerc = 95;
    nBins = 255;
    getHistogram(values, count, nBins);
    cumSum = getWidth() * getHeight();
    tissueValue = cumSum * tissueThreshPerc / 100;
    cumSumValues = count;

    for (i = 1; i < count.length; i++) {
        cumSumValues[i] += cumSumValues[i - 1];
    }

    for (i = 1; i < cumSumValues.length; i++) {
        if (cumSumValues[i - 1] <= tissueValue && tissueValue <= cumSumValues[i]) {
            setThreshold(i, 255);
            setOption("BlackBackground", false);
            run("Convert to Mask");
        }
    }

    run("Median...", "radius=2");
    run("Watershed");
    saveAs("tiff", origen +"Masks\\"+nombre+"_BlueMask");

    run("Analyze Particles...", "size=0.01-Infinity summarize");
    run("Create Selection");

    close();

    close();

    open(origen + lista[j]);

    // Only Green Image
    run("Delete Slice");

    run("Restore Selection");
    run("Set Measurements...", "area mean integrated area_fraction display redirect=None decimal=3");
    run("Measure");
    close();
}
```

12.3. Process green image without red image

```
origen = getDirectory("Images to process");
lista = getFileList(origen);
File.makeDirectory(origen + "Masks\\");
setBatchMode(true);
for (j = 0; j < lista.length; j++) {
    showProgress(j + 1, lista.length);
    open(origen + lista[j]);
    run("Delete Slice");
    nombre = lista[j];
    setBackgroundColor(0, 0, 0);
    run("Duplicate...", "duplicate");
    run("Gaussian Blur...", "sigma=1");
    run("Split Channels");
    id = getImageID();
    selectImage(id + 1);
    run("Duplicate...", "duplicate");
    tissueThreshPerc = 95;
    nBins = 255;
    getHistogram(values, count, nBins);
    cumSum = getWidth() * getHeight();
    tissueValue = cumSum * tissueThreshPerc / 100;
    cumSumValues = count;
    for (i = 1; i < count.length; i++) {
        cumSumValues[i] += cumSumValues[i - 1];
    }
    for (i = 1; i < cumSumValues.length; i++)
        if (cumSumValues[i - 1] <= tissueValue && tissueValue <= cumSumValues[i]) {
            setThreshold(i, 255);
            setOption("BlackBackground", false);
            run("Convert to Mask");
        }
    run("Median...", "radius=2");
    saveAs("tiff", origen + "Masks\\" + nombre + "_Blue");
    run("Analyze Particles...", "size=0.01-Infinity summarize");
    run("Create Selection");
    run("Copy");
    close();
    selectImage(id + 1);
    run("Restore Selection");
    run("Set Measurements...", "area mean integrated area_fraction display redirect=None decimal=3");
    run("Measure");
    close();
    selectImage(id + 2);
    run("Duplicate...", "duplicate");
    tissueThreshPerc = 95;
    nBins = 255;
    getHistogram(values, count, nBins);
    cumSum = getWidth() * getHeight();
    tissueValue = cumSum * tissueThreshPerc / 100;
    cumSumValues = count;
    for (k = 1; k < count.length; k++) {
        cumSumValues[k] += cumSumValues[k - 1];
    }
    for (k = 1; k < cumSumValues.length; k++)
        if (cumSumValues[k - 1] <= tissueValue && tissueValue <= cumSumValues[k]) {
            setThreshold(k, 255);
            setOption("BlackBackground", false);
            run("Convert to Mask");
        }
    run("Median...", "radius=2");
    saveAs("tiff", origen + "Masks\\" + nombre + "_2");
    run("Analyze Particles...", "size=0.01-Infinity summarize");
    run("Create Selection");
    run("Copy");
    close();
    selectImage(id + 2);
    run("Restore Selection");
    run("Set Measurements...", "area mean integrated area_fraction display redirect=None decimal=3");
    run("Measure");
    close();
}
```

12.4. Process red image without green image

```
origen = getDirectory("Images to process");
lista = getFileList(origen);
File.makeDirectory(origen + "Masks\\");
setBatchMode(true);
for (j = 0; j < lista.length; j++) {
    showProgress(j + 1, lista.length);
    open(origen + lista[j]);
    run("Delete Slice");
    nombre = lista[j];
    setBackgroundColor(0, 0, 0);
    run("Duplicate...", "duplicate");
    run("Gaussian Blur...", "sigma=1");
    run("Split Channels");
    id = getImageID();
    selectImage(id + 0);
    run("Duplicate...", "duplicate");
    tissueThreshPerc = 95;
    nBins = 255;
    getHistogram(values, count, nBins);
    cumSum = getWidth() * getHeight();
    tissueValue = cumSum * tissueThreshPerc / 100;
    cumSumValues = count;
    for (i = 1; i < count.length; i++) {
        cumSumValues[i] += cumSumValues[i - 1];
    }
    for (i = 1; i < cumSumValues.length; i++)
        if (cumSumValues[i - 1] <= tissueValue && tissueValue <= cumSumValues[i]) {
            setThreshold(i, 255);
            setOption("BlackBackground", false);
            run("Convert to Mask");
        }
    run("Median...", "radius=2");
    saveAs("tiff", origen + "Masks\\" + nombre + "_0");
    run("Analyze Particles...", "size=0.01-Infinity summarize");
    run("Create Selection");
    run("Copy");
    close();
    selectImage(id + 0);
    run("Restore Selection");
    run("Set Measurements...", "area mean integrated area_fraction display redirect=None decimal=3");
    run("Measure");
    close();
    selectImage(id + 2);
    run("Duplicate...", "duplicate");
    tissueThreshPerc = 95;
    nBins = 255;
    getHistogram(values, count, nBins);
    cumSum = getWidth() * getHeight();
    tissueValue = cumSum * tissueThreshPerc / 100;
    cumSumValues = count;
    for (k = 1; k < count.length; k++) {
        cumSumValues[k] += cumSumValues[k - 1];
    }
    for (k = 1; k < cumSumValues.length; k++)
        if (cumSumValues[k - 1] <= tissueValue && tissueValue <= cumSumValues[k]) {
            setThreshold(k, 255);
            setOption("BlackBackground", false);
            run("Convert to Mask");
        }
    run("Median...", "radius=2");
    saveAs("tiff", origen + "Masks\\" + nombre + "_2");
    run("Analyze Particles...", "size=0.01-Infinity summarize");
    run("Create Selection");
    run("Copy");
    close();
    selectImage(id + 2);
    run("Restore Selection");
    run("Set Measurements...", "area mean integrated area_fraction display redirect=None decimal=3");
    run("Measure");
    close();
}
```

12.5. Exemplary macro for color threshold analysis with ImageJ

```
run("Set Measurements...", "area integrated area_fraction display redirect=None decimal=3");

imgName=getTitle();
run("Duplicate...", "title=1.tif");

run("Color Threshold...");

min=newArray(3);
max=newArray(3);
filter=newArray(3);
a=getTitle();
run("HSB Stack");
run("Convert Stack to Images");
selectWindow("Hue");
rename("0");
selectWindow("Saturation");
rename("1");
selectWindow("Brightness");
rename("2");
min[0]=30;
max[0]=240;
filter[0]="pass"; //oder stop
min[1]=130;
max[1]=255;
filter[1]="pass";
min[2]=0;
max[2]=255;
filter[2]="pass";

for (i=0;i<3;i++){
  selectWindow(""+i);
  setThreshold(min[i], max[i]);
  run("Convert to Mask");
  if (filter[i]=="stop")  run("Invert");
}
imageCalculator("AND create", "0","1");
imageCalculator("AND create", "Result of 0","2");
for (i=0;i<3;i++){
  selectWindow(""+i);
  close();
}
selectWindow("Result of 0");
close();
selectWindow("Result of Result of 0");
rename(a);

run("Create Selection");
selectWindow(imgName);
run("Restore Selection");

run("Measure");
```

13. Acknowledgements

First of all, I would like to express my gratitude to my supervisor Professor Agnes Görlach, for giving me the opportunity to work on this research project and acquire my doctor's degree of medical science.

I am sincerely grateful to my mentor and scientific advisor, Dr. rer. nat. Damir Kračun for his guidance, his support and patience throughout this entire time. It is under his continuous supervision and thoughtful instructions despite his own research projects in the US that I acquainted myself with scientific work, project planning and data analysis. Thanks to his huge contribution I gained my scientific knowledge and am about to obtain my doctoral degree.

I would also like to sincerely thank Ivan Kanchev for teaching me the fundamentals of histology. From paraffin embedding, microtome cutting to histological stainings, he provided valuable tips and suggestions for improvement. With the help of his histopathological expertise, I was able to master the different steps of histology and to identify pathologies in murine tissues.

My special thanks also go to the postdoctoral researcher Dr. Andreas Petry who introduced me to molecular biological techniques.

These acknowledgments would not be complete without mentioning my lab colleagues, especially Sebahat Özer, Kilian Hierdeis and Mathieu Klop, but also Andreas Seidel, Anna Knirsch and Dr. Benjamin Trautz, who all helped and assisted throughout this project.

I would also like to acknowledge the support I received from my current employer and mentor Professor Tilo Biedermann, thank you for providing me the opportunity to finalize my doctoral research study.

Lastly, I am deeply grateful to my parents, my dear brother and my loving husband as well as my caring friends for their continuous support, appreciation and encouragement. Thank you for always believing in me.